

Differentiation of Basic Calcium Phosphate and Calcium Pyrophosphate deposition in articular cartilage

Thesis

for the degree of

doctor rerum naturalium (Dr. rer. nat.)

approved by the Faculty of Natural Sciences of Otto von Guericke University Magdeburg

by M.Sc. Sina Stücker

born on 12.02.1995 in Brilon

Examiner: Prof. Dr. Jessica Bertrand

Prof. Dr. Rik Lories

submitted on: 09.09.2024

defended on: 21.02.2025

Abstract

Osteoarthritis (OA) is a degenerative disease of the joint that is accompanied by structural, functional and metabolic changes in articular structures including cartilage, menisci, synovium, and bone. Calcification of articular cartilage is a common event in OA joints and involves the pathological deposition of calcium crystals in the extracellular matrix. Intra-articular calcium crystals can be divided into Basic calcium phosphate (BCP) and Calcium pyrophosphate (CPP) crystals. Individual BCP crystals are of submicroscopic size and their formation is associated with cartilage degradation, chondrocyte hypertrophy and OA progression. CPP crystals are of larger, needle-shaped morphology and have been linked to chondrocyte senescence. Calcified deposits can be detected with various methods including conventional radiography, microscopy and spectroscopy that come with several limitations. Thus, detection and differentiation of BCP and CPP crystals in calcified cartilage remains difficult, leading to conflicting data on prevalence and distribution. The formation of BCP and CPP is proposedly determined by extracellular levels of inorganic phosphate (Pi) and pyrophosphate (PPi). However, the formation process largely remains elusive. Therefore, this thesis aimed to differentiate BCP and CPP calcification in articular cartilage in regards to prevalence, distribution and formation.

Calcification was detected using conventional radiography, and histological von Kossa staining. Crystals were identified using Raman spectroscopy. Radiological calcification was detected in 38% of patients. In contrast, histological cartilage calcification was found in 88% of patients, indicating the superior sensitivity of histological over radiological detection methods. Topologically, BCP was located on the cartilage surface and in the deep zone, while CPP deposition was limited to the superficial to intermediate cartilage.

To elucidate the formation of BCP and CPP in cartilage, I analysed the expression of enzymes of the extracellular PPi metabolism using quantitative RT-PCR. Additionally, enzymatic activity, Pi and PPi levels were assessed using specific assays. Specifically BCP-calcified cartilage showed elevated expression and activity of tissue non-specific-alkaline phosphatase (TNAP). This was accompanied by increased Pi concentration and an elevated Pi/PPi ratio, suggesting that BCP deposition in cartilage is driven by an imbalance in the extracellular PPi metabolism in favour of Pi. Instead, CPP deposition could not be explained by a dysregulated PPi metabolism. To investigate the formation of CPP, I induced chondrocyte calcification *in vitro*. In response to ATP, chondrocytes from CPP-calcified cartilage produced CPP, while BCP-cartilage-derived chondrocytes were only able to produce BCP, suggesting an inherent, ATP-associated mechanism for CPP formation. In light of the recent association between CPP calcification and senescence, I measured senescence-associated cytokines and chemokines in synovial fluid of BCP versus CPP-calcified joints by multiplex assay. CPP-calcified joints showed upregulated senescence-associated cytokines and chemokines, hinting towards increased senescence. In line with these findings, chondrocytes from heavily calcified menisci contained dense cytosolic

accumulations of CPP crystals. This was accompanied by elevated intracellular PPI concentrations and decreased Pi/PPI ratio, suggesting an intracellular pathway of CPP formation.

Zusammenfassung

Osteoarthrose (OA) ist eine degenerative Gelenkserkrankung, die mit strukturellen, metabolischen und funktionellen Einschränkungen in allen Bestandteilen des Gelenks einhergeht. Kalzifikation im Knorpel stellt ein häufiges Phänomen dar und entsteht durch die pathologische Ablagerung von Calciumkristallen in der extrazellulären Matrix. Intra-artikuläre Kalziumkristalle können in Basische Calciumphosphat (BCP) und Calciumpyrophosphat (CPP) Kristalle unterteilt werden. BCP Kristalle haben eine submikroskopische Größe und ihre Bildung hängt eng mit Knorpeldegradierung, OA Fortschreitung und einer hypertrophen Differenzierung von Chondrozyten zusammen. CPP Kristalle weisen eine größere, nadelförmige Morphologie auf und wurden kürzlich mit Seneszenz von Chondrozyten in Verbindung gebracht. Kalzifikationen können mit verschiedenen Methoden detektiert werden, unter anderem konventioneller Radiographie, Mikroskopie und Spektroskopie. Jede dieser Methoden weist jedoch Schwächen auf, die die Detektion und Differenzierung von BCP- und CPP-Kristallen im Knorpel erschweren. Dies führt zu widersprüchlichen Daten über Prävalenz und Verteilung von BCP- und CPP-Ablagerungen. Die Kristallbildung hängt mit der Konzentration von Phosphat (Pi) und Pyrophosphat (PPi) zusammen. Die genauen Mechanismen, die zur Ablagerung von BCP- oder CPP-Kristallen führen, sind allerdings noch nicht bekannt. Das Ziel dieser Arbeit ist es daher, BCP- und CPP-Kalzifikationen im Knorpel mit verschiedenen Methoden zu detektieren und im Hinblick auf Detektion, Prävalenz und Bildung zu differenzieren.

Kalzifikationen wurden radiologisch und histologisch detektiert. Die Art der Kristalle wurde mithilfe von Raman Spektroskopie identifiziert. In 38% der Patienten konnten radiologische Kalzifikationen des Kniegelenks festgestellt werden. Histologisch wurden dahingegen Kalzifikationen in 88% festgestellt. Während BCP-Ablagerungen auf der Knorpeloberfläche und in der tiefen Knorpelschicht zu finden waren, lagerten sich CPP-Kristalle ausschließlich in der mittleren Knorpelschicht ab.

Um die Kristallbildung im Knorpel zu untersuchen, habe ich die Expression von Enzymen des extrazellulären PPI-Metabolismus mittels quantitativer RT-PCR untersucht. Enzymatische Aktivität, sowie die Konzentration von Pi und PPI wurden mithilfe von speziellen Assays gemessen. BCP-kalzifizierter Knorpel zeigte dabei eine erhöhte Expression und Aktivität von tissue non-specific alkaline phosphatase (TNAP), begleitet von einer gesteigerten Pi-Konzentration sowie Pi/PPi Ratio. Folglich scheint die Bildung von BCP-Kristallen durch eine Dysregulation des extrazellulären PPI-Metabolismus gesteuert zu sein, während dies jedoch nicht die Bildung von CPP-Kristallen erklären kann. Zur Untersuchung der Bildung von CPP-Kristallen habe ich Chondrozyten aus kalzifiziertem Knorpel isoliert und diese mittels ATP zur Kalzifikation stimuliert. Chondrozyten aus CPP-kalzifiziertem Knorpel waren in der Lage, CPP- und BCP-Kristalle zu bilden, während Chondrozyten aus BCP-kalzifiziertem Knorpel lediglich BCP-Kristalle produzierten. Diese Beobachtung deutet auf einen inhärenten, ATP-assoziierten Mechanismus zur Bildung von CPP-Kristallen hin. Im Hinblick auf den kürzlich gezeigten Zusammenhang zwischen CPP-Kalzifikation und zellulärer Seneszenz im Knorpel, habe ich daraufhin

verschiedene Seneszenz-assoziierte Faktoren in der Synovialflüssigkeit aus BCP- und CPP-kalzifizierten Kniegelenken gemessen. CPP-Kalzifikation war mit einer erhöhten Konzentration einiger Seneszenz-assoziiierter Zytokine und Chemokine verbunden, was auf eine erhöhte Seneszenz in diesen Gelenken hindeuten könnte. *In vitro* zeigten Chondrozyten aus stark kalzifizierten Menisken eine große Ansammlung von CPP-Kristallen im Zytoplasma. Diese war mit einer erhöhten intrazellulären PPI-Konzentration sowie einer verminderten Pi/PPi Ratio verbunden. Insgesamt deuten diese Ergebnisse auf einen intrazellulären Mechanismus zur Bildung von CPP-Kristallen hin, während BCP-Kristalle vermutlich extrazellulär entstehen.

Contents

1	Introduction	1
1.1	Osteoarthritis	1
1.1.1	Clinical presentation and diagnosis	1
1.2	Pathophysiology of knee OA	2
1.2.1	Synovial membrane	2
1.2.2	Synovial fluid	3
1.2.3	Cartilage	3
1.2.4	Meniscus	5
1.2.5	Bone	5
1.3	Articular calcification	6
1.3.1	Basic calcium phosphate crystals	6
1.3.2	Calcium pyrophosphate dihydrate crystals	6
1.4	Detection of articular calcification	8
1.4.1	Radiography	8
1.4.2	Histological staining and light microscopy	9
1.4.3	Scanning electron microscopy	10
1.4.4	Raman spectroscopy	10
1.5	Calcification mechanism	11
1.5.1	Pyrophosphate metabolism	12
1.6	Aims	14
2	Materials and Methods	15
2.1	Materials	15
2.1.1	Equipment	15
2.1.2	Reagents	16
2.1.3	Consumables	17
2.1.4	Kits and Enzymes	17
2.1.5	Primers	18
2.1.6	Buffers and solutions	19
2.2	Histological methods	20
2.2.1	Sample collection and processing	20
2.2.2	Safranin-Orange/Fast Green staining	20
2.2.3	Von Kossa staining	20
2.2.4	Imaging and image analysis	20
2.2.5	Raman spectroscopy	21
2.2.6	Scanning electron microscopy and energy-dispersive X-ray spectroscopy	21
2.3	Molecular biological methods	22
2.3.1	RNA isolation and cDNA synthesis	22

2.3.2	Quantitative RT-PCR	22
2.4	Protein biochemical methods	24
2.4.1	Tissue homogenization	24
2.4.2	Enzymatic activity of ENPP1 and TNAP	24
2.4.3	Pi and PPI concentration	24
2.4.4	Multiplex cytokine assay	24
2.5	Cell culture methods	26
2.5.1	Isolation of primary articular chondrocytes	26
2.5.2	Isolation of primary meniscal fibrochondrocytes	26
2.5.3	Cultivation of primary articular chondrocytes and meniscal fibrochondrocytes.....	26
2.5.4	<i>In vitro</i> calcification	26
2.6	Statistical analysis	28
3	Results	29
3.1	Histology-directed Raman spectroscopy for accurate differentiation of articular calcification	29
3.1.1	Histological cartilage calcification is more prevalent than radiological calcification	31
3.1.2	Cartilage calcification is predominantly caused by BCP deposition	32
3.1.3	Discrete histology and distribution of BCP and CPP deposits in OA cartilage.....	32
3.2	Upregulated extracellular PPI metabolism as a driver of BCP deposition	35
3.2.1	Upregulated gene expression of PPI metabolism enzymes in BCP-calcified cartilage.	36
3.2.2	Upregulated TNAP activity and Pi levels in BCP-calcified cartilage.....	37
3.3	Intracellular and ATP-dependent induction of CPP deposition.....	39
3.3.1	ATP stimulation induces CPP formation <i>in vitro</i>	39
3.3.2	CPP calcification is associated with elevated levels of senescence-associated cytokines in synovial fluid	40
3.3.3	Intracellular CPP deposition is accompanied by elevated PPI levels in meniscal fibrochondrocytes	41
4	Discussion.....	44
4.1	Histology-directed Raman spectroscopy for accurate differentiation of articular calcification	44
4.1.1	Histological cartilage calcification is more prevalent than radiological calcification	44
4.1.2	Cartilage calcification is predominantly caused by BCP deposition	46
4.1.3	Discrete histology and distribution of BCP and CPP deposits in OA cartilage.....	47
4.2	Upregulated extracellular PPI metabolism as a driver of BCP deposition in OA cartilage	48
4.2.1	Upregulated gene expression of PPI metabolism enzymes in BCP-calcified cartilage.	48
4.2.2	Upregulated TNAP activity and Pi levels in BCP-calcified cartilage.....	49
4.3	Intracellular and ATP-dependent induction of CPP deposition.....	51
4.3.1	ATP stimulation induces CPP formation <i>in vitro</i>	51

4.3.2	CPP calcification is associated with elevated levels of senescence-associated cytokines in synovial fluid	52
4.3.3	Intracellular CPP deposition is accompanied by elevated PPI levels in meniscal fibrochondrocytes	53
5	Conclusion and Outlook	56
6	Abbreviations	57
7	List of Figures	60
8	List of Tables.....	61
9	References	62
10	Publications	82
11	Danksagung	83
12	Declaration of Honour	84
13	Curriculum vitae	85

1 Introduction

1.1 Osteoarthritis

Osteoarthritis (OA) is the most frequent form of arthritis. As a degenerative disease, OA is characterized by structural, functional and metabolic changes in the whole joint. Affected tissues include articular cartilage, synovium and subchondral bone, causing pain, joint stiffness and functional impairment [1]. The knee joint is the most common site of OA [2]. According to a systematic analysis for the Global Burden of Disease Study, an estimated 7.6% of the world population suffered from OA in 2020. This is equal to a total number of 595 million people [2]. Risk factors for OA development include obesity, injury, metabolic diseases (e.g. diabetes) and sociodemographic factors (e.g. age, female gender) [3]. In an aging population and rising rates of obesity, the prevalence of OA continues to increase steadily. From 2020 to 2050, cases of knee OA are set to increase by 75%, imposing a significant burden to the global health care system [2]. To date, there is no effective cure available. Current therapeutics mainly focus on pain relief with joint replacement surgery remaining the final treatment option [4].

1.1.1 Clinical presentation and diagnosis

Knee OA is a heterogeneous multifactorial disease. Affected tissues and clinical symptoms vary considerably, challenging accurate diagnosis. The European League Against Rheumatism (EULAR) recommends persistent knee pain, stiffness and reduced function as the main symptoms for diagnosis [5]. Besides physical examination, imaging adds additional value in making a differential diagnosis. Due to its easy availability, conventional radiography is often the first choice imaging method in clinical diagnostics [6]. Since pain and other OA symptoms are imprecise markers for disease severity [7], radiography is also used to grade the severity of structural changes in OA. The most commonly used system therefor is the Kellgren Lawrence (KL) grading system [8]. It describes five grades of OA severity based on radiographic findings such as joint space narrowing and osteophyte formation (Figure 1.1.1). Grade 0 shows a normal joint indicating no presence of OA. Grade 1 refers to doubtful space narrowing and possible osteophytes. Grades 2 and 3 show progressive joint space narrowing, osteophyte formation and beginning sclerosis, indicating minimal to moderate OA. Grade 4 is reserved for severe OA with large osteophytes, evident joint space narrowing, definite sclerosis and bone end deformity [8, 9].

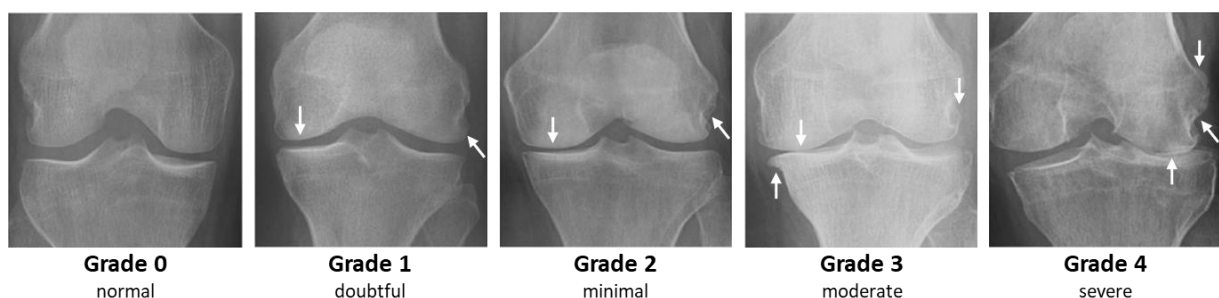


Figure 1.1.1: Kellgren Lawrence grading system. Grade 1 (no OA) shows a normal joint without OA. Grade 2 (doubtful OA) shows doubtful joint space narrowing (left arrow) and possible osteophytes (right arrow). Grade 2

(minimal OA) shows beginning joint space narrowing (left arrow) and osteophyte formation (right arrow). Grade 3 (moderate OA) is characterized by progressive osteophyte formation (left and right arrows) and evident narrowing of the joint space (middle arrow). In grade 4 (severe OA) the joint space is severely narrowed (left arrow) and bone ends show deformities and large osteophytes (right arrows) (adapted from [10]).

1.2 Pathophysiology of knee OA

The knee joint is among the largest and most complex joints in the human body. It enables movement between femur, tibia and patella. The bones are held in place by various ligaments, including anterior and posterior cruciate ligaments and medial and lateral collateral ligaments. By limiting rotation and translation, they stabilize the knee joint. The femoral condyles and the tibial plateau represent the articulating surfaces of the tibiofemoral joint and are covered by hyaline cartilage. For an even load distribution, the articulating surfaces are divided the medial and lateral meniscus [11] (Figure 1.2.1). The joint is enveloped by a capsule that is internally lined with synovial membrane. The capsule contains synovial fluid that fills up the joint space and lubricates the articulating surfaces to reduce friction during movement [12].

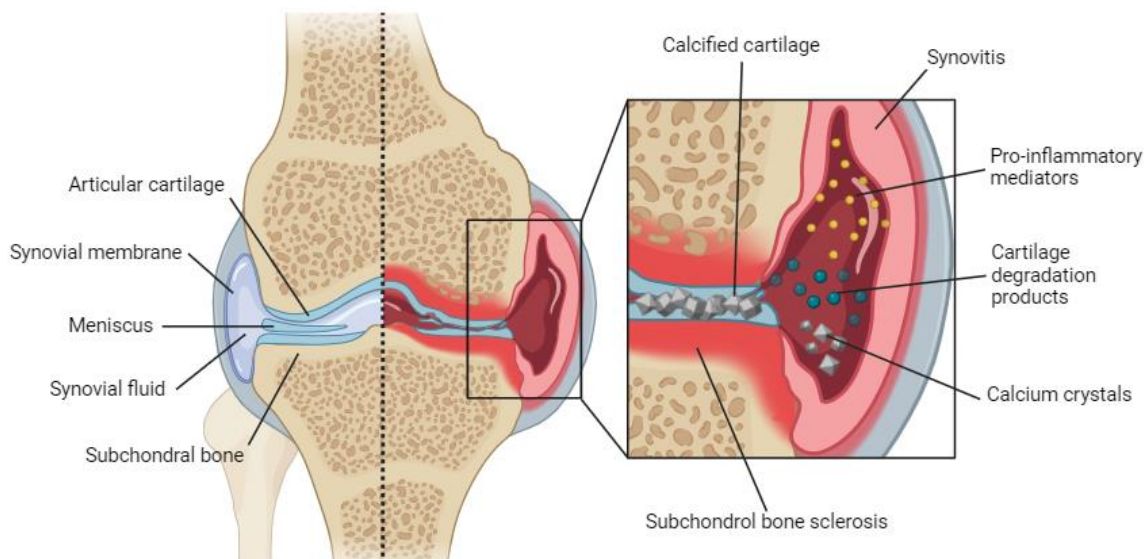


Figure 1.2.1: Structural changes during OA. Healthy knee with labelled anatomical structures (left). OA knee with marked structural changes (right). During OA, articular cartilage and meniscal fibrocartilage degenerate and calcify. Degradation products and calcium crystals are released into the synovial fluid, triggering synovial inflammation and the secretion of pro-inflammatory mediators. The subchondral bone becomes sclerotic, impairing mechanical stability (created with BioRender.com).

1.2.1 Synovial membrane

Traditionally, OA was considered a disease of hyaline cartilage and subchondral bone caused by mechanical overload. Today, OA is treated as a complex multifactorial pathology, involving virtually all intra-articular tissues, including a crucial synovial involvement. The synovial membrane is the connective

tissue lining the joint. It contains the synovial fluid inside the joint cavity and forms a physical barrier to surrounding fat and connective tissue. Structurally, it is composed of a thin inner layer of cells that covers an outer layer of loosely arranged fibro-collagenous tissue. Tissue-resident cells include fibroblasts, adipocytes and macrophages [13, 14].

During OA, the synovial membrane displays various changes, including hyperplasia, increased vascularization, inflammation and fibrosis [15] (Figure 1.2.1). The synovium is infiltrated by immune cells that produce high levels of inflammatory cytokines [16]. Synovial inflammation is closely linked to cartilage degeneration. Through the synovial fluid, inflammatory catabolic mediators of the synovium can diffuse into the cartilage [17]. Here, they can stimulate chondrocytes to produce matrix-degrading metalloproteinases (MMPs) and additional inflammatory cytokines [18, 19]. Vice versa, cartilage degradation products are released in the synovial fluid where they can trigger secondary inflammatory reactions in a cycle of synovial inflammation and cartilage degeneration [20].

1.2.2 Synovial fluid

The synovial fluid fills the joint cavity and has various functions, ranging from lubrication and mechanical support to intra-articular communication and nutrient exchange. As an ultrafiltrate of plasma, synovial fluid is filtered through the fenestrated capillaries in the synovial membrane. Synovial fibroblasts and chondrocytes secrete hyaluronic acid, lubricin and other lubricants that give the synovial fluid its viscous consistency for lubrication of the articulating surfaces. In addition, synovial fluid contains cytokines, growth factors and other soluble mediators, that provide a medium for cellular crosstalk between cartilage and synovium [17].

The composition of synovial fluid is dictated by the permeability of the synovial membrane. Healthy synovium has a low permeability, retaining lubricants and other large molecules within the synovial fluid. Inflamed synovium is more permeable, impairing its filtration function [21, 22]. Lubricants can diffuse out of the synovial fluid into the synovial membrane [23]. Here, they cause synovial edema due to their hydrophilic properties [24]. Decreased lubrication also increases friction on the cartilage surface, promoting its degradation [25]. With erosion of the cartilage surface, ECM degradation fragments are released into the synovial fluid [26] where they can drive synovial inflammation (Figure 1.2.1). These fragments also have proteolytic effects themselves, further aggravating cartilage damage [27, 28].

1.2.3 Cartilage

Hyaline articular cartilage is the most abundant type of cartilage in the human body and is essential for normal joint function. Lining the bone ends, articular cartilage provides a smooth surface for movement (Figure 1.2.1). It contains a dense ECM that is mainly composed of collagen fibers (primarily type II). These fibers are crosslinked to form a fibrillary network [29]. Non-collagenous ECM proteins include proteoglycans like aggrecan. Proteoglycans are highly hydrophilic due to their negatively charged glycosaminoglycan side chains. These side chains bind water, hydrating the spaces within the collagenous framework [30]. Water is the main component of cartilage and makes up 70-85% of its weight [31]. It provides lubrication, durability to compressive forces and nutrient transport to chondrocytes [12]. The chondrocyte is the only tissue-resident cell type and is responsible for consistent

ECM production and maintenance. As healthy articular cartilage is devoid of vasculature, chondrocytes function under low oxygen tension, mainly limiting their metabolism to anaerobic glycolysis [32]. This lack of vasculature, nerves and lymphatics also limits the regenerative capacity of articular cartilage.

The full thickness of articular cartilage ranges from 2-4mm and can be divided into four distinct zones (Figure 1.2.2). The superficial zone covers 10-20% of the total thickness and protects the underlying zones from shear stresses [33]. Fibers are oriented parallel to the cartilage surface, providing tensile strength to the tissue. Chondrocytes are relatively abundant in this zone and show a flattened ellipsoidal shape that follows the fiber orientation [34]. The intermediate zone makes up the majority of the total cartilage thickness (40-60%). Here, collagen fibers cross over each other to transition from horizontal to vertical orientation [35]. Chondrocytes are sparse and display a round and spherical shape [34]. The deep zone spans approximately 30% of the cartilage thickness. This zone contains collagen fibers perpendicular to the surface, anchoring the cartilage to the underlying subchondral bone. Along these fibers, chondrocytes are stacked in vertical columns. From superficial to deep zone, the proteoglycan content increases while the water content decreases. The tidemark marks the separation between the deep zone and the calcified cartilage that merges into the underlying subchondral bone at the cement line [36].

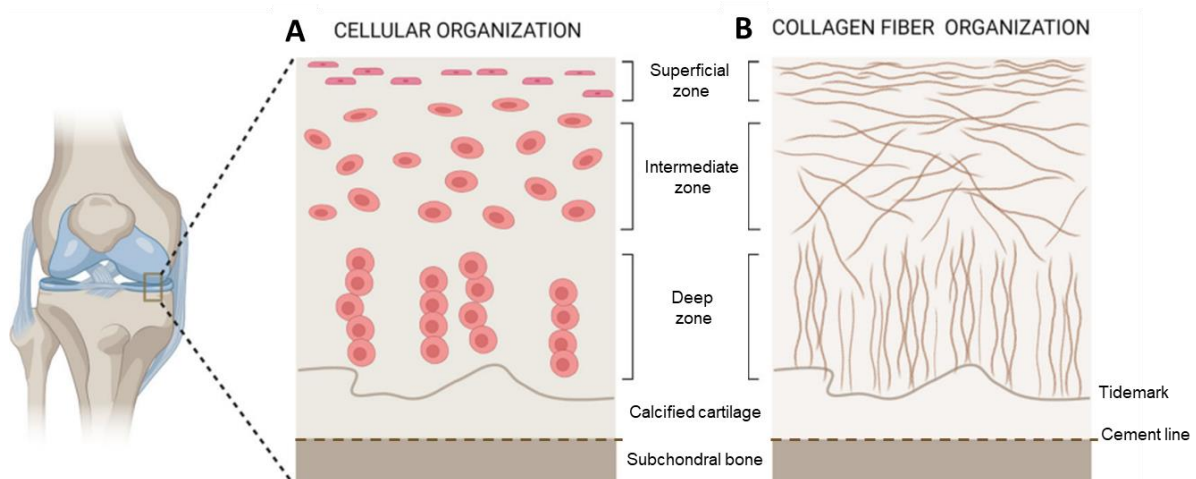


Figure 1.2.2: Zonal structure of articular cartilage. **A.** Cellular organization and **B.** Collagen fiber organization in articular cartilage (adapted from [37]).

During OA, the homeostasis of ECM production and degradation is disrupted. This leads to dramatic changes in ECM composition. While healthy chondrocytes normally reside in a stable quiescent phenotype, OA chondrocytes increase their proliferative activity in early stages of the disease. Nevertheless, the proteoglycan content of the ECM decreases, indicating inefficient compensation that may leave the cartilage in permanent degeneration [38]. Loss of proteoglycans is among the first changes in early OA. This increases tissue permeability and impairs mechanical stability, eventually causing cartilage degradation and thinning [39].

A hallmark of OA progression is the phenotypic shift of chondrocytes towards terminal hypertrophic differentiation. This state is similar to the terminal differentiation of growth plate chondrocytes during

bone formation and involves an increase in cell volume, alterations in ECM metabolism and bone mineral deposition [40]. Chondrocytes reduce the expression of cartilage-specific genes such as SOX9 and aggrecan. Simultaneously, the production and activity of MMPs and other matrix-degrading enzymes is upregulated. Elevated production of collagen type X and a concomitant inhibition of collagen type II synthesis weakens the collagen network and structural ECM integrity [40, 41]. In later stages of the disease, hypertrophic chondrocytes undergo apoptosis [41, 42] and the cartilage becomes hypocellular, impairing appropriate remodelling and regeneration [43].

1.2.4 Meniscus

The menisci are semi-circular structures of fibrocartilage that are positioned between the articulating surfaces of femur and tibia. They mainly function as shock absorbers and evenly distribute load between lateral and medial joint compartments [11]. In addition, they increase stability and lubrication of the articulating surfaces. The ECM is mainly composed of water and collagen. Meniscal fibrocartilage predominantly contains collagen type I, distinguishing it from articular cartilage that is rich in collagen type II [44]. Other ECM components include non-collagenous proteins such as fibronectin and proteoglycans that provide viscoelasticity to the tissue. During early stages of OA, meniscal fibrocartilage degenerates and stiffens, altering its biomechanical properties [45]. These degenerative changes increase the risk for meniscal tears, accelerating articular cartilage damage and OA progression. Vice versa, meniscal tears in a healthy knee may increase the risk of developing OA [46], indicating a complex relationship between these processes.

1.2.5 Bone

The cement line connects the calcified cartilage zone to the subchondral bone and represents an important site for nutrient supply. In OA, the cement line roughens and the tidemark duplicates. These changes are accompanied by defective remodelling of the subchondral bone that worsens with OA severity. [47]. Subchondral bone density and volume increases, while mineralization is reduced [48]. In addition, the periosteum forms bony outgrowths, referred to as osteophytes [49, 50]. Eventually, the subchondral bone becomes sclerotic, impairing mechanical integrity [51] (Figure 1.2.1). Blood vessels and nerve fibers breach the tidemark and innervate the non-calcified cartilage, contributing to OA pain [49, 52].

1.3 Articular calcification

Structural changes in OA joints are often accompanied by ectopic calcification. This pathological process is defined by the deposition of calcium-containing crystals in tissues that are not designated to calcify [53]. Unlike physiological calcification, pathological calcification does not serve a clear function and is associated with metabolic abnormalities [54]. In principle, all articular tissues can calcify, including synovium [55], tendons [56] and synovial fluid [57], but calcifications are primarily found in cartilage and menisci (Figure 1.2.1). These are directly associated with OA progression, driving cartilage degeneration [58] and synovial inflammation [59]. Intra-articular calcium crystals can be divided into two types with distinct morphology, size and cellular effects.

1.3.1 Basic calcium phosphate crystals

Basic calcium phosphate (BCP) crystals describe a group of amorphous crystals that can occur in different phases. Hydroxyapatite (HA) ($\text{Ca}_{10}(\text{PO}_4)_6(\text{OH})_2$) is the most common form of BCP in the human body as an anorganic component of bone and teeth [60]. HA is the most thermodynamically stable form of BCP. In its pure form, it has a Ca/P molar ratio of around 1.67. Other phases include octacalcium phosphate or tricalcium phosphate with varying Ca/P ratios and less thermodynamic stability [61]. Individual BCP crystals have a size of 1 nm [62], but they tend to agglomerate in clusters of micrometre size range [63].

The link between BCP crystals and OA is well established. BCP deposition actively contributes to OA progression, correlating with OA severity and the degree of cartilage degradation [64]. On cellular level, BCP deposition is directly associated with chondrocyte hypertrophy and positively correlates with collagen type X expression [65]. Induction of hypertrophy in healthy human chondrocytes promotes the formation of BCP. Vice versa, stimulation of chondrocytes with BCP induces hypertrophy and elevates the expression of hypertrophy markers such as collagen X and MMP-13 [66-68]. Chondrocyte hypertrophy is driven by the activation of canonical Wnt signalling. BCP crystals can promote this process by binding the canonical Wnt ligands via electrostatic interaction between protein and crystal surface. By accumulating around hypertrophic chondrocytes in OA cartilage, BCP crystals increase local Wnt ligand availability and promote canonical Wnt activation [64]. This pathway amplifies cartilage damage [69].

BCP crystals can also trigger inflammatory responses via direct contact with cell membranes [70] or interaction with membrane receptors of surface-bound proteins [64, 71]. For instance, BCP crystals can trigger the production of pro-inflammatory mediators such as IL-6. In turn, IL-6 amplifies chondrocyte calcification in a positive feedback loop [72]. Eventually, BCP crystals also induce cell death by apoptosis via MAPK-dependent nitric oxide production [73, 74].

1.3.2 Calcium pyrophosphate dihydrate crystals

First detected in arthritic joints in 1962 [75], calcium pyrophosphate dihydrate (CPP) crystals are larger, rhomboid or rod-shaped crystals of 1-20 μm diameter. In polarized light, they appear birefringent. Pure

CPP ($\text{Ca}_2\text{P}_2\text{O}_7 \cdot 2\text{H}_2\text{O}$) has a Ca/P molar ratio of approximately one. Within the joint, crystalline CPP can be present in a monoclinic or triclinic phase. Monoclinic CPP is more common and has a higher inflammatory potential [76], inducing inflammatory cytokine production in various articular cell types [77]. While BCP crystals are closely linked to chondrocyte hypertrophy, CPP crystals have been associated with a different phenotype, namely chondrocyte senescence [78]. Senescence describes a cellular state of irreversible cell cycle arrest to contain the proliferation of damaged cells [79]. It can be triggered by different stressors, for instance excessive mechanical loading, oxidative stress or DNA damage. Senescent cells characteristically produce various cytokines, growth factors and proteases, collectively described as the senescence-associated secretory phenotype (SASP) [80]. Cellular senescence has been commonly reported in OA synovium [81] and cartilage [82], particularly in damaged areas, correlating with cartilage degradation and OA severity [83]. Senescent chondrocytes produce matrix-degrading enzymes that aggravate cartilage damage [84] and have recently been implicated in cartilage calcification [42], specifically CPP deposition [78].

Unlike BCP, CPP is not normally present in the body. Therefore, CPP deposition is always considered pathological e.g. in the case of CPP deposition disease (CPPD). CPPD is an umbrella term that describes a collection of arthritis forms with CPP crystal involvement. Clinical phenotypes of CPPD are diverse, ranging from asymptomatic to gout-like inflammatory flares and often resemble OA. Although CPPD is regarded as a stand-alone arthropathy, it is often accompanied by OA-like degenerative changes to the joint, constituting a differential diagnosis to OA [85]. However, growing evidence suggests a more poly-articular and systemic nature of CPPD [86, 87]. In this regard, familial forms of CPPD are caused by rare genetic mutations [88]. Sporadic CPPD occurs in close correlation with age, referring back to the recently established association of CPP with cellular senescence. Considering the biochemical differences between BCP and CPP crystals and their clinical heterogeneity, accurate detection of intra-articular calcification is an important step in differential diagnostics.

1.4 Detection of articular calcification

While bone displays a homogeneous matrix and mineral composition, pathological calcification often varies in composition, structure and size [54]. Therefore, detection of intra-articular calcification and identification of involve crystal types prove rather difficult. Thus, the data regarding prevalence and distribution is inconsistent [89]. *In vivo* imaging of calcification is limited to non-invasive techniques such as ultrasonography, magnetic resonance imaging and conventional radiography, the latter being the most common. *Ex vivo* imaging techniques include histological staining combined with conventional light microscopy, or spectroscopic methods such as Raman spectroscopy.

1.4.1 Radiography

Radiography is the most commonly used method for *in vivo* detection articular calcifications in clinical practice. Due to its easy accessibility and cost effectiveness, radiography remains the standard imaging method for the diagnosis of calcium-crystal arthropathies [90]. Soft tissue calcification can be identified on radiographs due to their increased density compared to the surrounding tissue. Calcification occurs as linear or focal opacities in the joint space (Figure 1.4.1A), a phenomenon that is termed chondrocalcinosis (CC). CC is usually considered as CPP deposition. In fact, radiographic evidence of calcification is commonly used in the diagnosis of CPPD [91]. Struggling with nomenclature, the terms CC and CPPD are often used synonymously, even though CC is not specific to CPPD [92] and its absence does not exclude CPPD. The inconsistent use of these terms often cause confusion. To avoid assumption of involved crystal type, the term CC is substituted by the definitional term “radiological calcification” in this thesis. According to EULAR recommendations, a definite CPPD diagnosis relies on crystal identification and radiography is not able to distinguish between BCP and CPP deposition [85]. In addition, CC or rather radiological signs of calcification can also be observed in OA joint without CPPD diagnosis [93, 94]. To avoid premature assumptions of involved crystal types, the term radiological calcification will be used here instead.

As radiography only has a limited resolution, it only detects larger calcification, while smaller calcifications of less density often go undetected [95]. In later OA stages, advanced cartilage damage and joint space narrowing further exacerbates the detection of calcification [57]. Thereby, radiography likely underestimates the prevalence of articular calcification [96].

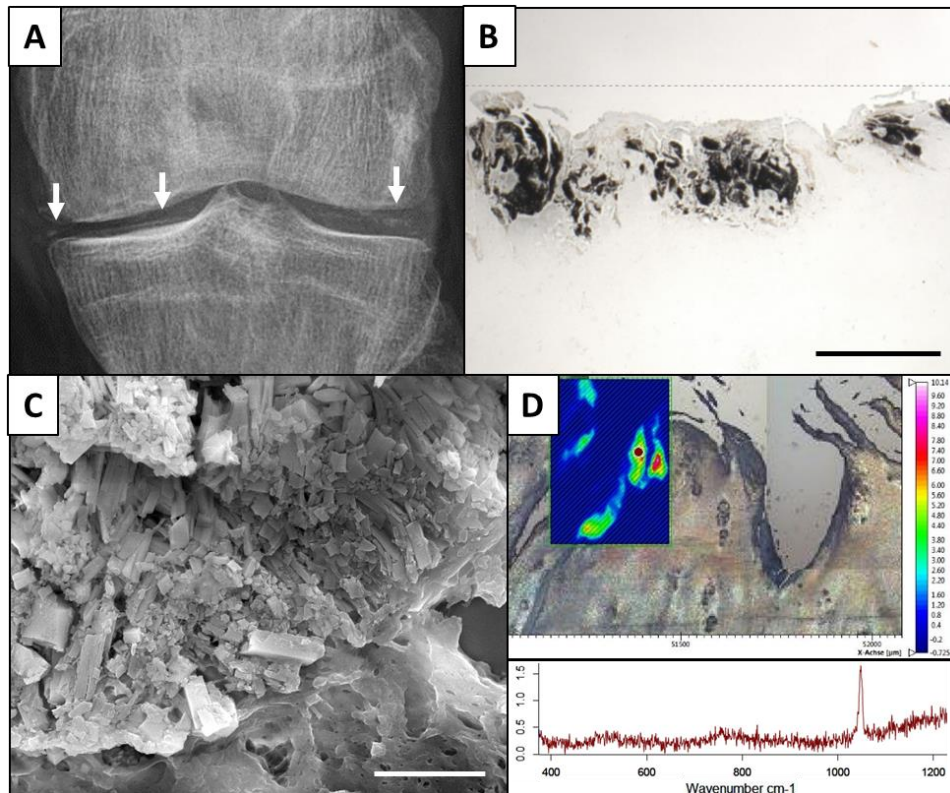


Figure 1.4.1: Different imaging methods for the detection of articular calcification. **A.** Representative knee radiograph with calcification presenting as visible white opacities in the joint space (white arrows). **B.** Representative von Kossa staining of articular cartilage with calcified deposits stained in black (scale bar 500µm). **C.** Representative SEM image of cartilage crystals embedded in cartilage (scale bar 5µm). **D.** Representative Raman spectrum (bottom) collected on a calcified part of a cartilage section (top).

1.4.2 Histological staining and light microscopy

Ex vivo, there are more detailed methods for visualizing calcification in articular tissues. Many of these methods involve the use of microscopy. Due to their birefringent properties, CPP crystals can be detected by polarized light. This property is utilized in synovial fluid analysis to detect the presence of CPP crystals. Synovial fluid analysis requires training and experience though and the results are largely observer-dependent [97]. It has also become clear that many CPP crystals do not appear birefringent [98, 99], rendering this analysis unreliable.

Microscopic detection of calcification in articular tissues is often facilitated by histological staining methods such as von Kossa staining. Von Kossa is a commonly used *in vitro* stain to detect calcified deposits in tissues and cells [100]. It is based on a chemical reaction between a silver nitrate staining solution and calcium in the calcified sample. As silver ions replace calcium ions, calcifications initially take on a brown colour that turns to black under light exposure (Figure 1.4.1B). Both BCP and CPP crystals contain calcium, so von Kossa is not able to differentiate between the two. In addition, the resolution of light microscopy is limited, exacerbating the detection of smaller aggregates, particularly for BCP crystals of submicroscopic size. The resolution limit of light microscopy also prohibits the evaluation of crystal morphology. Instead, morphological analysis of individual crystals requires more

high-resolution methods such as scanning electron microscopy. Therefore, determining the exact prevalence of articular calcification by radiography or light microscopy remains difficult and many calcification studies do not determine the type of detected calcium crystals [101].

1.4.3 Scanning electron microscopy

Scanning electron microscopy (SEM) has a manifold higher resolution than conventional light microscopy. By scanning the surface of a sample with a beam of electrons, SEM can create images in nanometer range [102], making it an ideal method for morphological analysis of individual calcium crystals (Figure 1.4.1C). SEM imaging is often combined with energy-dispersive X-ray spectroscopy (SEM-EDS) for chemical analysis. EDS scans the sample with X-rays and detects emitted X-rays. Based on these emission spectra, EDS can identify and measure chemical elements in a sample. Calculation of the calcium to phosphate (Ca/P) ratio enables precise identification of BCP and CPP crystals based on characteristic Ca/P ratios of 1.5 and 1, respectively [103]. Providing morphological and chemical data, SEM-EDS is a convenient tool for crystal analysis and differentiation and has been used in the context of cartilage calcification before [104, 105]. However, samples need to be sputter-coated by a conductive metal for high quality images. In addition, SEM imaging requires a low-pressure atmosphere and EDS detectors need liquid nitrogen cooling [102]. This rather elaborate sample preparation and costly operating principle limits the availability of SEM-EDS.

1.4.4 Raman spectroscopy

Raman spectroscopy is a type of vibrational spectroscopy for chemical characterisation of biomolecules. It utilizes the inelastic scattering of light and the so-called Raman effect. This effect occurs when photons of a monochromatic laser interact with the vibrational modes of chemical bonds within a sample. This interaction leads to an excitation of the laser photons. The emitted photons have a different energetic state compared to the photons that initially hit the sample. Raman spectroscopy measures this shift in energy as Raman spectra. Raman spectra represent distinct vibrational modes of molecules in the sample, providing qualitative information about its biochemical composition and structure [106]. Due to its non-invasive nature and simple sample preparation, Raman spectroscopy is a popular and versatile analysis tool in biomedical and material sciences [107]. In recent years, Raman spectroscopy is also increasingly used in *ex vivo* analysis of calcified tissues, allowing precise distinction of BCP and CPP crystals based on characteristic peaks in the Raman spectrum [108] (Figure 1.4.1D). Spectroscopic crystal type determination poses a unique advantage over radiographic and histological analysis, rendering it a powerful tool for identification of calcifications within articular tissues [109]. Since mechanistic understanding of intra-articular calcification is still lacking, accurate detection and differentiation of involved crystals may provide valuable insights into the calcification mechanism.

1.5 Calcification mechanism

Physiological calcification as in the context of bone remodelling or fracture healing [110], proceeds in an orderly, highly controlled fashion. In contrast, pathological calcification occurs rather spontaneous and disordered and mechanistic understanding of this process is still lacking [54]. Generally, calcification is a complex process that can be divided into two steps: crystal nucleation and growth. The former requires a local supersaturation of ions, particularly phosphate. In the body, 85% of extracellular phosphate exists in the form of free inorganic phosphate (Pi) while the rest is bound to proteins or cations e.g. calcium or magnesium [111]. During crystal nucleation, phosphate binds to calcium and precipitates as crystal precursor complexes in the ECM. These precursors exist in amorphous phases and can be converted to mature crystalline forms under certain conditions [53]. These “pro-calcifying” conditions include the exposure to calcification promoters and a deficiency of calcification inhibitors, meaning an imbalance of calcification promoters and inhibitors [54]. Various factors have been proposed as calcification promoters, including cells, proteins and macromolecules. For instance, hypertrophic chondrocytes produce matrix vesicles that are able to concentrate phosphate and calcium ions. These matrix vesicles have been reported in calcified tissues such as bone [112] and cartilage [113]. Synovial fibroblasts also seem to have the ability to form calcium crystals in a yet to be identified mechanism [114]. In addition to cellular calcification promoters, ECM components can function as calcification promoters. Particularly collagen fibrils are critical for calcification as they provide a template for crystal nucleation and growth. Assembled collagen fibrils contain gap zones with charged amino acids. These amino acids bind amorphous crystal precursors and attract calcium and phosphate ions [115]. Once converted into stable crystalline forms, deposits grow along the collagen fibers. Proteoglycans and other non-collagenous proteins (NGPs) regulate this process by binding to collagen fibers [116, 117] and concentrating additional crystal precursors. This process eventually results in uncontrolled extrafibrillar crystal growth [118].

In environments supersaturated with calcium and phosphate ions (e.g. blood or synovial fluid), the body produces endogenous calcification inhibitors. These inhibitors bind pre-nucleated calcium phosphate complexes to prevent crystal growth [119]. One of these endogenous calcification inhibitors is inorganic pyrophosphate (PPi), a potent inhibitor of BCP formation. PPi binds to amorphous calcium phosphate and prevents the crystallization to mature BCP [120]. PPi also prevents BCP crystal growth by occupying growth sites [121]. In addition, PPi inhibits the release of Pi. Thereby, PPi deficiency disrupts bone mineralization [122]. Chondrocytes usually produce large quantities of PPi to prevent BCP formation in the non-calcified cartilage matrix [123]. However, the effects of PPi on calcification are bimodal as excessive PPi levels cause the deposition of CPP crystals [124, 125]. Therefore, the nature of the phosphate substrate is a key determinant in the pathological calcification process. In particular, the balance of PPi and Pi proposedly guides the crystal formation [125, 126].

1.5.1 Pyrophosphate metabolism

As byproducts of many biosynthetic reactions, PPI and Pi are ubiquitous ions in the human body. The synthesis of biological macromolecules requires the hydrolysis of adenosine triphosphate (ATP). A molecule of ATP can be hydrolysed to adenosine diphosphate (ADP) and Pi or adenosine monophosphate (AMP) and PPI. The former reaction takes place more often but the latter produces more energy [127]. In calcifying cells such as osteoblasts and chondrocytes, the ratio of free PPI to Pi is regulated by the PPI metabolism. This metabolism comprises a group of membrane enzymes that participate in extracellular transport and degradation of ATP and its metabolites (Figure 1.5.1).

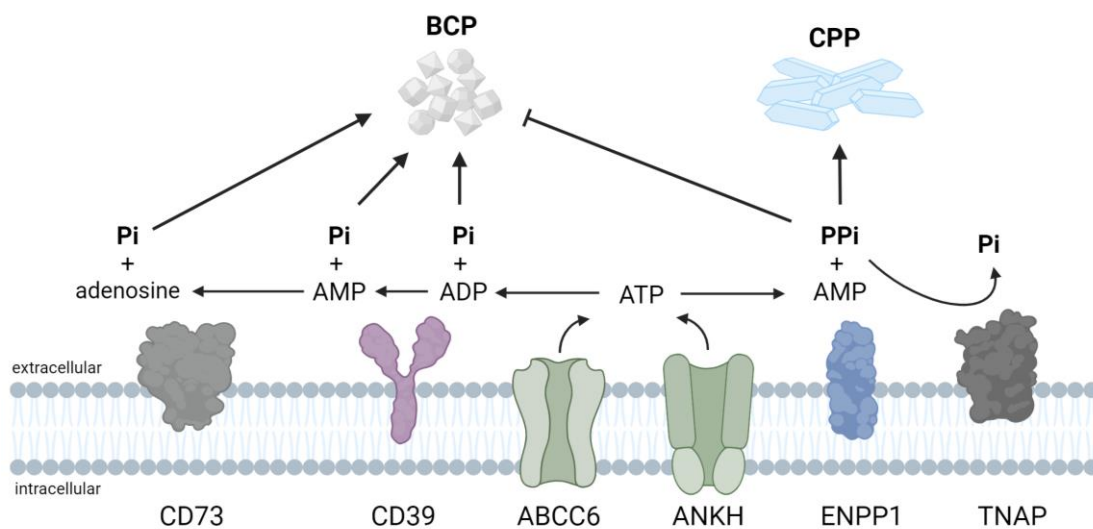


Figure 1.5.1: Calcium crystal formation is determined by extracellular phosphate (Pi) and pyrophosphate (PPI) ions. High Pi levels promote BCP deposition, while PPI has an inhibitory effect. Instead, excess PPI leads to CPP formation. The extracellular Pi/PPI ratio is regulated by the extracellular PPI metabolism. Adenosine triphosphate (ATP) is exported from the cell via the transmembrane transporters progressive ankyloses homolog (ANKH) and ATP-binding cassette subfamily C member 6 (ABCC6). Outside the cell, ATP is progressively hydrolysed to adenosine monophosphate (AMP) by CD39, releasing two Pi ions. AMP can be further degraded to adenosine and Pi by CD73. On the other hand, ectonucleotide pyrophosphatase/phosphodiesterase 1 (ENPP1) directly degrades ATP into AMP via elaboration PPI that can further be transformed into Pi by tissue-nonspecific alkaline phosphatase (TNAP) (created with BioRender.com and adapted from [128]).

The transmembrane protein progressive ankylosis homolog (ANKH) transports intracellular ATP to the extracellular space [129]. The hepatic ATP-binding cassette subfamily C number 6 (ABCC6) protein has a similar function, mediating cellular ATP efflux. Extracellularly, ATP is converted into AMP by CD39, elaborating two Pi molecules, the phosphate component of BCP crystals [130]. On the other hand, ATP can also be degraded into AMP and PPI. This reaction is catalyzed by ectonucleotide pyrophosphatase/phosphodiesterase 1 (ENPP1) and increases local extracellular PPI levels [131], the anionic component of CPP. The by-product AMP is further degraded into Pi and adenosine by CD73. Downstream of ENPP1, tissue-nonspecific alkaline phosphatase (TNAP) converts PPI into Pi. Both

reactions elevate local Pi levels in favour of BCP formation. As part of a self-regulatory feedback loop, adenosine inhibits TNAP activity, limiting TNAP-mediated Pi release [132].

Disturbances in this metabolism can shift the sensitive balance of PPI and Pi in favor of one or the other crystal type. In this context, pathological calcification could be viewed as a local metabolic disease. For instance, inactivating mutations in ENPP1 and ABCC6 reduce extracellular PPI. These mutations can cause calcification disorders as Pseudoxanthoma elasticum (PXE) and generalized arterial calcification of infancy (GACI) [133, 134]. Deficiency of CD73 causes arterial and joint calcification via upregulation of TNAP activity and subsequent reduction of PPI levels [135, 136]. Loss-of-function mutations in TNAP deplete Pi levels, causing hypophosphatasia that manifests in a hypomineralization of bone and teeth [137]. As neither BCP nor CPP calcification is curable, understanding the calcification process may help to identify potential intervention targets and advance the development of treatment options.

1.6 Aims

With rising incidence of degenerative arthropathies such as OA, articular calcification is a frequent problem in the aging population. It is caused by the deposition BCP or CPP crystals that have heterogeneous biochemical properties and clinical phenotypes. As accurate detection and differentiation of involved crystal types remains difficult, there is conflicting data on prevalence and distribution of articular BCP and CPP deposition. Therefore, the first part of this thesis sought to detect and differentiate the type of calcification in articular cartilage of OA patients by combining histological staining with Raman spectroscopy.

Mechanistically, pathological calcification is considered an active and complex multifactorial process that lacks understanding. Specifically, the mechanism(s) that determine what crystal type is formed, remain elusive. As distinct phosphate sources, extracellular Pi, PPI and its metabolism are proposed as important factors in crystal formation. Therefore, the second part of this thesis aimed to identify changes in the PPI metabolism in articular cartilage with regards to the crystal type detected in the tissue.

The specific questions this thesis intended to answer were:

- Does histology-directed Raman spectroscopy improve the detection of cartilage calcification in comparison to conventional radiography?
- What is the prevalence and distribution of BCP and CPP deposition in OA cartilage detected by this method?
- Is there a difference in the PPI metabolism in cartilage depending on the presence and type of calcification detected in the tissue?

2 Materials and Methods

2.1 Materials

2.1.1 Equipment

All equipment that was used in the experiments for this thesis is listed in Table 1.

Table 1: List of instruments and equipment.

Equipment	Manufacturer
Biological Safety Cabinets S2020 1.5 Biological Safety Cabinets KS 18	Thermo Scientific
Bio-Plex 200	Bio-Rad Laboratories
Binder CO2 incubator	Binder Labortechnik GmbH
Senterra II Confocal Raman Microscope	Bruker
Centrifuge Heraeus, Fresco 17 Centrifuge Heraeus Megafuge 16R	Thermo Scientific
ChemieDoc MP Imaging Systems	Bio-Rad Laboratories
Embedding Center Shandon HistoCentre 2	GMI
Inverse microscope Axio Observer Z1	Zeiss
Inverse microscope BX51	Olympus
Inverse microscope Eclipse TS100	Nikon
Microplate reader Infinite F200 Pro	Tecan
Microplate reader Infinite M Plex	Tecan
Microtome Hyrax M55	Zeiss
QuantStudio 6 Flex	Applied Biosystems
Perfect Spin Plate Spinner C1000-PEQ-230EU	Applied Biosystems
Platform rocker SSL24	Stuart
Roll mixer RS-TR05	Phoenix Instrument
Rotator Fa-45-30-11	Phoenix Instrument
Scale ALC-810.2 Scale A 120 S	Eppendorf
Scanning electron microscope	FEI/Philips
Shaking Incubator Thermo Mixer C	IKA

Tissue processor TP1020	Eppendorf
Tube Revolver Rotator	Leica Biosystems
T100 Thermal cycler	Bio-Rad Laboratories
Vortex Genie 2 Mixer	Bohemia
Water bath Thermolab 1070	GFL

2.1.2 Reagents

Chemical reagents that were used in the experiments are listed below (Table 2).

Table 2: List of reagents and manufacturer.

Reagents	Manufacturer
Acetic acid	Carl Roth
Adenosin-5'-triphosphate magnesium salt (A9187)	Sigma
Canada balsam	Carl Roth
DMEM (11965092)	Gibco™
Ethanol denatured 70%, 80%, 96%, 99,8%	Carl Roth
Fast Green FCF	Sigma Aldrich
Fetal bovine serum (FBS)	PAN-Biotech
Formaldehyde 4%	Otto Fischar
HEPES	Carl Roth
MgCl ₂	Carl Roth
Nuclease-free water	Carl Roth
QIAzol lysis reagent	QIAGEN
Penicillin/Streptomycin (10,000 U/mL)	Biochrom AG
Protease Inhibitor Cocktail (cOmplete ULTRA Tablets)	Roche
Pyrogalllic acid	Carl Roth
Safranin Orange	AppliChem
Silver nitrate	Carl Roth
Sodium pyruvate	Sigma Aldrich
Sodium thiosulfate	Carl Roth
Thymidine monophosphate nitrophenyl ester (PNTM)	Sigma Aldrich
Tris	Carl Roth

Triton-X100	Sigma Aldrich
Trypsin/EDTA	Biochrom AG
Xylene (isomers)	Carl Roth

2.1.3 Consumables

Consumables that were used for the experiments are listed in Table 3.

Table 3: List of consumables and manufacturer.

Consumables	Manufacturer
Cell culture flask	Greiner
Cell scraper	Sarstedt
Cell strainer (100, 70, 40 μ M)	Greiner
Cover glasses (24x50mm)	Thermo Scientific
Cover slips 12mm	Paul Marienfeld
Filter pipette tips (10, 200, 1000 μ L)	Sarstedt
Microtome blades A35	pfm medical
Petri dishes	Sarstedt
Pipette tips (10, 200, 1000, 5000 μ L)	Sarstedt
Safe-lock tubes (0.2, 0.5, 1.5, 2ml)	Eppendorf
Sterile filters (0.22 μ M)	TPP
Stripettes (5, 10, 25, 50ml)	Greiner
Superfrost Plus Microscope Adhesion Slides	Epredia
Syringes (20ml)	BD
Tubes (15ml, 50ml)	Greiner
Well plates (12-well, 24-well)	Greiner

2.1.4 Kits and Enzymes

All kits and enzymes that were used in this thesis are listed in Table 4.

Table 4: List of kits and enzymes.

Name	Manufacturer
High-Capacity cDNA Reverse Transcription Kit (4368814)	Thermo Scientific
RNeasy® Plus Micro Kit	QUIAGEN
Alkaline Phosphatase Assay Kit (ab83369)	Abcam
Pierce BCA Protein Assay (23227)	Thermo Scientific
Human XL Cytokine Luminex® Performance Assay (LKTM014)	R&D Systems
SYBR®Green Mastermix (4309155)	Thermo Scientific
Pronase (<i>Streptomyces griseus</i>)	Roche
Phosphate Assay Kit (ab65622)	Abcam
Pyrophosphate Assay Kit (ab112155)	Abcam
Collagenase IV (<i>Clostridium histolyticum</i>)	Worthington

2.1.5 Primers

All primers used for qRT-PCR were purchased from Metabion (Martinsried) at a stock concentration of 100µM. Prior to use, primers were diluted to 10µM in nuclease-free water. Primer sequences are listed below (Table 5).

Table 5: Human primer sequences.

Gene	Product length	Sequence (5'-3')	
GAPDH	90 bp	Forward Reverse	CCC ACT CCT CCA CCT TTG AC AGC CAA ATT CGT TGT CAT ACC AG
TNAP	137 bp	Forward Reverse	GACCTCCTCGGAAGACACTC TGAAGGGCTTCTTGTCTGTG
ENPP1	246 bp	Forward Reverse	GTC GTC AGT GGT CCT GTG TT GTC ATG CTT CCC ATG CAC AC
ANKH	204 bp	Forward Reverse	GGC AGT GGC GAT TTT GAC AG ATC ACG AAA CAG AGC GTG AGT
CD73	111 bp	Forward Reverse	CCA GTC CAC TGG AGA GTT CC CGA CAC TTG GTG CAA AGA AC
CD39	116 bp	Forward Reverse	ACTTATGGAAGATACAAAGGAGTCT TCAACCCACAGCAAGCAA
ABCC6	195 bp	Forward Reverse	AAG GAA CCA CCA TCA GGA GGA G ACC AGC GAC ACA GAG AAG AG G

2.1.6 Buffers and solutions

All buffers and solutions that were prepared during the experiments are listed below (Table 6).

Table 6: List of buffers and solutions with ingredients.

Solution	Ingredients
Chondrocyte medium	DMEM (4.5g/mL glucose, L-glutamine) + 10% FBS + 1% Penicillin/Streptomycin + 1% sodium pyruvate
Collagenase digestion (articular chondrocytes)	1mg/mL collagenase IV in chondrocyte medium
Collagenase digestion (meniscal fibrochondrocytes)	1.8mg/mL collagenase IV in meniscal fibrochondrocyte medium
HEPES lysis buffer	50mM HEPES in dH ₂ O (pH7.5) + 1% Triton-X
HEPES sample buffer	50mM HEPES in dH ₂ O (pH7.5)
Meniscal fibrochondrocyte medium	DMEM (4.5g/mL glucose, L-glutamine) + 10% FBS + 1% Penicillin/Streptomycin
PC-1 buffer	1.6mM MgCl ₂ in dH ₂ O (pH8.1) + 0.2M Tris
Phosphate buffered saline (PBS)	Ready to use (#D8537)
Pronase digestion	1mg/mL pronase in DMEM
Safranin-Orange solution	2% Safranin-Orange in dH ₂ O

2.2 Histological methods

2.2.1 Sample collection and processing

Articular cartilage, meniscus and synovial fluid samples were obtained from OA patients the time of elective knee joint replacement. Prior to surgery, patients provided written informed consent. Patients with post-traumatic osteoarthritis or previous surgery on the ipsilateral knee were excluded. All procedures were approved by the Institutional Review Board (IRB) of the Medical School, Otto-von-Guericke University Magdeburg (IRB No. 28/20). Radiographs were taken by the department of radiology at the Otto-von-Guericke University Magdeburg. Radiological calcification was determined and scored by radiograph evaluation. OA severity was assessed radiographically according to the KL score. Histological assessment of OA severity was done using the OARSI score. Synovial fluid samples were frozen in liquid nitrogen and stored at -80°C. Full thickness cartilage samples of approximately 1x0.5cm were taken from the main loading area of the tibia plateau. Cartilage and meniscus samples were fixed in 4% formaldehyde for a minimum of 24h, dehydrated and embedded in paraffin. For histological staining, samples were cut into consecutive sections of 4µm thickness on a microtome and mounted on microscope adhesion slides.

2.2.2 Safranin-Orange/Fast Green staining

Before staining, paraffin sections were deparaffinised using Xylene. After paraffin removal, sections were rehydrated using a degrading ethanol series and washed in dH₂O. Rehydrated cartilage sections were stained with Fast Green for 1min, followed by a 1% acetic acid wash for 30s and 30min of incubation in 2% Safranin-Orange solution. Subsequently, sections were dehydrated with 96% and 100% ethanol and xylene before mounting with Canada balsam on glass cover slides.

2.2.3 Von Kossa staining

Sections of cartilage and menisci were deparaffinised and rehydrated as described above (2.2.2). Deparaffinised sections were incubated in 5% silver nitrate in dH₂O for 1h under light exposure and washed in dH₂O. Tissue sections were incubated in 1% pyrogalllic acid in dH₂O for 3min and washed, followed by a 3min incubation in 5% sodium thiosulfate in dH₂O. Subsequently, sections were dehydrated using an increasing series of ethanol (96% and 100%) and xylene and mounted with Canada balsam [138].

2.2.4 Imaging and image analysis

Stained sections were imaged on a Zeiss Axio Observer Z1 using a 2.5x objective (Axio Observer, Axiocam 702 mono, HXP 120V, Zeiss) with a light source intensity of 4.2V and an exposure time of 7ms. Images were analysed using ImageJ software (Version 1.53). Von Kossa staining was quantified by applying a threshold and measuring the stained area percentage.

2.2.5 Raman spectroscopy

BCP and CPP crystals were identified using a confocal Raman microscope (Bruker Senterra II, Software OPUS 7.8, Bruker). For tissue analysis, sections were deparaffinized with xylene and air dried to remove any paraffin residue. Corresponding von Kossa images served as templates to guide region of interest (ROI) selection. Raman spectra were mapped on a grid of individual measurement points with a distance of 10 μ m in x and y direction. A 785nm laser with a power of 50mW and a 10x/0.25 objective with a focal spot of 1.915 μ m were used to scan ROIs. Measurements were obtained in a spectral range of 50-1410 cm^{-1} to cover signature peaks for both crystals (BCP: 960 cm^{-1} , CPP: 1050 cm^{-1}). The resolution was set to 1.5 cm^{-1} . Each point was measured once with an integration time of 500ms. *In vitro* calcification of chondrocytes on coverslips was mapped on a grid with 5 μ m distance between individual measurement points using 20x/0.40 and 50x/0.65 objectives with an integration time of 1000ms. After mapping, Raman spectra were normalized. Outliers were manually removed and replaced by an average of surrounding spectra. Integration of normalized spectra at 960 cm^{-1} and 1050 cm^{-1} yielded heat maps visualizing BCP and CPP deposition, respectively.

2.2.6 Scanning electron microscopy and energy-dispersive X-ray spectroscopy

SEM imaging was performed on a FEI XL30 ESEM-FEG (FEI/Philips) with a secondary electron (SE) detector at 10kV under $\sim 5 \times 10^{-5}$ mbar environmental pressure. Cartilage sections were deparaffinized and air dried as described in 2.2.5. Before imaging, samples were sputter-coated with gold at 25mA for 4min. Images were taken in SE mode. EDS (EDAX-AMETEK) was used to determine the elemental composition of calcified deposits. The accelerating voltage was set to 10kV. ROIs for imaging and EDS measurements were selected based on corresponding von Kossa images.

2.3 Molecular biological methods

2.3.1 RNA isolation and cDNA synthesis

Fresh cartilage tissue was snap frozen in liquid nitrogen. Frozen samples were manually homogenized in liquid nitrogen by mortar and pestle. Pulverized tissue was lysed in QIAzol lysis reagent (QIAGEN) on rotation at 4°C overnight. RNA was isolated by phenol/chloroform extraction and RNeasy® Plus Micro Kit (QIAGEN). After extraction, RNA was dissolved in nuclease-free water. Concentration and quality of extracted RNA were measured on a microplate reader (Tecan Infinite F200 Pro). For cDNA synthesis, the Applied Biosystems™ High-Capacity cDNA Reverse Transcription Kit (Thermo Scientific) was used. Therefore, 1µg RNA was diluted in 10µL nuclease-free water and mixed with the same volume of master mix containing reverse transcriptase, primers and nucleotides as listed below (Table 7). The reaction was performed in a thermal cycler using a four step protocol (25°C 10min, 37°C 120min, 85°C 5min, 4°C hold). Transcribed cDNA was diluted in 80µL nuclease-free water and kept at 4°C.

Table 7: Reverse transcription master mix.

Reagents	Volume
10x RT Buffer	2.0µL
25x dNTP-Mix (100mM)	2.0µL
10xRT Random Primer	0.8µL
MultiScribe Reverse Transcriptase (50U/µL)	1.0µL
RNAse Inhibitor	1.0µL
Nuclease-free water	3.2µL

2.3.2 Quantitative RT-PCR

Quantitative RT-PCR was performed on a QuantStudio 6 Flex PCR system according to the protocol below (Table 8).

Table 8: Step-wise qRT-PCR protocol.

Step	Temperature	Time
Initial denaturation	95°C	15min
denaturation	95°C	30s
40 cycles of annealing	60°C	30s
elongation	72°C	30s
Dissociation	95°C 60°C 95°C	15s each

In a 384-well plate, 2.5 μ L of cDNA was mixed with 7.5 μ L of master mix containing SYBR®Green Mastermix (Thermo Scientific) and primers for the gene of interest (Table 9).

Table 9: Master mix for quantitative RT-PCR.

Reagents	Volume
SYBR®Green Mastermix	5 μ L
Forward primers (10 μ M)	0.5 μ L
Reverse primers (10 μ M)	0.5 μ L
Nuclease-free water	1.5 μ L

For quantification, relative standard curves for each gene of interest were included on each plate. All samples and standards were run in duplicates and gene expression was normalized to the expression of glyceraldehyde-3-phosphate dehydrogenase (GAPDH).

2.4 Protein biochemical methods

2.4.1 Tissue homogenization

Frozen cartilage samples were pulverized with mortar and pestle and solved in 50mM HEPES sample buffer (pH7.5) including protease inhibitor cocktail (Roche). Samples kept on a rotator at 4°C overnight. Protein concentration was measured colorimetrically by Pierce BCA protein assay kit (Thermo Scientific) according to manufacturer's instructions. Therefore, samples were diluted 2.5 fold in PBS and mixed with 200µL of working solution in a 96-well plate. Supplied standards were included on each plate. After 30min of incubation at 37°C, the absorbance at 560nm was measured on a microplate reader (Tecan Infinite F200 Pro). A standard curve was created to calculate protein concentration in sample wells.

2.4.2 Enzymatic activity of ENPP1 and TNAP

ENPP1 activity of cartilage lysates was assessed by colorimetric conversion of Thymidine monophosphate nitrophenyl ester (PNTM) (Sigma). Therefore, 10µL of samples was mixed with 100µL of PC-1 buffer including 1mM PNTM and protease inhibitor cocktail (Roche). After 1h incubation at 37°C in the dark, the absorbance at 410nm was measured on a microplate reader. Measured absorbance values were normalized to the protein concentration in the sample.

TNAP activity was determined with the colorimetric Alkaline Phosphatase Assay Kit (ab83369, Abcam) that was used according to the manufacturer's instructions. Briefly, 20µL of samples was mixed with 60µL of supplied assay buffer and 50µL of 5mM p-Nitrophenyl phosphate solution. After 1hr incubation in the dark, the conversion of p-Nitrophenyl phosphate substrate into colored p-Nitrophenyl measured at 405nm. Supplied standards were included on each plate. Calculated TNAP activity in sample wells was normalized to protein concentration.

2.4.3 Pi and PPi concentration

Pi concentration in cartilage lysates was quantified with a colorimetric Phosphate Assay Kit (ab65622 Abcam). Therefore, 10µL of sample was diluted in 190µL dH₂O. For the reaction, 200µL of Phosphate reagent was added to all sample and standard wells. After 30min in the dark, the absorbance at 650nm was measured. PPi concentration was measured using a Pyrophosphate Assay Kit (ab112155, Abcam). Here, 10µL of sample was diluted in 40µL HEPES sample buffer in a black 96-well plate. 50µL of assay solution containing 1x PPi sensor was added to each sample and standard well. After 10 min incubation protected from light, fluorescence was measured on a microplate reader at 316/456nm (Excitation/Emission).

2.4.4 Multiplex cytokine assay

Synovial fluid concentrations of IL-6, IL-7, IL-8, IL-10, IL-13, IL-15, IL-1ra (IL-1 receptor antagonist), granulocyte-macrophage colony stimulating factor (GM-CSF), Fms-like tyrosine kinase 3 (FLT3) Ligand, platelet-derived growth factor-AB/BB (PDGF-AB/BB), vascular endothelial growth factor (VEGF), eotaxin, macrophage inflammatory protein-1b (MIP-1b), MIP-3b and growth-regulated proteins

(GROa, GROb) were measured using the Human XL Cytokine Luminex® Performance Assay (LKTM014, R&D Systems) as instructed by the manufacturer. Thawed synovial fluid samples were centrifuged for 4min at 16000g to remove any cellular component and diluted 1:1 in provided calibrator diluent RD6-65. 50µL of sample, supplied standard or control was added to each well. All samples, standards and controls were mixed with the same volume (50µL) of Microparticle Cocktail containing magnetic antibody-coated microparticles. After a 2h incubation on a shaker at 800rpm protected from light, wells were washed using a hand-held microplate magnet to prevent loss of microparticles. After three washes, 50µL of Biotin-Antibody cocktail was added and incubated for 1h at 800rpm in the dark. Wells were washed again followed by 30min incubation with Streptavidin-PE. After a final wash, the plate was read on a Bio-Plex 200 Analyzer (Bio-Rad) by measuring mean fluorescence intensity. Measurement parameters were set to a reporter gain of 3631, a flow rate of 60µL/minute and 50 count/region. For each analyte, a standard curve was created to quantify the concentration in sample wells.

2.5 Cell culture methods

2.5.1 Isolation of primary articular chondrocytes

Cartilage from the tibial plateau was dissected into small pieces of approximately 1mm and digested with pronase at 1mg/mL in DMEM for 30min at 37°C. A second digestion was done with collagenase type IV (1mg/mL in DMEM supplemented with 10% FBS, 1% penicillin/streptomycin and 1% sodium pyruvate) overnight at 37°C. The remaining pieces were manually homogenized by repeated pipetting. The solution was filtered (40µm strainer) and centrifuged (700g, 5min). The pellet of cells was resuspended in DMEM with 10% FBS, 1% penicillin/streptomycin and 1% sodium pyruvate and plated in a cell culture flask.

2.5.2 Isolation of primary meniscal fibrochondrocytes

Meniscal fibrocartilage was cut into small pieces of approximately 1mm and digested with collagenase type IV (1.8mg/mL per 1.5mg tissue weight in DMEM supplemented with 10% FBS and 1% penicillin/streptomycin) overnight at 37°C. The solution was spun down at 700g for 5min. The pellet was resuspended in 10% FBS and 1% penicillin/streptomycin, transferred to a petri dish and kept at 37°C. After two days, the remaining pieces were manually homogenized by repeated pipetting. The solution was filtered through strainers of decreasing pore size (100µm, 70µm, 40µm) and transferred into a cell culture flask.

2.5.3 Cultivation of primary articular chondrocytes and meniscal fibrochondrocytes

Cells were cultured at 37°C, 98% relative humidity and 5% CO₂. Primary articular chondrocytes were cultured in chondrocyte-specific medium containing DMEM supplemented with 10% FBS, 1mM sodium pyruvate and 1% penicillin/streptomycin. Primary meniscal fibrochondrocytes were cultured in DMEM supplemented with 10% FBS and 1% penicillin/streptomycin.

2.5.4 *In vitro* calcification

Primary articular chondrocytes were seeded in 12-well plates at a density of 5x10⁴ cells/well. Seeded cells were left to attach overnight. To induce calcification, cells were stimulated with 1mM ATP (Sigma) or 5% calciprotein particles (kindly provided by the Department of Musculoskeletal Medicine, University of Lausanne, Switzerland). Briefly, calciprotein particles were synthesized in DMEM supplemented with 10% FBS, 1% penicillin/streptomycin, 1% L-Glutamine, 1mM CaCl₂ and 3.5mM Pi at 37°C for 7d [139]. Cells were stimulated with calciprotein particles and ATP for 24h. Medium was removed and cells were washed in PBS, fixed in 4% formalin and kept in PBS at 4°C until Raman analysis.

Primary meniscal fibrochondrocytes were seeded in 12-well plates at a density of 7x10⁴ cells/well. After 24h, medium was aspirated and cells were washed in cold PBS. On ice, cells were manually detached from the plate with a cell scraper, transferred into tubes and centrifuged at 700g for 5min at 4°C. The cell pellet was resuspended in HEPES lysis buffer and kept at -20°C until measuring Pi and PPi concentrations. For Raman analysis of produced crystals, cells were seeded on coverslips in 24-well

plates at a density of 3×10^4 cells/well. After 24h, medium was removed and cells were washed and fixed in 4% formalin. Fixed cells were kept in PBS at 4°C until Raman analysis.

2.6 Statistical analysis

Statistical analysis was performed in GraphPad Prism V.9 (GraphPad Prism Software). Data are presented in bar graphs as or dot plots. The method of data presentation is indicated in the respective figure legend. Normality of data distribution was tested by Shapiro-Wilk test and QQ-plot. In case of normal distribution, data were compared by t-test or ordinary one-way ANOVA with Dunnett's multiple comparisons test. Non-parametric data are analyzed by Mann-Whitney or Kruskal-Wallis test with Dunn's multiple comparisons test. Parametric data are presented with mean. Non-parametric data are presented with median. For correlation analysis, individual values are plotted in scatter plots. Parametric data were correlated with Pearson correlation. For correlation of non-parametric data, Spearman correlation was used. A p-value of $p < 0.05$ was considered statistically significant under consideration of 95% confidence intervals.

3 Results

3.1 Histology-directed Raman spectroscopy for accurate differentiation of articular calcification

For detection and characterization of articular calcifications, I used a combination of conventional radiography, histological staining and Raman spectroscopy [140]. Therefore, cartilage was collected from 83 OA patients that underwent knee arthroplasty. OA severity and radiological calcification were assessed and scored by radiograph evaluation. As radiographs showed calcifications of varying severity, the degree of radiological calcification was graded into four stages from 0 (no visible calcification), 1 (mild focal calcification), 2 (moderate peripheral calcification) to 3 (severe areal calcification) (Figure 3.1.1A, white arrows) [140]. According to radiograph analysis, 34% of patients (28/83) displayed intra-articular calcification (grades 1-3) (Figure 3.1.1B).

More than half (55%) of included patients were male (46/83), while 45% (37/83) were female. Gender distribution was relatively balanced for radiological grades 0 (m=29, f=26), 1 (m=2, f=3) and 3 (m=4, f=6). Merely patients with moderate radiological calcification (grade 2) were predominantly male (m=11, f=2) (Figure 3.1.1B). Patients' age was comparable across different grades of radiological calcification (Figure 3.1.1C). Mean age values ranged from 63.49 (grade 0) to 69.30 (grade 3) ($p=0.14$), refuting age as a sole cause radiological calcification. Median KL grades ranged from 3.00 (grade 0) to 4.00 (grade 2) and did not differ significantly between calcification grades ($p=0.22$) (Figure 3.1.1D). This indicated similar radiological OA severity independent of radiological calcification.

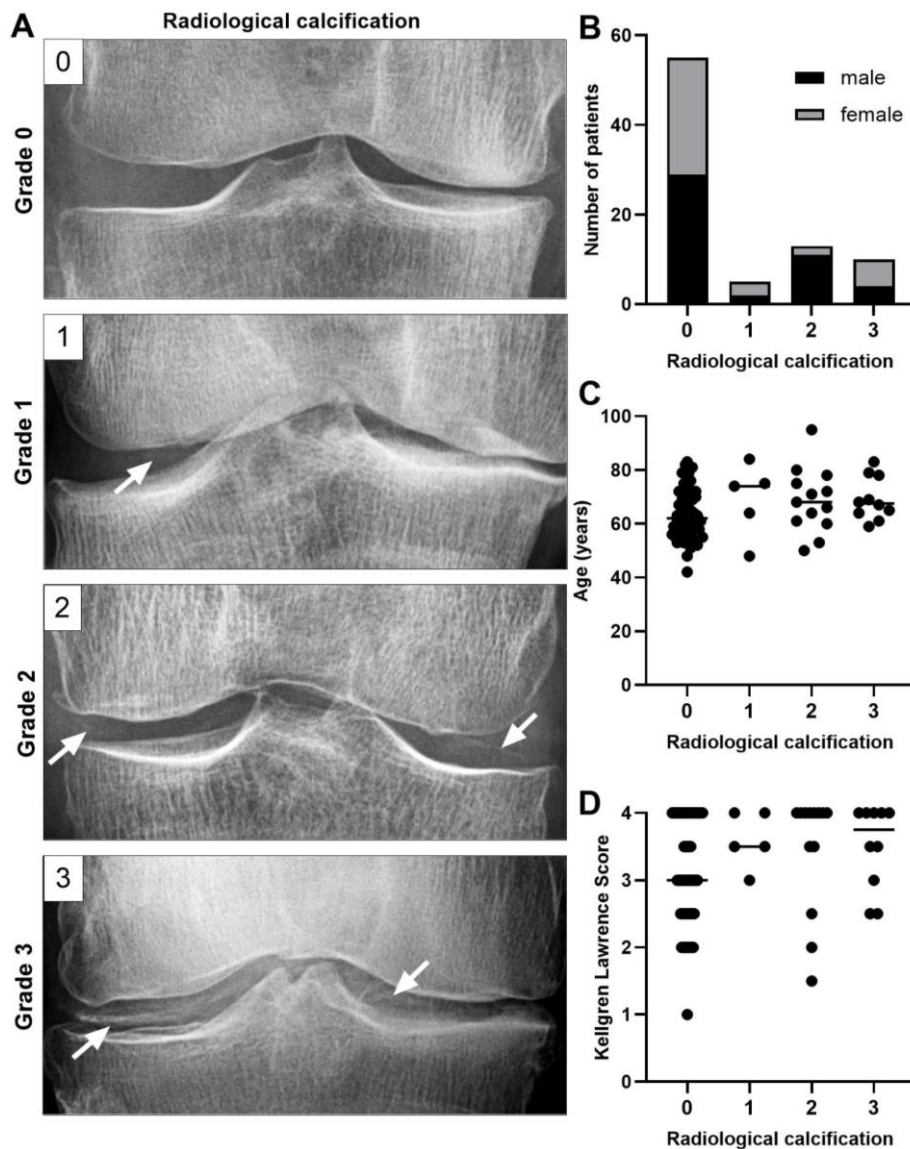


Figure 3.1.1: Demographic information of the patient cohort and radiological detection of articular calcification. **A.** Representative radiographs of articular calcification graded by severity from 0 (no visible calcification), 1 (mild focal calcification), 2 (moderate peripheral calcification) to 3 (severe areal calcification) with arrows indicating calcifications. **B.** Number and gender distribution of patients per radiological calcification grade (grade 0: m=29, f=26, grade 1: m=2, f=3, grade 2: m=11, f=2, grade 3: m=4, f=6). **C.** Mean age of patients graded by radiological calcification (grade 0: 63.49 ± 1.26 , grade 1: 69.00 ± 6.13 , grade 2: 68.69 ± 3.32 , grade 3: 69.30 ± 2.55 , n=83, p=0.14). **D.** Median Kellgren Lawrence grade of patients graded by radiological calcification (grade 0: 3.00 ± 0.11 , grade 1: 3.50 ± 0.19 , grade 2: 4.00 ± 0.24 , grade 3: 3.75 ± 0.20 , n=83, p=0.22) (adapted from [140]). Data are presented as individual values with mean and were analysed using ordinary one-way ANOVA followed by Dunnett's multiple comparisons test for C. For D, data are presented as individual values with median and were analysed by Kruskal-Wallis test followed by Dunn's multiple comparisons test.

3.1.1 Histological cartilage calcification is more prevalent than radiological calcification

In a second step, cartilage calcification was visualized histologically by von Kossa staining. Regardless of radiological calcification, cartilage samples often displayed evident histological calcification of black color (Figure 3.1.2A) [140]. Quantification of the von Kossa stained area showed cartilage calcification in 88% (73/83) of patients (Figure 3.1.2B), yielding a more than two-fold higher prevalence than radiograph analysis (Figure 3.1.1B). Thus, histological calcification was far more frequent than radiological calcification, emphasizing the superiority of histology in the detection of articular calcification. Nevertheless, the histologically calcified area was positively correlated with the grade of radiological calcification ($p=0.006$) (Figure 3.1.2B). Particularly severe radiological calcification (grade 3) translated to a large calcified area stained by von Kossa of up to 8%. This correlation acknowledged the adequacy of radiography for the detection of larger calcified deposits. Even in the absence of radiological calcification (grade 0) cartilage samples often displayed von Kossa-positive areas though (Figure 3.1.2A-B), highlighting the limitation of radiography to detect smaller calcifications.

In contrast, the calcified area did not correlate with the patients age, discounting articular calcification as a simply age-related phenomenon ($p=0.12$) (Figure 3.1.2C). The size of histological calcification further correlated with the severity of cartilage damage assessed by the OARSI score ($p=0.03$) (Figure 3.1.2D), indicating the destructive potential of calcium crystal to cartilage integrity. Unsurprisingly, cartilage damage was rather advanced with a median OARSI of three. Since cartilage samples were collected from end stage OA patients during joint replacement surgery, cartilage damage was to be expected.

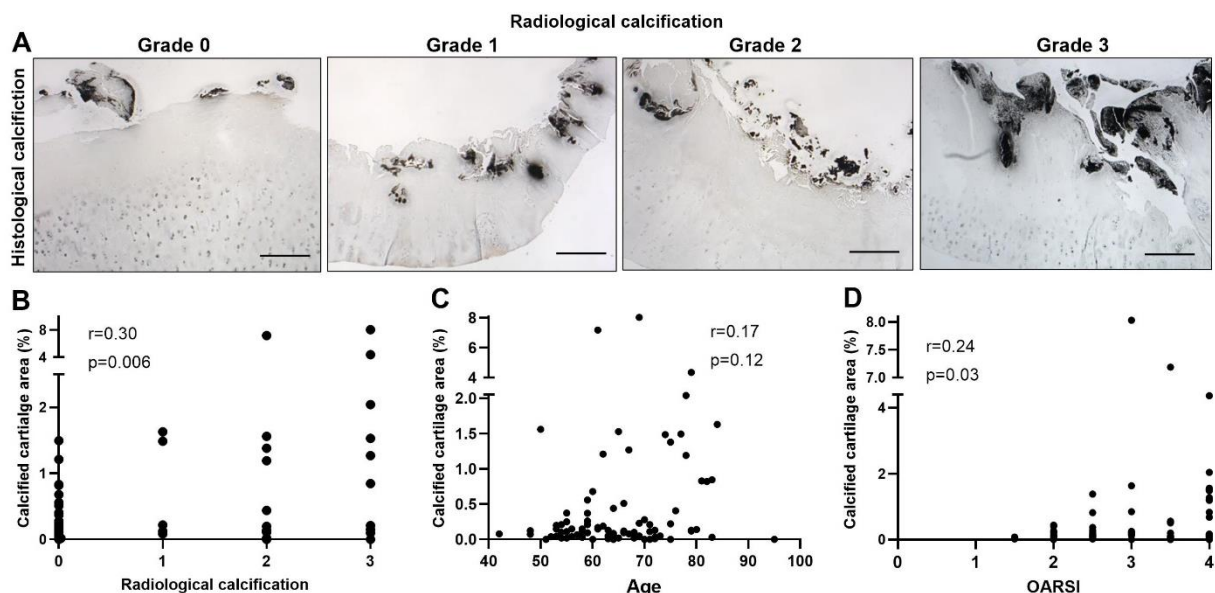


Figure 3.1.2: Histological detection of articular calcification. **A.** Representative von Kossa-stained cartilage samples for each grade of radiological calcification (scale bars=100 μ m). **B.** Spearman correlation of radiological calcification grade and calcified cartilage area ($n=83$, $r=0.30$, $p=0.006$). **C.** Spearman correlation of patient age with calcified cartilage area ($n=83$, $r=0.17$, $p=0.12$). **D.** Spearman correlation of calcified cartilage area with OARSI score ($n=83$, $r=0.24$, $p=0.03$) (adapted from [140]).

3.1.2 Cartilage calcification is predominantly caused by BCP deposition

Following the detection of cartilage calcification, I determined the type of calcium crystal present in the tissue. To do so, I combined Kossa staining with Raman spectroscopy, developing a fast and easy protocol for qualitative crystal analysis in articular tissues [140]. Raman spectroscopy can differentiate BCP and CPP crystals by distinct peaks in the Raman spectrum at 960cm^{-1} and 1050cm^{-1} , respectively (Figure 3.1.3B). Using this method, BCP crystals were detected in 75% of cartilage samples (62/83) (Figure 3.1.3A), making it the predominant calcium crystal in OA cartilage. In contrast, CPP was only identified in 22% (18/83) patients, discounting the common misinterpretation of radiological calcification as CPP deposition. Instead, in this cohort, radiological calcification was often BCP-mediated. In the presence of radiological calcification (grades 1-3), 39% (11/28) of patients exclusively contained BCP calcifications while only 25% (7/28) showed exclusive CPP calcification. Interestingly, in 10% of patients (8/83), BCP and CPP crystal were located in close proximity within the same cartilage section (Figure 3.1.3A-B), indicating a possible existence of mixed endotypes or crystallopathies [140].

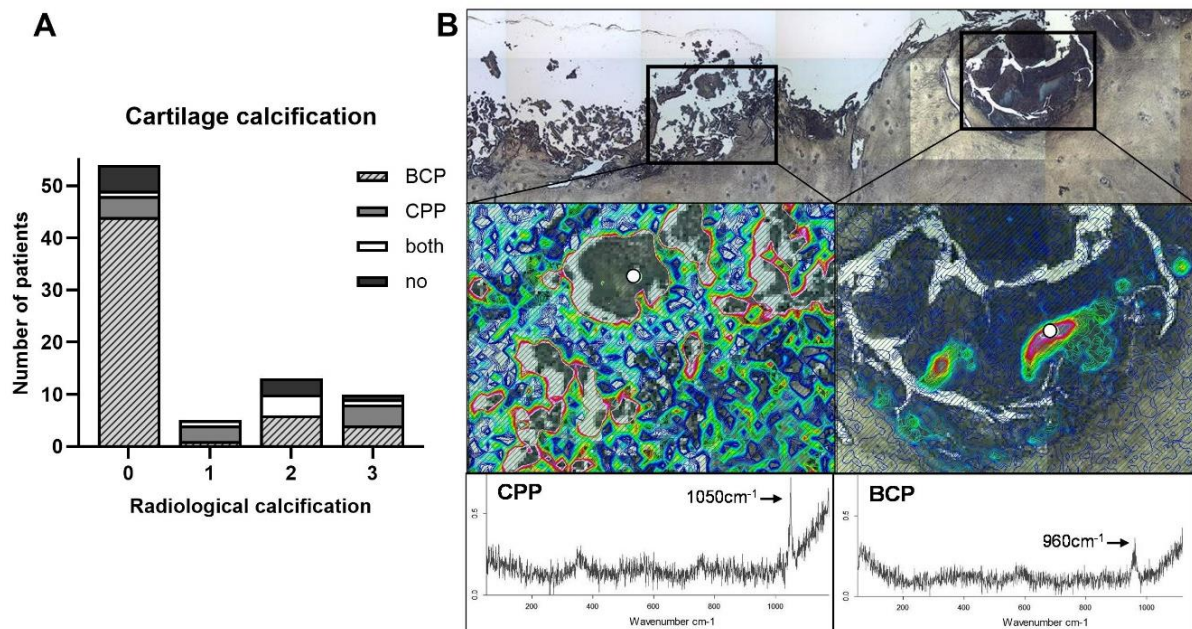


Figure 3.1.3: Identification of calcium crystals in cartilage by Raman spectroscopy. **A.** Calcium crystal types in cartilage graded per radiological calcification grade (grade 0: BCP=44, CPP=4, both=1, no=5, grade 1: BCP= 1, CPP=3, both=1, grade 2: BCP=6, both=4, no=3, grade 3: BCP=3, CPP=4, both=1, no=1, n=83). **B.** Representative image of calcified cartilage (top) with heat maps of CPP (middle left) and BCP (middle right) deposition and matching Raman spectra below (adapted from [140]).

3.1.3 Discrete histology and distribution of BCP and CPP deposits in OA cartilage

In correspondence with the spectroscopic identification of the calcification type, I was able to infer crystal-specific histological patterns for BCP and CPP deposition in von Kossa-stained cartilage. BCP displayed as compressed variably sized nodules of frail appearance. In most cases, these were loosely

attached to the cartilage surface (Figure 3.1.4A-B) [140]. Occasionally, BCP deposits were found buried in the deep zone close to the zone of calcified cartilage. In contrast, CPP was exclusively located in the superficial to intermediate cartilage zone, accumulating in solid definitive pockets (Figure 3.1.4A and C). Peripherally, CPP could also appear less dense granular, needle-shaped clusters. These presumably indicate earlier calcification stages that may gradually solidify to calcified CPP pockets.

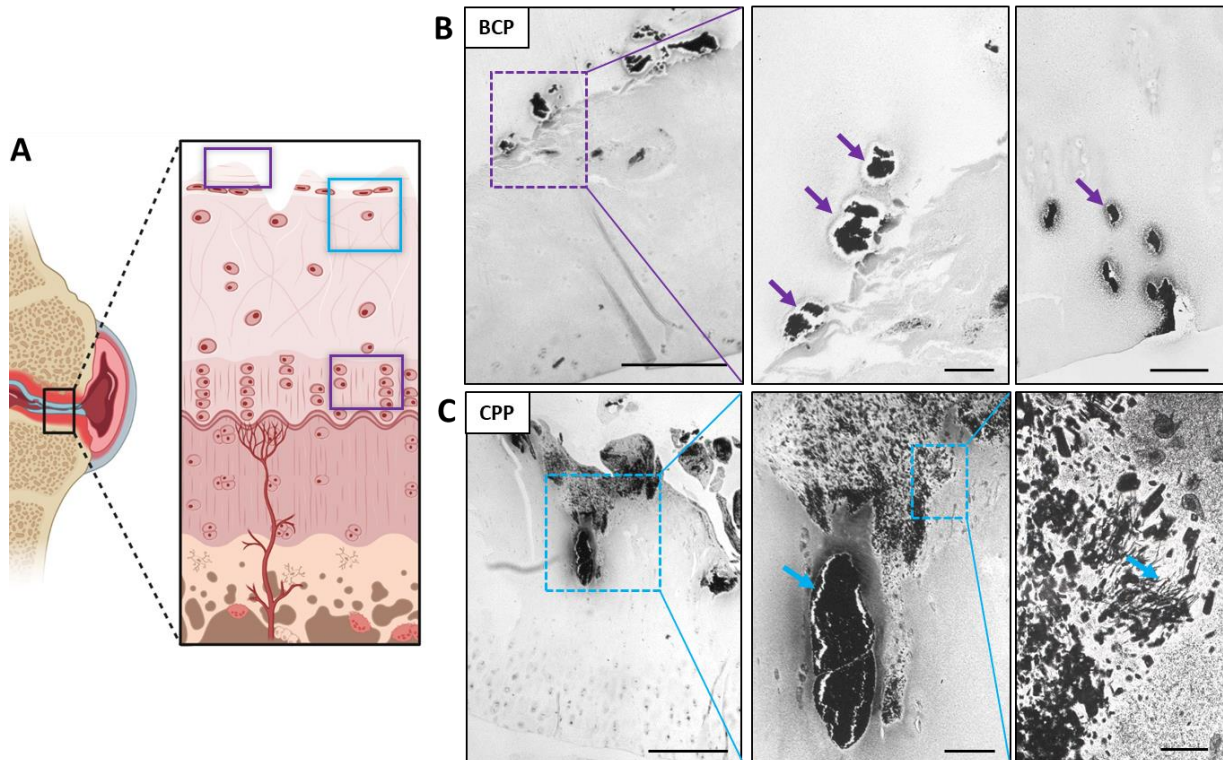


Figure 3.1.4: Histological presentation of BCP and CPP deposition in articular cartilage. **A.** Schematic location of BCP (purple rectangles) and CPP (blue rectangle) deposits in articular cartilage. **B.** Representative von Kossa images showing fragments of clumped BCP (purple arrows) on the cartilage surface (left, scale bars: 500 μ m, 100 μ m) and in the deep zone (right, scale bar: 100 μ m) **C.** Representative von Kossa images of CPP deposits (blue arrows) in large condensed bodies (left and middle, scale bars: 500 μ m, 100 μ m) or as granular, needle-shaped clusters (right, scale bar: 20 μ m) in the superficial and intermediate cartilage zone (adapted from [140]).

For more detailed morphological distinction of BCP and CPP, cartilage, sections with representative BCP and CPP calcifications were imaged by SEM-EDS (Figure 3.1.5) [138]. As observed at a lower resolution on von Kossa images, BCP clumped in chunks that were loosely attached to the cartilage surface. In the deep zone BCP accumulated in empty chondrocyte lacunae (Figure 3.1.5A). EDS analysis detected calcium and phosphate with a weight percentage ratio of approximately 1.5, that is characteristic of BCP. CPP instead was more embedded in the tissue, presenting as densely stacked crystals (Figure 3.1.5B). This needle-like appearance was already indicated by von Kossa staining (Figure 3.1.4C), appearing more pronounced in high resolution SEM imaging. EDS analysis detected calcium and phosphate at a CPP-specific Ca/P ratio of 1. These results corroborate the previous observations of CPP in von Kossa staining.

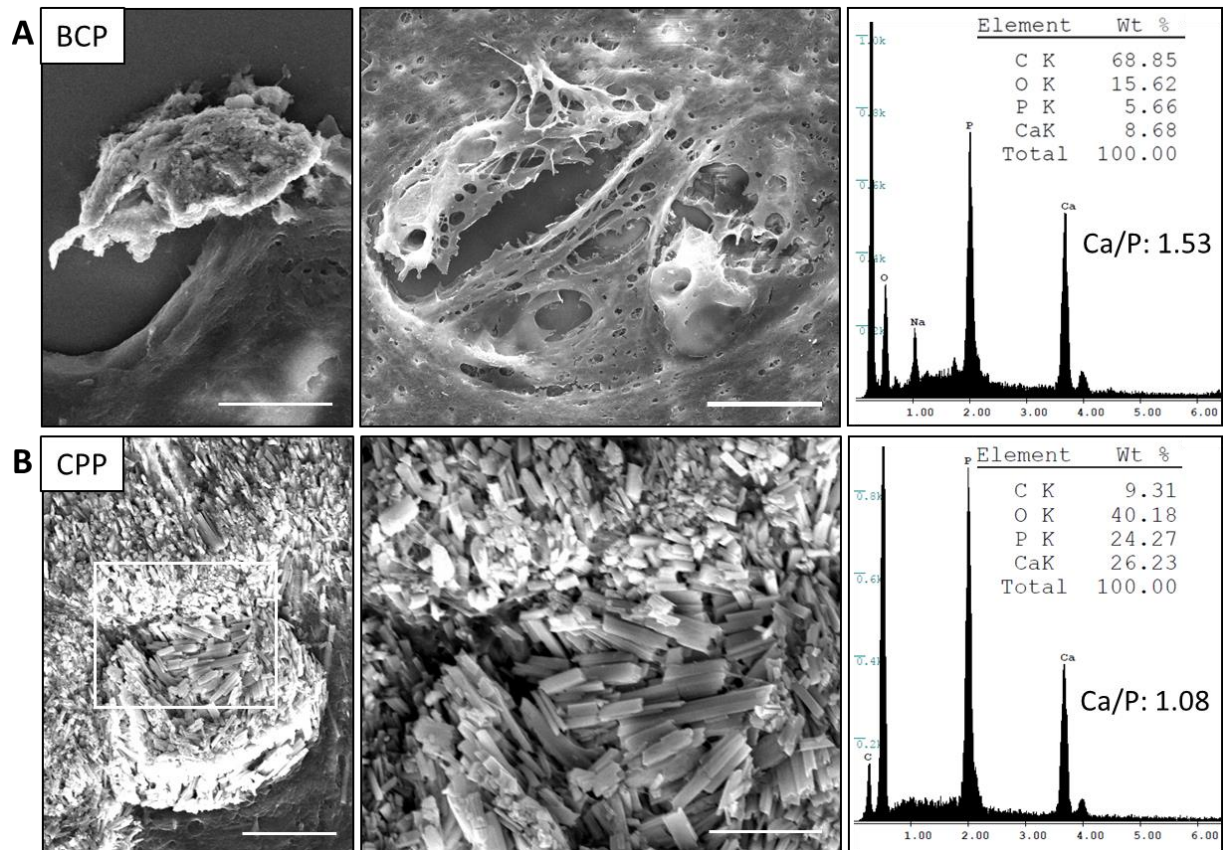


Figure 3.1.5: Scanning electron imaging and energy dispersive X-ray spectroscopy (SEM-EDS) of cartilage calcifications. **A.** Representative SEM image of a clumped BCP agglomerate on the cartilage surface (left) and in a chondrocyte lacunae in the deep zone (middle). Corresponding EDS analysis (right), revealed a characteristic Ca/P ratio of 1.5 (scale bars: 10 μ m). **B.** Representative SEM image of densely stacked rhomboid-shaped CPP crystals embedded in cartilage with characteristic EDS-measured Ca/P ratio of 1 (scale bars: 10 μ m, 5 μ m) (adapted from [138]).

3.2 Upregulated extracellular PPI metabolism as a driver of BCP deposition

After analyzing prevalence, distribution and morphology of BCP and CPP calcification, the second part of this thesis aimed to elucidate the calcification mechanism in cartilage. Therefore, I focused on the extracellular PPI metabolism as a potential determinant of crystal type formation. In this context, gene expression levels of the candidate enzymes TNAP, CD73, CD39, ENPP1, ANKH and ABCC6 were analyzed in cartilage in regards to histological calcification visualized by von Kossa. Cartilage RNA was extracted and gene expression was analyzed using qRT-PCR (Figure 3.2.1) [141]. Gene expression of the phosphatase TNAP was markedly upregulated in histologically calcified cartilage compared to non-calcified cartilage (Figure 3.2.1A, $p < 0.0001$). Similarly, gene expression of CD73 was elevated in calcified cartilage too (Figure 3.2.1B, $p = 0.003$). Instead, CD39 gene expression did not differ significantly with regards to histological cartilage calcification (Figure 3.2.1C, $p = 0.73$). Calcified cartilage also showed greatly increased gene expression of the pyrophosphatase ENPP1 (Figure 3.2.1D, $p < 0.0001$). In addition, gene expression of the ATP efflux transporter ANKH was evidently elevated in the presence of cartilage calcification (Figure 3.2.1E, $p < 0.0001$). This was also the case for ABCC6, although the effect was less pronounced (Figure 3.2.1F, $p = 0.02$). As most of these PPI metabolism enzymes showed elevated gene expression in calcified cartilage, calcification may underlie an imbalance of the extracellular PPI metabolism [141].

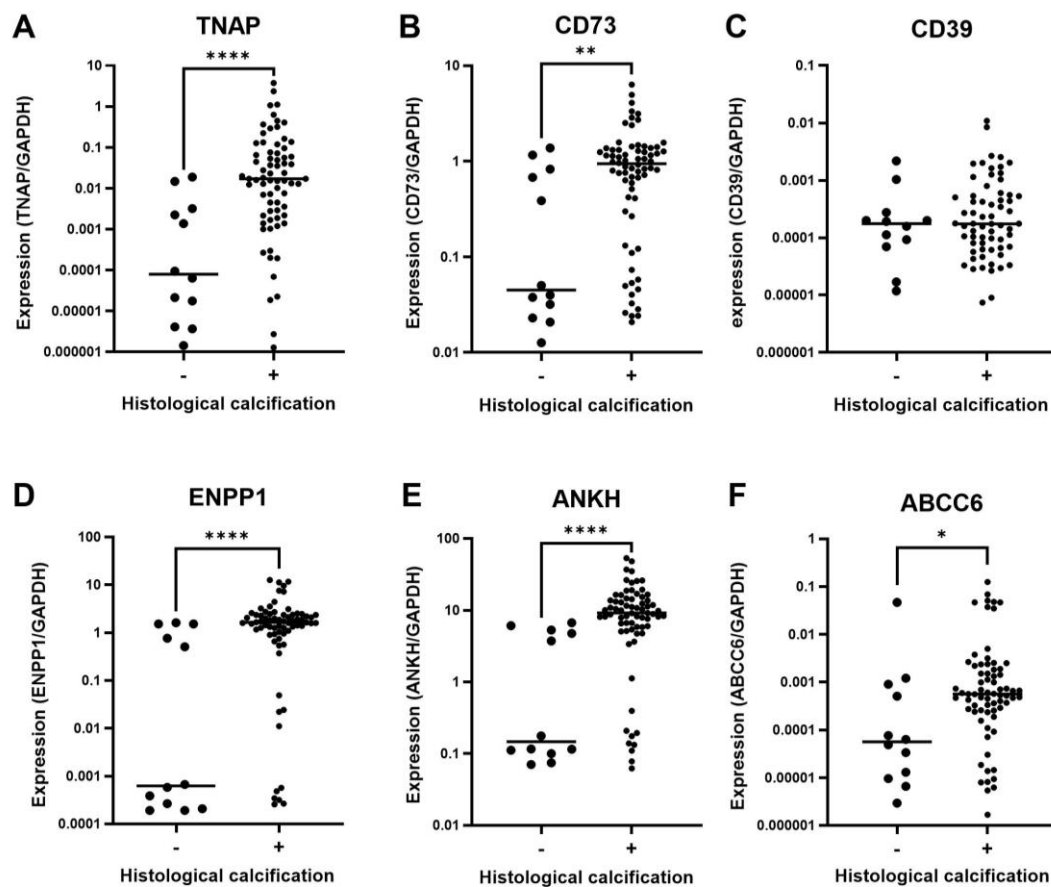


Figure 3.2.1: Gene expression of PPI metabolism enzymes in cartilage in the presence (+) compared to the absence (-) of histological calcification. Median mRNA expression of **A.** TNAP ($p < 0.0001$, $n = 83$), **B.** CD73

($p=0.003$, $n=82$), **C.** CD39 ($p=0.73$, $n=79$), **D.** ENPP1 ($p<0.0001$, $n=83$), **E.** ANKH ($p<0.0001$, $n=82$), and **F.** ABCC6 ($p=0.02$, $n=83$) in non-calcified and calcified cartilage (adapted from [141]). Data are presented as individual values with median on log₁₀ scale and were analysed using Mann-Whitney test. *= $p\leq 0.05$, **= $p\leq 0.01$, ****= $p\leq 0.0001$.

3.2.1 Upregulated gene expression of PPI metabolism enzymes in BCP-calcified cartilage

In order to attribute the calcification-associated changes in gene expression to a specific crystal type, calcified cartilage were analyzed by Raman spectroscopy. Spectroscopic crystal identification was performed as described and cartilage samples were classified by the detected crystal type. Cartilage samples containing both crystal types were excluded for the following crystal-specific analysis to prevent blending and isolate BCP- from CPP-related effects. Classification by crystal type showed an evident upregulation of TNAP gene expression specifically in BCP-calcified cartilage (Figure 3.2.2A, $p=0.0001$) [141]. TNAP gene expression in CPP-calcified was comparable to cartilage without calcification. CD73 gene expression was upregulated in both BCP- and CPP-calcified cartilage (Figure 3.2.2B, $p=0.01$). A similar pattern was observed for ANKH, showing elevated expression in BCP- and CPP-calcified cartilage (Figure 3.2.2E, $p=0.0001$). Gene expression levels of CD39 ($p=0.24$) and ABCC6 ($p=0.06$) did not differ significantly with regards to calcification or crystal type (Figure 3.2.2C and F). Similarly to TNAP, ENPP1 was specifically overexpressed in BCP- but not CPP-calcified cartilage (Figure 3.2.2D, $p=0.0001$). Thus, upregulated gene expression of TNAP and ENPP1 detected in calcified cartilage (Figure 3.2.1A and D) could be specifically attributed to BCP deposition (Figure 3.2.2A and D). This suggests that BCP deposition in particular may be driven by an upregulation of the extracellular PPI metabolism [141].

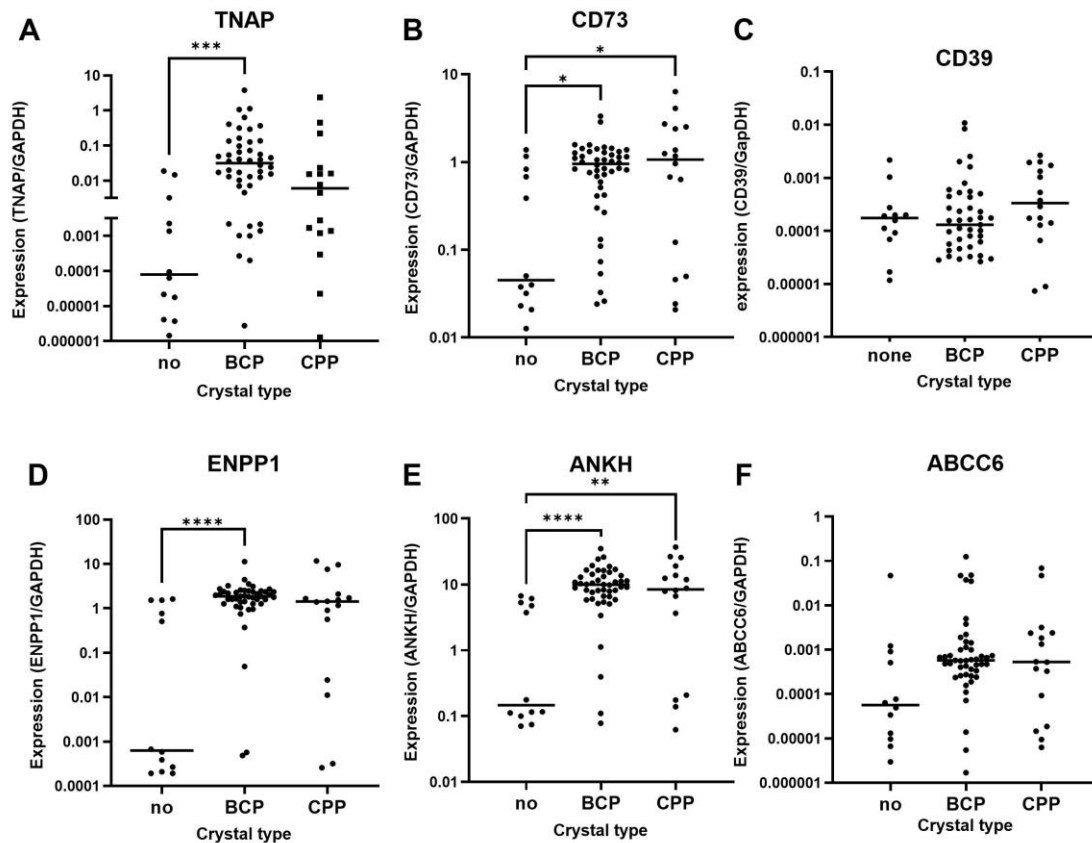


Figure 3.2.2: Gene expression of PPI metabolism enzymes in cartilage classified by the type of calcification in the tissue. Median mRNA expression of **A.** TNAP ($p=0.0001$, $n=74$), **B.** CD73 ($p=0.01$, $n=74$), **C.** CD39 ($p=0.24$, $n=71$) **D.** ENPP1 ($p=0.0001$, $n=74$), **E.** ANKH ($p=0.0001$, $n=74$) and **F.** ABCC6 ($p=0.06$, $n=74$) in non-calcified, BCP- and CPP-calcified cartilage (adapted from [141]). Data are presented as individual values with median on log₁₀ scale and were analysed by Kruskal-Wallis test followed by Dunn's multiple comparisons test. $*$ = $p\leq 0.05$, $**$ = $p\leq 0.01$, $***$ = $p\leq 0.001$ $****$ = $p\leq 0.0001$.

3.2.2 Upregulated TNAP activity and Pi levels in BCP-calcified cartilage

With a focus on the BCP-specific upregulation of TNAP and ENPP1 expression, I aimed to investigate potential associated metabolic changes. Therefore, I assessed the enzymatic activity of TNAP and ENPP1 in cartilage lysates as a proxy for Pi and PPI production. Activity levels were measured by the colorimetric conversion of a synthetic substrate for the respective enzyme (Figure 3.2.3) [141]. With no changes between non-, BCP- and CPP-calcified cartilage, ENPP1 activity was independent of calcification and crystal type (Figure 3.2.3A, $p=0.40$). In contrast, TNAP activity was specifically upregulated in BCP-calcified cartilage (Figure 3.2.3B, $p=0.004$).

As the main respective products of TNAP and ENPP1, Pi and PPI levels were measured in the same samples as before, using colorimetric and fluorescence assays. Similarly to ENPP1 activity, PPI levels did not differ between non-, BCP- and CPP-calcified cartilage (Figure 3.2.3C, $p=0.56$) [141]. Pi levels instead were significantly increased in BCP-calcified cartilage (Figure 3.2.3D, $p=0.02$), matching the

upregulated TNAP activity detected before (Figure 3.2.3B). In addition, the Pi/PPi ratio was increased in BCP-calcified cartilage (Figure 3.2.3E, $p=0.03$). This highlights the importance of the relation of both ions in the calcification process. As a product of TNAP, Pi levels directly correlated with TNAP activity (Figure 3.2.3G, $r=0.43$, $p=0.0002$) while there was no correlation observable for ENPP1 and PPI (Figure 3.2.3F, $r=0.17$, $p=0.18$).

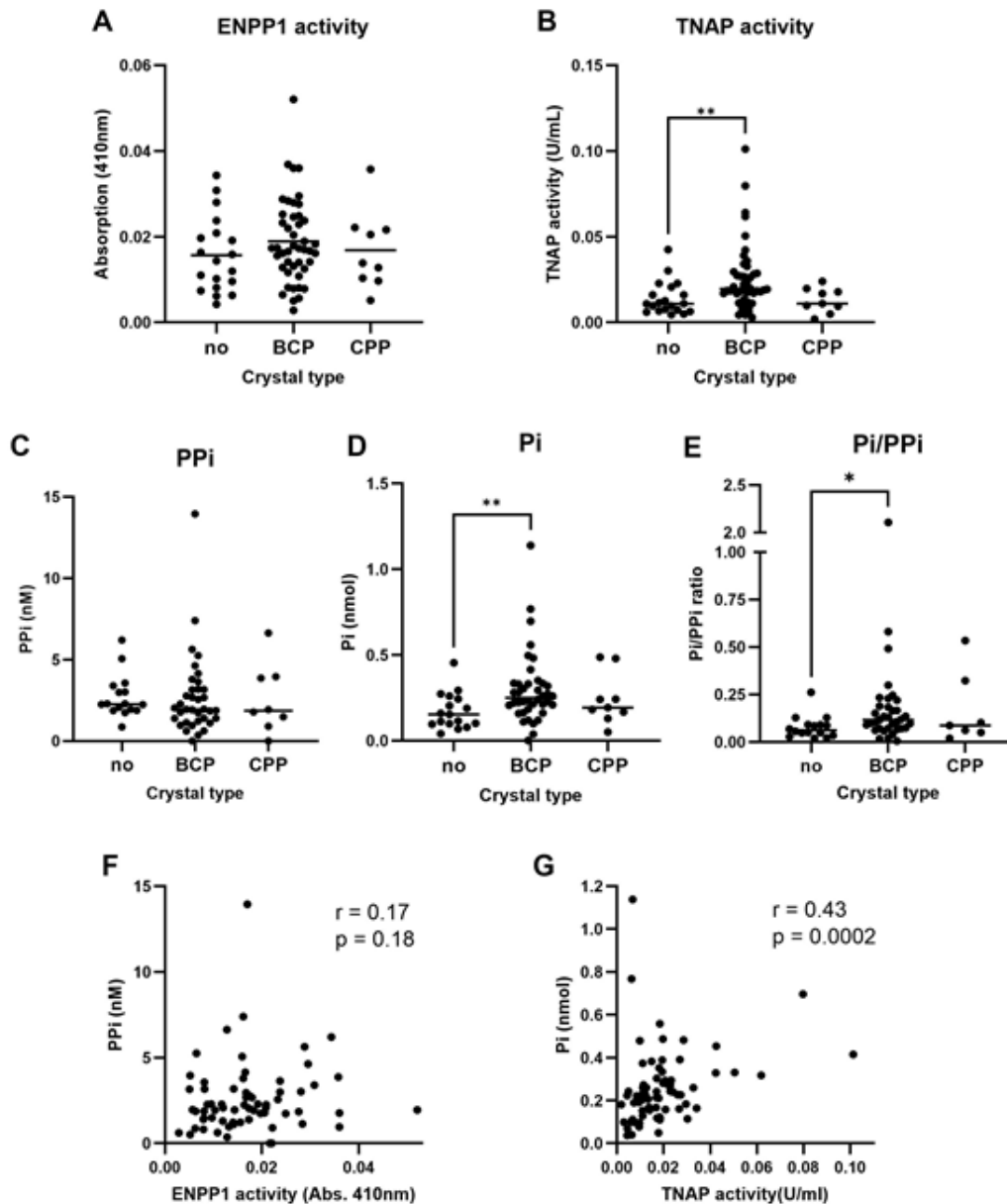


Figure 3.2.3: TNAP and ENPP1 activity and concentrations of Pi and PPI in articular cartilage **A.** Median ENPP1 activity ($n=73$, $p=0.40$) and **B.** TNAP activity ($n=75$, $p=0.004$) in cartilage classified by the type of calcification. Levels of **C.** PPI ($n=60$, $p=0.56$) and **D.** Pi ($n=66$, $p=0.02$) and **E.** their ratio ($n=58$, $p=0.03$) in non-calcified, BCP- and CPP-calcified cartilage. **F.** Spearman correlation of cartilage ENPP1 activity and PPI levels ($n=67$, $r = 0.17$, $p=0.18$). **G.** Spearman correlation of cartilage TNAP activity and Pi levels ($n=72$, $r=0.43$, $p=0.0002$) (adapted from [141]). Data are presented as individual values with mean and were analysed using ordinary one-way ANOVA followed by Dunnett's multiple comparisons test for A. For B-E, data are presented as individual values with median and were analysed using Kruskal-Wallis test followed by Dunn's multiple comparisons test. $*=p\leq 0.05$, $**=p\leq 0.01$.

3.3 Intracellular and ATP-dependent induction of CPP deposition

Retrospective analysis of calcified cartilage identified increased TNAP-mediated Pi content as a driver of BCP deposition. However, CPP deposition could not be explained by a dysregulated extracellular PPI metabolism. Instead, CPP deposition seems to be regulated by additional factors that have yet to be identified.

3.3.1 ATP stimulation induces CPP formation *in vitro*

Taking a prospective approach to calcification, I induced and characterized calcification *in vitro*. With the aim of identifying characteristics unique to CPP deposition, chondrocytes were isolated from calcified cartilage, cultured in the presence of calcification promoters and monitored for calcification. To induce calcification, chondrocytes were stimulated with calciprotein particles or ATP that act as calcification promoters. As an amorphous precursor form of BCP, calciprotein particles naturally resulted in BCP deposition (Figure 3.3.1A-B, left panel). In contrast, ATP stimulation lead to a more diverse calcification process. While chondrocytes isolated from BCP-calcified cartilage responded with BCP deposition (Figure 3.3.1A, right panel), chondrocytes from CPP-calcified cartilage produced both crystal types following ATP stimulation (Figure 3.3.1B, right panel). Interestingly, BCP presented as spherical deposits located on top of the monolayer of chondrocytes. Instead, CPP appeared as individual crystals. While some of these crystals were located in the extracellular space between the cells, a majority appeared to occupy the cytoplasm (Figure 3.3.1B, blue arrows). This observation suggests that CPP deposition may be regulated by an ATP related cell-intrinsic factor.

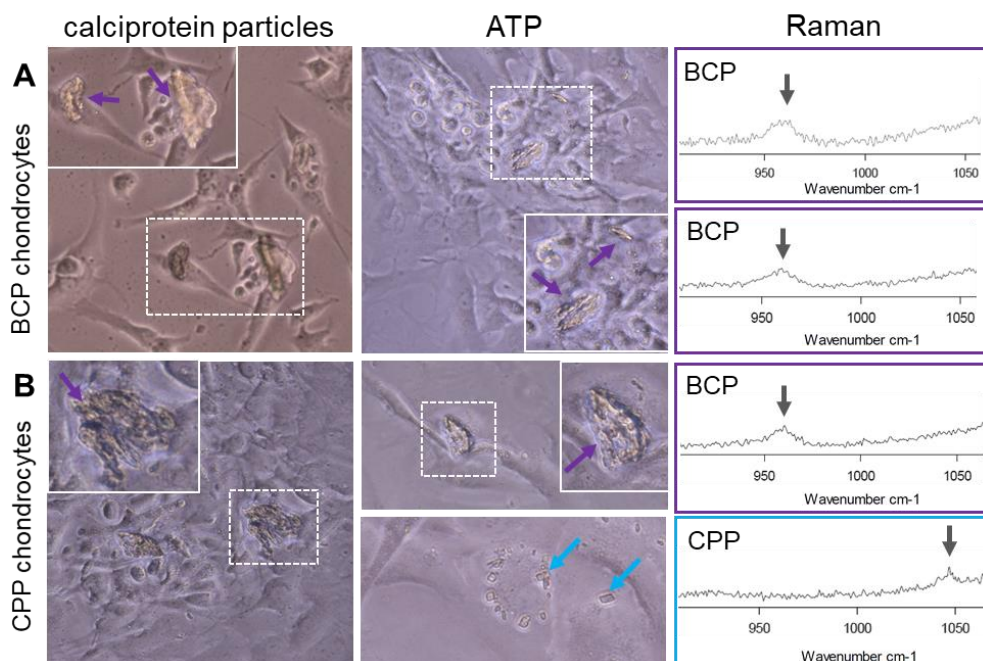


Figure 3.3.1: *In vitro* calcification of human primary chondrocytes stimulated with calciprotein particles or ATP. Representative Raman spectra of detected crystals are located on the right. **A.** In response to calciprotein particles (left panel) and ATP (right panel), they produced BCP crystals (purple arrows). **B.** Chondrocytes isolated from CPP-calcified cartilage produced BCP (purple arrows) in response to calciprotein particles (left panel). ATP induced the formation of both BCP (purple arrows) and CPP crystals (blue arrows) (right panel).

3.3.2 CPP calcification is associated with elevated levels of senescence-associated cytokines in synovial fluid

In view of ATP-induced *in vitro* CPP formation, disruptions in ATP synthesis are commonly reported in OA. For instance, OA chondrocytes often display mitochondrial dysfunction that precedes and promotes cellular senescence [142, 143]. Chondrocyte senescence is a common phenomenon in OA cartilage [82, 83] and has been proposed to be involved in CPP deposition [78]. Further elucidating this link, I compared intra-articular concentrations of senescence-associated mediators in the context of cartilage calcification. To this end, various inflammatory mediators that can be released by senescent cells, were measured in synovial fluid by magnetic-bead based multiplex assay in respect to the crystal type detected in corresponding cartilage samples. Here, CPP deposition in cartilage was associated with elevated synovial fluid levels of senescence-associated cytokines, chemokines and growth factors (Figure 3.3.2) [144]. Specifically, the pro-inflammatory cytokines IL-15 and GM-CSF were upregulated in synovial fluid of patients with CPP compared to BCP cartilage calcification (Figure 3.3.2A, IL-15: $p=0.0007$, GM-CSF: $p=0.02$). Similarly, IL-1ra and IL-10 were significantly higher in synovial fluid of CPP- compared to BCP-calcified joints (Figure 3.3.2B, IL-1ra: $p=0.003$, IL-10: $p=0.01$). Synovial fluid concentrations of the growth factors PDGF-AB/BB and VEGF (Figure 3.3.2C, PDGF-AB/BB: $p=0.04$, VEGF: $p=0.04$) as well as the chemokines MIP-1b (Figure 3.3.2D, $p=0.01$) were also higher in patients with articular CPP deposition. Collectively, these data show an elevated synovial fluid cytokine profile in CPP- compared to BCP-calcified joints that may indicate increased senescence [144].

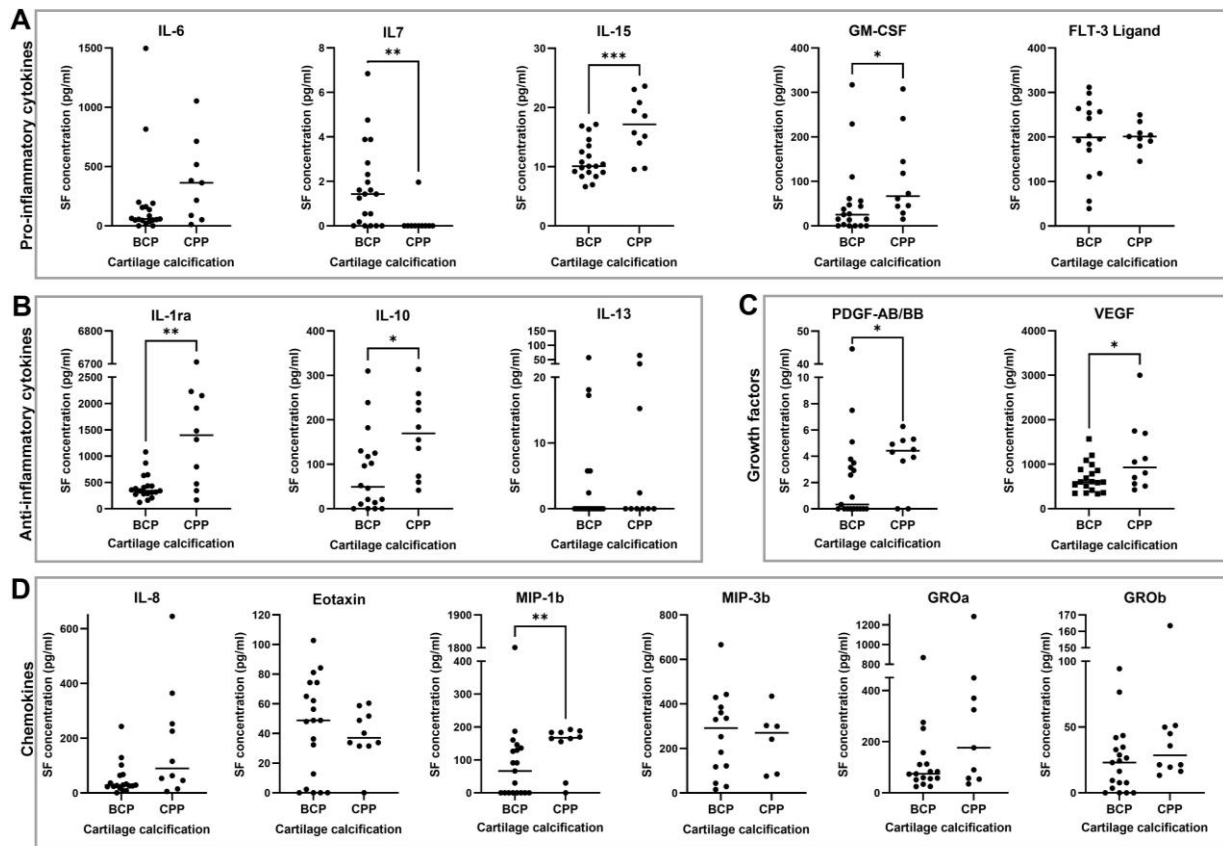


Figure 3.3.2: Synovial fluid concentrations of senescence-associated mediators classified by the crystal type detected in corresponding cartilage tissue. Concentrations of various senescence-associated mediators in synovial fluid of BCP- and CPP-calcified joints including (A) pro-inflammatory cytokines (IL-6: p=0.06, n=28, IL-7: p=0.002, n=30, IL-15: p=0.0007, n=29, GM-CSF: p=0.02, n=29, FLT3-Ligand: p=0.92, n=25) (B) anti-inflammatory cytokines (IL-1ra: p=0.003, n=29, IL-10: p=0.01, n=28, IL-13: p=0.64, n=28) (C) growth factors (PDGF-AB/BB: p=0.04, n=29, VEGF: p=0.04, n=29) and (D) chemokines (IL-8: p=0.06, n=28, Eotaxin: p=0.69, n=29, MIP-1b: p=0.01, n=29, MIP-3b: p=0.77, n=20, GROa: p=0.18, n=26, GROb: p=0.13, n=29) (adapted from [144]). Data are presented as individual values with mean and were analysed by unpaired two-sided t-test for IL-15, FLT3-Ligand, VEGF, Eotaxin, and MIP-3b. Data are presented as individual values with median and were analysed by Mann-Whitney test for IL-6, IL-7, GM-CSF, IL-1ra, IL-10, IL-13, PDGF-AB/BB, IL-8, MIP-1b, GROa and GROb. *= $p \leq 0.05$, **= $p \leq 0.01$, ***= $p \leq 0.001$.

3.3.3 Intracellular CPP deposition is accompanied by elevated PPi levels in meniscal fibrochondrocytes

In addition to calcification of articular cartilage, meniscal fibrocartilage is a frequent site of calcification. In particular, menisci often show very extensive forms of CPP deposition. For specific investigation into CPP calcification, I collected menisci from eight end-stage OA patients during knee replacement surgery. Similar to articular cartilage samples, menisci were stained with von Kossa and detected calcifications were analyzed by Raman spectroscopy. Spectroscopic analysis of calcified deposits

revealed large meniscal CPP deposits in 3 out of 8 patients. Patients with meniscal CPP deposition did not differ in age or KL grade from patients without meniscal CPP (Figure 3.3.3A).

In a second step, I isolated chondrocytes from meniscal fibrocartilage with and without CPP deposition. Isolated meniscal fibrochondrocytes were cultured and observed for spontaneous microscopic calcification. Meniscal fibrochondrocytes from donors without meniscal calcification served as a control and displayed no evident *in vitro* calcification (Figure 3.3.3B). Von Kossa staining of corresponding meniscus sections revealed no calcification in the tissue. In contrast, von Kossa images of calcified menisci displayed large CPP deposits embedded in the tissue (Figure 3.3.3C), presenting the peculiar nodular and granular histology of CPP that has been described in articular cartilage above (3.1.3.). In contrast to cartilage, there was no apparent distribution pattern of CPP in menisci, depositing both at the outer margins and deep inside the tissue. Interestingly, fibrochondrocytes isolated from these calcified menisci contained large accumulations of evident, easily visible crystals. Inside these cells, the cytoplasm was packed with vibrant, needle-shaped crystals (Figure 3.3.3C, white arrow), resembling CPP deposits embedded in cartilage (Figure 3.1.4C and Figure 3.1.5B) and CPP crystals formed in response to ATP (Figure 3.3.1B). In contrast to the densely crystal-filled cytoplasm, the nucleus usually remained visible and free of crystals (Figure 3.3.3C, black arrow). Occasional crystals could also be found outside the cells. These extracellular crystals were markedly less frequent compared to the density of intracellular crystal accumulation. Spectroscopic analysis validated these crystals as CPP, showing the characteristic Raman band at 1050cm^{-1} (Figure 3.3.3C). Appositely, intracellular P_i levels were elevated in CPP-containing chondrocytes (Figure 3.3.3E, $p < 0.0001$) while intracellular Pi levels were similar to those of chondrocytes without crystals (Figure 3.3.3D, $p = 0.45$). Accordingly, the Pi/PP_i ratio was decreased in the presence of intracellular CPP (Figure 3.3.3F, $p = 0.001$), proposing an intracellular mechanism for CPP formation.

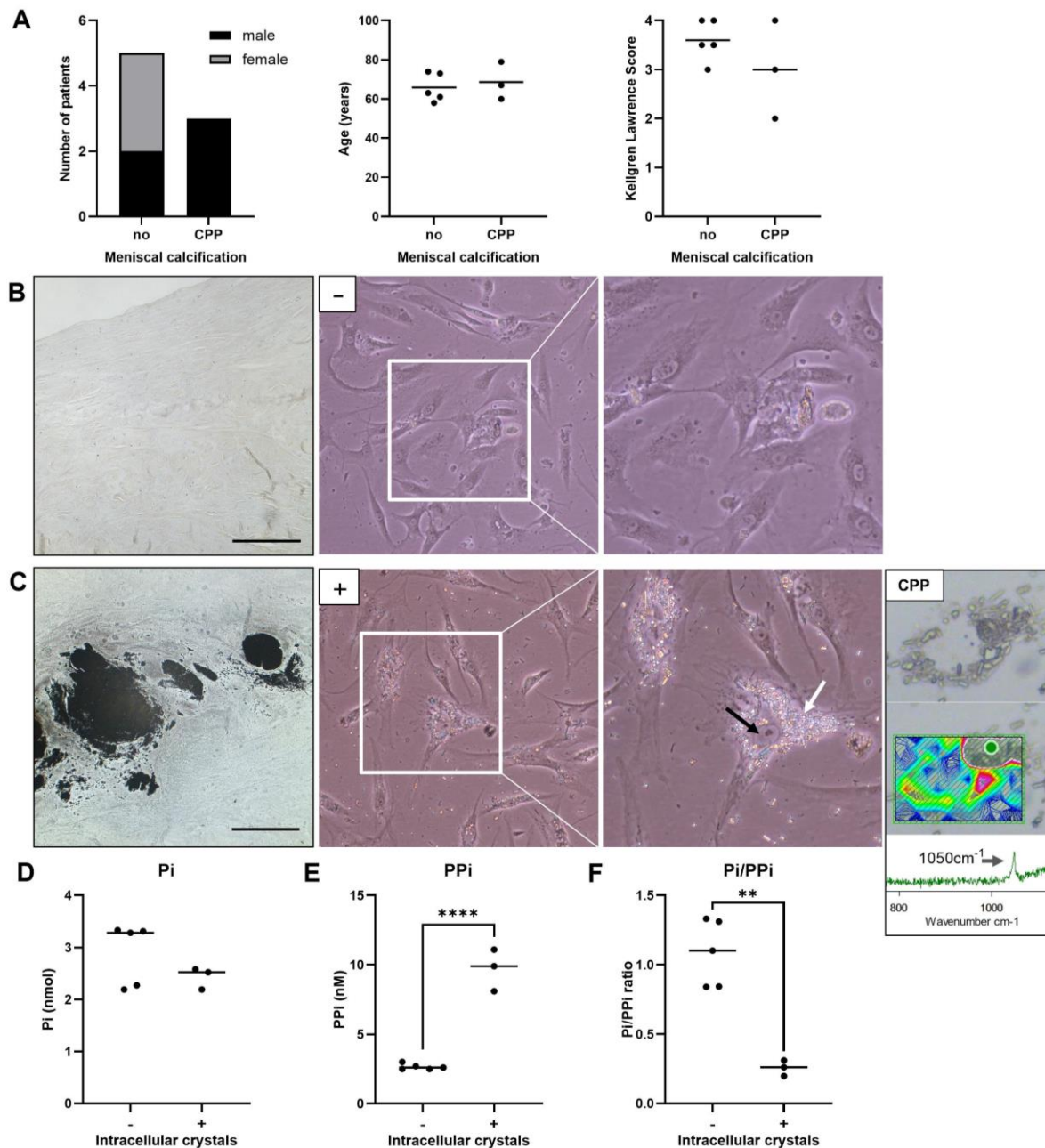


Figure 3.3.3: Intracellular CPP deposition in meniscal fibrochondrocytes with von Kossa staining of corresponding menisci. **A.** Demographic information on the cohort of patients grouped by the presence of meniscal CPP deposition. Number and gender (left, no: m=2, f=3, CPP: m=3, f=0), age (middle, no: 65.80 ± 3.25 , CPP: 68.67 ± 5.55 , $n=8$, $p=0.65$) and Kellgren Lawrence grade (right, no: 3.60 ± 0.19 , CPP: 3.00 ± 0.58 , $n=8$, $p=0.27$) **B.** Representative light microscopy images from meniscal fibrochondrocytes without intracellular calcification (-) isolated from non-calcified meniscus tissue (left, scale bar: $200\mu\text{m}$). **C.** Representative light microscopy images of meniscal fibrochondrocytes containing intracellular CPP crystals (+) derived from CPP-calcified meniscus (left, scale bar: $200\mu\text{m}$) with a representative Raman spectrum of a CPP-filled chondrocyte (right). **D.** Cellular concentration of Pi ($n=8$, $p=0.45$) **E.** Cellular concentration of PPI ($n=8$, $p<0.0001$). **F.** Ratio of cellular Pi to PPI in meniscal fibrochondrocytes in regards to intracellular CPP deposition ($n=8$, $p=0.001$). Data in A are presented as individual values with mean and were analysed using an unpaired two-sided t-test. Data in D are presented as median and were analysed using Mann-Whitney test for D. In E and F, data are presented as individual values with mean and were analysed using unpaired t-test. **= $p \leq 0.01$, ****= $p \leq 0.0001$.

4 Discussion

The involvement of articular calcification in joint degeneration and OA progression is well recognized. Calcified deposits in cartilage cause abrasive mechanical damage, ECM degradation and cell death. Calcium crystals can also shed into the synovial fluid, triggering inflammatory reactions that further drive calcification. They exist in two major types that share overlapping clinical presentations while being associated with distinct underlying cellular phenotypes and etiologies. Thus, differentiation in the context of detection and formation remains challenging [145]. Therefore, the main aim of this thesis was to differentiate and characterize BCP and CPP deposition in cartilage, assessing prevalence, distribution and formation.

4.1 Histology-directed Raman spectroscopy for accurate differentiation of articular calcification

4.1.1 Histological cartilage calcification is more prevalent than radiological calcification

The first part of this thesis focused on detection and differentiation of articular calcification. Since crystal type differentiation remains difficult, there is inconsistent data on the prevalence of BCP and CPP deposition in cartilage. By combining histological von Kossa staining with Raman spectroscopy, this thesis established a convenient protocol for precise identification of BCP and CPP deposition in cartilage. As the standard imaging method in clinical practice, conventional radiography served as a comparison. Conventional radiography detected articular calcifications in 34% of patients (28/83) (Figure 3.1.1A-B), coinciding with studies on other OA patient cohorts that detected radiological calcification in 31% to 35% [57, 146]. Still, reported prevalence values vary considerably from 9% [147] up to 40% [148], highlighting the weak reliability of radiography in detecting articular calcification. In addition, most studies in this context include large community-based cohorts and determine the prevalence of radiological calcification in the general population without specifying involved crystal types [149, 150]. In these studies, radiological evidence of calcification is often equated with CPP deposition [148], reinforcing this common misinterpretation. Instead, radiological calcification more often involves BCP deposition (Figure 3.1.3A).

In addition, radiograph interpretation and evaluation requires training and is at least partially dependent on the observer [151]. Radiograph evaluation could be further impaired by advanced OA severity, particularly severe joint space narrowing, that is not uncommon in end stage OA patients. Severe joint space narrowing or osteophytosis have been mentioned as an impediment to accurate detection of calcification before [95, 152]. These limitations likely contribute to the mediocre accuracy for radiography in detecting articular calcification. The lack of sensitivity of radiography in detecting articular calcification has been recognized before with sensitivity estimates of around 50% [151, 152], favoring detection methods with higher resolution and sensitivity that are less affected by OA-related articular changes such as ultrasonography [153] or computed tomography [154].

Despite its limited sensitivity, radiography did present in various levels of severity (Figure 3.1.1A). Since there is no standard grading system for radiological calcification available, a novel system was developed here to assess the severity of radiological calcification. Therefore, patients were classified into grades 0-3 based on the presence and extend of calcifications on radiographs (Figure 3.1.1A-B). Gender distribution and age between these grades were relatively even (Figure 3.1.1B-C). While an equal calcification prevalence for both genders has been reported before, the radiological calcification has been associated with an increased age average [149]. Due to lack of a grading system, literature findings refer to the mere presence of radiological calcification, not considering the extend or severity as done here. Radiographic OA severity assessed by KL score did not change with the grade of radiological calcification (Figure 3.1.1D). This is supported by the current view in literature, stating that radiological calcification does not seem to worsen radiographic changes in OA [147, 155, 156]. As the applied grading system is novel and self-established, data on reliability is still lacking and onward application requires further validation.

Histological analysis revealed calcifications in 88% of cartilage samples (Figure 3.1.2A-B), pointing out a large discrepancy between histological and radiological calcification (34%). Histological analysis in other studies provided similar values of cartilage calcification in 92% [58] to 100% of donors [65]. In this study, von Kossa staining revealed calcifications even in the absence of radiological calcification (grade 0) (Figure 3.1.2B), indicating a vast underestimation of articular calcification by radiography. Nonetheless, the calcified cartilage area increased with radiological calcification grade (Figure 3.1.2B), indicating that larger calcification are adequately detected by both radiography and histology. Considering its low resolution [95], radiography seems to be particularly insensitive to smaller calcifications. In addition, localization of detected deposits proves rather challenging on conventional radiographs [157] as radiologically visible calcification often represent calcification of meniscal fibrocartilage [58]. Thus, histology represents a superior method for the detection of articular calcification. The invasive sample collection and rather elaborate processing largely limits application to research purposes though.

In view of the cartilage degeneration, the calcified cartilage area positively correlated with cartilage damage measured by OARSI (Figure 3.1.2D). Although, some studies report calcifications in the absence of severe cartilage damage, these often only assess cartilage integrity macroscopically instead of histologically [91, 158] or focus on non-weight-bearing joints such as the shoulder [159]. Studies on weight-bearing joints instead demonstrate a robust correlation between cartilage calcification and damage [65, 160, 161]. In addition to mechanical damage, crystals can also induce proteolytic ECM degeneration [162]. These findings emphasize the inseparable link between cartilage calcification, degradation and OA progression. The causative chain of these events remains a topic of ongoing research and debate, though.

In contrast, the calcified cartilage area did not correlate with patient age (Figure 3.1.2C). According to epidemiological data, articular calcification frequency increases with age [157, 161], proposing calcification as a secondary effect to normal aging [91]. Age-related changes such as decreasing water

or proteoglycan content may likely contribute to the calcification process [163]. Nonetheless, mounting evidence supports an age-independent calcification of cartilage [58, 65, 160], reinforcing the lack of age-association observed here.

4.1.2 Cartilage calcification is predominantly caused by BCP deposition

Raman analysis identified BCP as the most common crystal type present in 75% of all cartilage samples (Figure 3.1.3). CPP was only found in 13%, while 10% of samples contained both crystals. Studies directly comparing BCP and CPP calcification in OA cartilage are rare and often lack generalizability due to limited sample size [105]. Thus, the sample size of 83 cartilage samples attests a strength of this study.

Many articular calcification studies focus on CPP detection in synovial fluid without considering BCP [164]. Thus, crystal-specific prevalence data is inconsistent. While some studies identified BCP as the most common crystal type in OA synovial fluid [165], others found the combination of BCP and CPP to be more frequent than any crystal type alone [166, 167]. Some never observed both crystal types in the same sample [168] and yet others most frequently reported findings of CPP [169, 170]. Furthermore, these studies do not specify the source of synovial crystals.

The few studies that focus on cartilage calcification most frequently detect BCP in up to 100% of cartilage samples at the time of arthroplasty [65, 104]. This data ties in with the frequent detection of BCP in this study (Figure 3.1.3). According to general consensus, cartilaginous CPP deposition is less common than BCP. Literature reports CPP in cartilage of roughly 13-20% of OA patients [65, 171], consistent with the present CPP frequency of 18% (Figure 3.1.3). In 10% of patients, both crystals were detected in the same cartilage section, demonstrating that BCP and CPP calcifications are not mutually exclusive. This coexistence of BCP with CPP in cartilage has been reported before [65, 104], suggesting the possibility of mixed endotypes.

Surprisingly, Raman analysis often solely detected BCP in the presence of radiological calcification (Figure 3.1.3A). Crystals other than CPP as the cause of radiological calcification have been acknowledged before, usually defined as a rarity though. For instance, an early study from 1966 ascribed 5% of radiological calcification to calcium crystals other than CPP [172]. In contrast, patients with radiological calcification in this cohort more often displayed exclusive BCP than CPP deposition in cartilage (Figure 3.1.3A). This emphasizes that radiological calcification does not necessarily reflect CPP deposition, stressing the relevance of radiographic BCP deposition and its accurate detection. On the other hand, some histological CPP calcifications were not visible on radiographs (Figure 3.1.3A). Thus, radiological calcification does not prove the deposition of CPP, while CPP cannot be excluded by negative radiographs. These findings challenge the synonymy of radiological calcification and CPP deposition [151, 154]. Similarly, detection of CPP in a singular joint is often equated with CPPD pathology [148, 171] despite the recommendation of additional diagnostic criteria [85]. In fact, CPPD has been proposed as a systemic pathology with poly-articular involvement [86]. Since this study focused on singular knee joints as the most common site for articular calcification [95], systemic changes and CPPD diagnostics cannot be evaluated based on the current data. These terminological

inconsistencies and the coexistence of both crystals accentuate the need for differential detection and analysis. Although the awareness for differentiated detection has increased in recent years [173], crystal-specific research is still underrepresented. Therefore, the strength of the present study lies in the integration of radiographic, histological and spectroscopic data to systematically compare BCP and CPP calcifications in cartilage.

Naturally, these findings come with limitations. Radiography encompasses the full joint, whereas histology and Raman analysis are limited to a small area of cartilage [58]. Also, soft tissue calcification does not proceed homogeneously [174], so smaller, initial or peripheral calcifications could be missed. Conscious of these limitations, samples were taken from the main loading area of the tibia plateau, arguably representative for each patient. Sampling large areas, or ideally, the full cartilage, in a cohort of this size is methodologically challenging and would go beyond the scope of this thesis.

Histological sample processing may raise the concern of losing calcified deposits. Inherent to the methodology, this limitation cannot be avoided. However, BCP and CPP are resilient and, in contrast to monosodium urate crystals in gout [175], can hardly be dissolved [176]. Histological and spectroscopic detection also underlies the light microscopic resolution limit ($>1\mu\text{m}$), that misses individual BCP crystals [65]. Likewise, Raman spectroscopy underlies a similar resolution limit, in this case $2\mu\text{m}$. As BCP tends to deposit in aggregates though [177], this technical limitation may be neglectable here.

4.1.3 Discrete histology and distribution of BCP and CPP deposits in OA cartilage

Morphological studies on cartilage calcification are limited and mostly focus on a singular crystal type. Histologically, CPP is frequently determined on the basis of birefringence under polarized light [176] even though it has become clear that a majority of CPP crystals lack this birefringent appearance [99, 178]. Histomorphological studies on cartilage calcification often lack crystal determination altogether. Therefore, this thesis directly compared the histomorphology and distribution of BCP and CPP in cartilage at different magnifications, using both light microscopy and SEM imaging. This approach revealed distinct von Kossa patterns for BCP and CPP in cartilage that were reflected by SEM imaging. BCP presented as spherical, rather smooth deposits that were loosely attached to the surface (Figure 3.1.4A, Figure 3.1.5A). This observation is supported by earlier electron microscopy studies, describing BCP deposits as irregular clumps on the surface [179] and highlights the relevance of BCP over CPP in superficial cartilage damage. In fact, severe CPP deposition has been observed in cartilage with a smooth surface [180]. BCP also accumulated around hypertrophic chondrocytes in the deep zone (Figure 3.1.4A-B), reinforcing its association with chondrocyte hypertrophy [181]. In view of this localization, apoptosis has been suggested as a mechanism for BCP deposition before. Apoptotic chondrocytes in the deep zone release apoptotic bodies that increase towards the subchondral bone and co-localize with BCP deposition [182]. These apoptotic bodies can accumulate calcium and phosphate ions, providing nucleation centers for BCP crystals [42, 53, 182].

In contrast, CPP deposition was limited to the superficial and intermediate zone. Dating back to early SEM and transmission electron microscopy studies, this peculiar location of CPP in the middle cartilage

zone has been reported before. While some of these studies observed CPP deposition adjacent to chondrocytes in areas with a high content of poorly organized collagen [183], others detected it independent of collagen [184, 185]. Early CPP deposition is described as scattered needle-shaped crystals [186]. These were already visible at low magnifications on von Kossa stained cartilage (Figure 3.1.4C). These granular clusters seem to condense to focal deposits distinctively outlined from the surrounding matrix, replacing resident chondrocytes [185, 187]. Consistently, dense CPP pockets were observed adjacent to clusters of dispersed CPP crystals (Figure 3.1.2B). Reportedly, linear CPP deposits are oriented parallel to the cartilage surface [188], presumably following the orientation of collagen fibers [189]. In line with this, superficial deposits aligned parallel to the cartilage surface while deeper CPP deposits showed a perpendicular orientation (Figure 3.1.4). This pattern matches the orientation of the collagen fibers in intermediate and superficial cartilage zones (Figure 1.2.2). A more recent study by Nguyen and colleagues found no difference in the crystal content between superficial and deep zone [104]. However, that study combined superficial and deep layers of the medial and lateral tibio-femoral compartment, while the present study focussed on the primarily affected tibial compartment.

Despite their frequent coexistence in the same sample, BCP and CPP were never observed in the same cartilage zone (Figure 3.1.4). A similar spatial separation of BCP and CPP deposition has been mentioned before [65, 180], suggesting distinct underlying etiologies.

4.2 Upregulated extracellular PPI metabolism as a driver of BCP deposition in OA cartilage

4.2.1 Upregulated gene expression of PPI metabolism enzymes in BCP-calcified cartilage

With the aim of elucidating the calcification process, I investigated the extracellular PPI metabolism as a regulator of local extracellular Pi and PPI. Therefore, gene expression of PPI metabolism enzymes were measured in cartilage in respect to calcification. TNAP, CD73, ENPP1 and ANKH were considerably upregulated in calcified over non-calcified cartilage (Figure 3.2.1A, B, D and E). Many of these enzymes have been more or less extensively studied in the context of calcification, often without specifying involved crystal types. The strength of this thesis represents the differentiation of crystal types within calcified cartilage. With this information, expression levels CD73 and ANKH were found to be upregulated in both BCP- and CPP-calcified cartilage (Figure 3.2.2B and E). Gain-of-function mutations in the ANKH gene are known to elevate extracellular PPI levels and promote CPP deposition [88], supporting the upregulated ANKH expression in CPP-calcified cartilage (Figure 3.2.2E). Surprisingly, BCP-calcified cartilage displayed a similarly upregulated ANKH expression. Recent evidence proposed a non PPI-transporter role for ANKH. ANKH also seems to interact with the phosphate transporter PiT-1 expression [190, 191], allowing a potential role in BCP deposition. In addition, ANKH mediates ATP efflux independent of extracellular PPI [129]. During chondrogenesis, ANKH expression and function seems to require phosphate and calcium [190], further supporting a potential role in BCP calcification.

CD73 is mostly studied in vascular calcification so data on its role in articular calcification is still missing. In aortic calcification, high CD73 rather than CD39 expression has been reported [192], supporting the upregulation of CD73 but not CD39 expression in calcified cartilage. Via conversion of AMP into adenosine and Pi, CD73 likely promotes BCP deposition by elevating Pi levels [136]. In contrast, adenosine is known to inhibit TNAP [132]. Thus, CD73 could possibly be involved in CPP formation by inhibiting TNAP-mediated hydrolysis of PPi to Pi.

Most importantly, elevated expression of TNAP and ENPP1 was specific to BCP-calcified cartilage (Figure 3.2.2A and D). Both of these enzymes have been extensively studied in the context of OA and ectopic calcification. Mutations in ENPP1 and TNAP are the cause of various inherited calcification disorders [137, 193, 194]. ENPP1 expression shows a negative correlation with cartilage calcification and OA severity [195], while ENPP1 deficiency promotes OA progression [196]. These protective effects are likely based on the ENPP1-mediated elaboration of PPi that subsequently inhibits BCP formation. Therefore, ENPP1 holds a reputation as an inhibitor of BCP calcification. Paradoxically, ENPP1 expression was upregulated in BCP-calcified (Figure 3.2.2D). In fact, there is evidence linking ENPP1 to BCP formation. For instance, ENPP1 overexpression promoted osteoblast differentiation *in vitro* [197]. In meniscal fibrochondrocytes, upregulated ENPP1 expression induced BCP matrix calcification [198], possibly through increased downstream breakdown of PPi by TNAP. Consistently, TNAP expression was also upregulated in BCP-calcified cartilage here (Figure 3.2.2A). Overexpression of TNAP has been linked to calcification *in vivo* [199] and BCP formation *in vitro* [104, 200] and was accompanied by elevated CD73 expression [104]. TNAP expression also stimulated transdifferentiation of synovial fibroblasts and vascular smooth muscle cells into mineralizing cells [200, 201].

4.2.2 Upregulated TNAP activity and Pi levels in BCP-calcified cartilage

In OA cartilage, TNAP expression has been located in the upper zone [202], matching the superficial location of BCP deposits (Figure 3.1.4A, Figure 3.1.5A). Likewise, TNAP activity was upregulated in BCP-, but not CPP-calcified cartilage (Figure 3.2.3B). Upregulated TNAP activity has also been detected in mineralizing growth plate and hypertrophic OA chondrocytes [203, 204]. Yet, data on TNAP activity in human OA cartilage, particularly in the context of crystal-specific calcification remains limited. One of the few studies in this context localized high TNAP activity in the deep zone of OA cartilage [205], corresponding to diffuse BCP deposition around chondrocytes observed here (Figure 3.1.4A, Figure 3.1.5A). As the main product of TNAP, Pi was also upregulated in BCP-calcified cartilage, correlating with TNAP activity (Figure 3.2.3D and G). This was accompanied by an increased Pi/PPi ratio (Figure 3.2.3E), favouring BCP formation [126].

Increased ENPP1 activity is known to cause CPP deposition via excess PPi liberation from ATP [206]. Against expectation, CPP-calcified cartilage was not associated with elevated ENPP1 activity or PPi concentration. Instead, ENPP1 activity and PPi levels were comparable in calcified and non-calcified cartilage regardless of crystal type. This lack of effect may be ascribed to the limited number of exclusively CPP-calcified cartilage samples, especially in comparison to BCP-calcified samples.

Samples containing both crystals were excluded from these analyses to isolate crystal-specific effects. Thereby, detection of smaller effects may require larger sample numbers.

Further, total Pi and PPI concentrations were measured here, whereas specifically the extracellular ratio of these ions proposedly regulates cartilage calcification. While extracellular ion levels are easily detected in fluids or cell culture, tissue measurements remain challenging.

In the context of articular calcification, PPI concentrations are usually measured in synovial fluid. Healthy synovial fluid contains PPI in a narrow range of $10 \pm 0.5 \mu\text{M}$ [207], while its concentration is significantly elevated in synovial fluid of CPP-calcified joints [208, 209]. For Pi and PPI levels in cartilage, reference values are missing. Similarly, enzymatic expression and activity were measured in full thickness cartilage, possibly concealing small, local changes. Indeed, there is evidence for variations in mineralisation potential for chondrocytes of different cartilage zones. Superficial zone chondrocytes seem to calcify less than deep zone chondrocytes and display lower TNAP activity [210]. Colorimetric assays like those applied here are based on the conversion of synthetic substrates, producing a colorimetric signal. This is a standard and widely applied method to measure phosphatase activity. However, their specificity and sensitivity have been criticized by some authors. Thus, in recent years, new detection approaches have been proposed, including fluorescence or nano-based strategies [211], which may be useful to validate the current data.

In combination with the spatial separation of BCP and CPP in the same sample, these findings suggest that calcification may be regulated by a very localized microenvironment. Considering its peculiar localization, CPP deposition in particular may be under tight spatial limitation. In line with this, *in vitro* CPP calcification was associated with a very localized increase in PPI [212]. Thus, investigating the spatial expression of PPI metabolism enzymes may be of great value for future research. Future studies may also consider enzymatic interactions for a more comprehensive insight into calcification as a multifactorial process. For instance, TNAP is able co-localize with ENPP1 and reduce ENPP1-mediated PPI formation [213]. This could explain the comparable ENPP1 activity and PPI levels in calcified and non-calcified cartilage (Figure 3.2.3A and C). Conversely, ENPP1 deficiency fully inhibited *in vitro* calcification even under supplementation with Pi [197]. Double-knock out of TNAP and ENPP1 in mice did not disrupt skeletal mineralization [213], suggesting a tight counterbalance of both enzymes in regulating calcification. Thus, elevated ENPP1 expression in BCP-calcified cartilage may serve to compensate for TNAP upregulation in an attempt to restore a balance between both enzymes.

Collectively, these findings show that BCP deposition in cartilage is driven by an imbalance in the extracellular PPI metabolism. Specifically, upregulated TNAP activity and an elevated Pi/PPI ratio favour the formation of BCP crystals. CPP deposition instead cannot fully be explained by a dysregulated PPI metabolism, suggesting other or additional mechanism.

4.3 Intracellular and ATP-dependent induction of CPP deposition

4.3.1 ATP stimulation induces CPP formation *in vitro*

In a prospective approach to calcification, I aimed to characterize the mechanism of CPP deposition. To do so, chondrocytes isolated from BCP and CPP-calcified cartilage were stimulated to calcify by supplementation with calciprotein particles or ATP. Calciprotein particles are amorphous calcium phosphate precursors and are used in short-term calcification assays, inducing *in vitro* calcification within 24h [139]. They can also promote transdifferentiation into mineralizing cells [214]. Consistently, calciprotein particles induced BCP deposition by both BCP- and CPP-chondrocytes (Figure 3.3.1A-B). Considering BCP as the mineral of the calcified cartilage zone and its common physiological deposition during endochondral ossification [215], chondrocytes may have the inherent ability to precipitate BCP.

The role of ATP in calcification appears to be more controversial. While ATP inhibited calcification in canine tenocytes [216], it stimulated calcification in meniscal fibrochondrocytes [101]. In fact, a more recent study demonstrated bivalent effects of ATP on calcification [217]. While promoting calcification at low concentrations, ATP seems to inhibit it at high concentrations. Unfortunately, these studies did not determine the calcification type, a common limitation in calcification studies. Upon ATP stimulation, I detected CPP crystals in chondrocytes from CPP-calcified cartilage (Figure 3.3.1B). This observation is consistent with ATP being the main source of extracellular PPi [218]. Similarly, ATP induced CPP formation in matrix vesicles, while the absence of ATP resulted in BCP formation [203]. CPP-calcified joints also showed high synovial fluid levels of ATP that correlated with PPi concentration [219].

In addition to CPP crystals, CPP-chondrocytes also precipitated BCP crystals in response to ATP. In contrast, chondrocytes from BCP-calcified cartilage merely produced BCP (Figure 3.3.1). As ATP can also be metabolized to Pi, BCP formation is not unlikely. In the presence of a collagen matrix, ATP stimulated BCP precipitation via rapid Pi release [220, 221], suggesting that the local enzymatic environment may determine the preferred crystal type that is formed. In addition, ATP is essential for the phosphorylation of ECM proteins that facilitates their function as nucleation centers [220]. The universal detection of BCP during *in vitro* calcification supports the hypothesis of an inherent BCP-forming ability of chondrocytes. The ability for CPP formation instead seems to be conserved in cartilage and isolated chondrocytes, hinting at a cell-intrinsic mechanism for CPP calcification.

Topologically, BCP deposits also appeared to sit on top of the chondrocyte monolayer attached to the cells. This observation is consistent with BCP deposition being driven by a dysregulated extracellular PPi metabolism discussed in the previous chapter. In contrast, CPP appeared as individual crystals. These often seem to be located inside the cells, possibly suggesting an intracellular source of CPP. An intracellular mechanism of CPP formation may explain why CPP deposition in cartilage could not be explained by a dysregulated extracellular PPi metabolism. In line with this, CPP stimulation decreased mitochondrial membrane potential, resulting in reactive oxygen species (ROS) generation and ATP release [222, 223]. Conversely, exogenous ATP has been shown to induce oxidative stress, premature

senescence and oscillations in intracellular calcium levels [224, 225], supporting the proposed link of CPP deposition and chondrocyte senescence [78].

4.3.2 CPP calcification is associated with elevated levels of senescence-associated cytokines in synovial fluid

In chondrocytes, a majority of ATP is produced in mitochondria, creating ROS in the process [226]. A dysbalance of ATP and ROS formation drives OA progression and induces chondrocyte senescence [227, 228]. Senescence is common process in OA cartilage and correlates with disease severity [82]. Importantly, senescence has also been implicated in the calcification of OA chondrocytes, inducing crystal production, which further drives ROS generation [229, 230]. In view of this link, I measured a panel of inflammatory mediators in the context of cartilage calcification, comparing the effect of BCP and CPP cartilage calcification on the joint environment. Specifically, I measured various senescence-associated cytokines, chemokines and growth factors in synovial fluid in BCP- versus CPP-calcified joints. Crystal-type specific concentrations of these factors in synovial fluid have not been compared before. Synovial fluid of CPP-calcified joints demonstrated increased levels of pro-inflammatory cytokines (IL-15, GM-CSF) (Figure 3.3.2A), growth factors (PDGF-AB/BB, VEGF) (Figure 3.3.2C) and chemokines (MIP-1b) (Figure 3.3.2D). These factors are part of the characteristic SASP and are commonly secreted by senescent cells [231]. Of interest, many of these factors have also been linked to calcification, albeit mostly to vascular calcification [232]. MIP-1b for example is secreted by senescent vascular smooth muscle cells [233], contributing to atherosclerosis. Conversely, some of these factors are produced upon calcium crystal exposure. For instance, serum MIP-1b levels are increased in coronary artery calcification [234] and BCP crystals induce MIP-1b secretion *in vitro* [235]. Similarly, VEGF secreted by chondrocytes stimulated vascular smooth muscle cell calcification *in vitro* [236]. In addition, VEGF was highly expressed in atherosclerotic lesions [237]. GM-CSF expression is reportedly promoted by CPP crystals [238]. Recently, cerebrovascular calcification has been associated with elevated PDGF-BB serum levels in aging mice. Moreover, PDGF-BB promoted osteogenic differentiation and phosphate transporter PiT-1 expression in cerebral microvasculature [239]. PDGF-BB was also able to promote ROS generation by elevating cellular calcium homeostasis [240]. This way, PDGF-BB may advance both senescence and calcification.

IL-15 is an important cytokine for skeletal mineralization, impairing osteoblast function and bone mineralization when deficient [241]. Interestingly, IL-15 stimulated the release of proteases [242] and correlated with pain and OA severity [243]. Unfortunately, none of these studies identified involved crystal types. An involvement of MIP-1b, VEGF or PDGF-AB/BB in articular calcification has not been assessed yet. Thus, upregulated synovial fluid levels of MIP-1b, GM-CSF, VEGF and PDGF-AB/BB in CPP-calcified joints may be the first evidence for their involvement in CPP deposition.

These findings suggest CPP-calcified cartilage as a potential source for elevated synovial fluid cytokine concentrations. Accordingly, chondrocytes are known to release pro-inflammatory cyto- and chemokines [244] and ROS into synovial fluid, driving cartilage senescence and degradation [245, 246]. Abreu and colleagues found an increased frequency of CPP deposition in areas of direct contact with

synovial fluid (e.g. hyaline cartilage) compared to areas without (e.g. tendons and ligaments) [148]. Conversely, CPP crystals induced chondrocytes senescence *in vitro* [78, 247]. Recent studies established a link between chondrocyte calcification and senescence via Krüppel-like factor 10 (Klf10). *In vitro*, Klf10 knockdown ameliorated chondrocyte calcification, dysfunctional mitochondrial ATP synthesis and senescence by inhibiting ROS production [247, 248]. *In vivo*, Klf10 knockdown attenuated cartilage senescence, calcification and degeneration [247]. Another study identified increased expression of sortilin and alkaline phosphatase during chondrocyte senescence and calcification [249]. Thus, elevated synovial fluid levels of IL-7, IL-15, GM-CSF, PDGF-AB/BB and MIP-1b in CPP-calcified joints may indicate increased articular senescence.

Surprisingly, CPP-calcified joints also showed elevated levels of the anti-inflammatory cytokines IL-1ra and IL-10 (Figure 3.3.2B). These findings contrast the reportedly higher inflammatory potential of CPP over BCP crystals *in vitro* [250] that has been ascribed to their sharp needle-like morphology [251]. Instead, both IL-1ra and IL-10 [252] ameliorate calcification in cartilage [253] and vasculature [254, 255]. On the other hand, BCP [251, 256] and CPP [257, 258] crystals can induce their release. Thus, increased levels of IL-10 and IL-1ra in synovial fluid may serve to antagonize the high concentrations of pro-inflammatory factors.

Sample number restrictions for SASP profiling only enabled the comparison of synovial fluid samples of BCP and CPP calcified joints, excluding non-calcified joints for reference. The BCP group included more samples than the CPP group. Further, sample collection was limited to the time of joint replacement, enabling only a single measurement per patient. This makes it difficult to determine a causation chain. Thus, it remains unclear whether upregulated cytokine levels in synovial fluid precede or follow calcification. In addition, the extend of senescence in corresponding cartilage samples was not measured here. As senescence and the characteristic secretion of SASP factor is common in OA cartilage [82, 259] and OA chondrocytes frequently secrete SASP factors, elevated cytokine levels observed in CPP-calcified joints may indicate increased senescence.

4.3.3 Intracellular CPP deposition is accompanied by elevated PPI levels in meniscal fibrochondrocytes

While BCP deposition is driven by a dysregulated extracellular PPI metabolism in favor of Pi, CPP appears to be linked to increased senescence, a largely internal process. In favor of an intracellular origin of CPP formation, spontaneous CPP calcification densely accumulated inside the cytoplasm of meniscal fibrochondrocytes (Figure 3.3.3B). *In vitro*, CPP crystals inside chondrocytes have been reported before, although in very few numbers [260]. While literature predominantly localizes CPP in the extracellular space, there is some evidence for an intracellular CPP formation site. Vijen and colleagues identified ANKH mutants with intracellular location [261]. Overexpression of these mutants decreased extracellular PPI while still promoting calcification. Unfortunately, the type and cellular location of these calcifications were not specified.

Intracellular CPP deposition in meniscal fibrochondrocytes was accompanied by increased intracellular PPI but not Pi levels (Figure 3.3.3C-D) and a decreased Pi/PPI ratio (Figure 3.3.3F). *In vitro*, elevated PPI levels were measured in chondrocytes [262] and fibroblasts [263] of patients with hereditary CPPD before, although not in combination with an evident intracellular CPP deposition as observed here. Thus, decades ago, speculations on an intracellular PPI overproduction emerged [263]. Accordingly, a case report from 1995 described a patient with temporomandibular joint calcification showing intracellular and intra-mitochondrial CPP deposition [260]. However, subsequent research exclusively focussed on extracellular PPI metabolism. Hence, there is much less known about intracellular than extracellular PPI metabolism. For instance, ENPP1 is mostly studied as part of the extracellular PPI metabolism, but appears to also have intracellular effects. Overexpression of ENPP1 or its isoform ENPP2 increased intracellular PPI in chondrocytes, while extracellular PPI was only affected by ENPP1 [264, 265].

In fact, the large majority of PPI production takes place in mitochondria inside the cell [266, 267]. The extracellular PPI metabolism belongs to the few extra-mitochondrial mechanism of PPI synthesis [268]. Due to charge and polarity, PPI cannot diffuse across cellular membranes, requiring specialized transporters or channels for externalization [269]. Alternatively, PPI can be hydrolysed to Pi by cytosolic inorganic pyrophosphatases. These are reportedly involved in calcification of osteoblasts, without affecting extracellular PPI levels [270]. Thereby, dysregulation of these gatekeepers of intracellular PPI may cause a build-up and local supersaturation of PPI in the cytoplasm, potentially predisposing this site for CPP formation. Additionally, mitochondria contain high levels of calcium and are known to mineralize during bone formation in the growth plate [271]. Growth plate chondrocytes also contain high levels of Pi that can precipitate to amorphous calcium phosphate upon mitochondrial calcium release [272, 273]. In a similar manner, intracellular PPI may cause CPP formation inside the cell, especially considering that cellular senescence is accompanied by a cytosolic calcium overload [274].

Further, CPP crystals have membranolytic effects via disintegration and local thinning of the phospholipid bilayer [275]. The irregular sharp-edged morphology of CPP (Figure 3.1.5B) and their high negative surface charge probably contributes to the membranolytic properties of CPP [275]. Crystals with smoother and less negative surfaces such as BCP appear to be less membranolytic [275, 276]. Thereby, intracellular CPP deposition may cause affected cells to rupture and release their crystal content. This could explain the occasional finding of extracellular crystals (Figure 3.3.3B). Morphological studies further found a preferred deposition of CPP around cellular debris [180, 277], possibly representing remnants of ruptured cells. Within a collagenous ECM, extracellular CPP may subsequently accumulate and grow along collagen fibers [189].

The main limitation of this study poses the small number of samples, particularly those containing intracellular CPP crystals. To confirm the existence of an intracellular CPP formation, further validation is needed, e.g. by expanding the sample size to increase statistical power. The present study was also limited to Pi and PPI measurements. Thus, it would be interesting to consider intracellular calcium or senescence markers in following experiments. In addition, assessing mitochondrial activity in the

presence of intracellular CPP crystals could be a next step to identify underlying intracellular calcification pathways.

5 Conclusion and Outlook

This is the first study to characterize and directly compare BCP and CPP calcification in cartilage, assessing distribution, morphology and formation processes. With the combination of histological von Kossa staining with spectroscopic Raman analysis, this thesis established a simple and convenient protocol for detection and characterization of articular calcification.

Thereby, BCP was determined as the predominant crystal type in calcified OA cartilage, located superficially and in the deep zone. Mechanistically, BCP precipitates outside of chondrocytes driven by a dysregulation of the extracellular PPI metabolism. Particularly, BCP deposition is favored by elevated TNAP activity and Pi content. Instead, CPP deposition is far less common and often accompanied by BCP. Topologically, CPP deposits are limited to the intermediate cartilage zone and seem to be associated with increased senescence. The underlying mechanisms of this association could not be answered in this thesis and require further investigation. The peculiar location of BCP and CPP in cartilage could not be addressed here either and may depend on spatial omics techniques to be answered.

For the first time, excessive cytoplasmic CPP deposition in combination with elevated intracellular PPI was observed, suggesting the existence of an intracellular formation. Thereby, this thesis provides new evidence for the understudied hypothesis of an intracellular CPP formation pathway. However, the underlying mechanisms of how CPP may form inside the cell remain open and require further research. This work also indicates increased senescence in calcified OA joints. Detailed comparison of the senescent state of CPP- against BCP-calcified cartilage in future studies may help to unravel its role in the calcification process.

Taken together, this study demonstrates an extracellular deposition of BCP in articular cartilage driven by elevated TNAP activity and Pi, while providing evidence for an intracellular CPP formation pathway.

6 Abbreviations

ABCC6	ATP-binding cassette subfamily C number 6
ADP	Adenosine diphosphate
AMP	Adenosine monophosphate
ANKH	Progressive ankylosis homolog
ANOVA	Analysis of variance
ATP	Adenosine triphosphate
BCP	Basic calcium phosphate
°C	Degrees Celsius
CaCl ₂	Calcium chlorid
CC	Chondrocalcinosis
CD	Cluster of differentiation
cDNA	Complementary deoxyribonucleic acid
cm ⁻¹	Wavenumber
CPP	Calcium pyrophosphate dihydrate
CPPD	Calcium pyrophosphate dihydrate deposition disease
Ca/P	Calcium phosphate
d	Days
dH ₂ O	Distilled water
dNTP	Deoxyribonucleotide triphosphate
DMEM	Dulbeco's modified eagle medium
DNA	Deoxyribonucleic acid
ECM	Extracellular matrix
EDTA	Ethylenediaminetetraacetic acid
EDS	Energy-dispersive X-ray spectroscopy
ENPP1	Ectonucleotide pyrophosphatase/phosphodiesterase 1
EULAR	European League Against Rheumatism
f	Female
FBS	Fetal bovine serum
FLT3	Fms-like tyrosine kinase 3
g	Gravity
GACI	Generalized arterial calcification of infancy
GAPDH	Glyceraldehyd-3-phosphate-dehydrogenase
GM-CSF	Granulocyte-macrophage colony stimulating factor
GRO	Growth-regulated protein
HA	Hydroxyapatite
HEPES	4-(2-hydroxyethyl)-1-piperazineethanesulfonic acid
h	Hours
IL	Interleukin

IL-1ra	Interleukin-1 receptor antagonist
IRB	Institutional Review Board
KL	Kellgren Lawrence
Klf10	Krüppel-like factor 10
kV	Kilovolt
m	Male
MgCl ₂	Magnesium dichloride
mg	Milligram
min	Minutes
MIP	Macrophage inflammatory protein
mL	Milliliter
mM	Millimolar
mm	Millimeter
MMP	Matrix metalloproteinase
ms	Milliseconds
mW	Milliwatt
NGP	Non-collagenous protein
nm	Nanometer
OA	Osteoarthritis
OARSI	Osteoarthritis Research Society International
PBS	Phosphate buffered saline
PDGF-AB/BB	Platelet-derived growth factor AB/BB
Pi	Inorganic phosphate
PiT	Inorganic phosphate transporter
PNTM	Thymidine monophosphate nitrophenyl ester
PPi	Inorganic pyrophosphate
PXE	Pseudoxanthoma elasticum
r	Pearson correlation coefficient
qRT-PCR	Quantitative reverse transcription polymerase chain reaction
RNA	Ribonucleic acid
ROI	Region of interest
ROS	Reactive oxygen species
rpm	Revolutions per minute
RT	Reverse transcription
SASP	Senescence associated secretory phenotype
s	Seconds
SE	Secondary electron
SEM	Scanning electron spectroscopy
TNAP	Tissue non-specific alkaline phosphatase
Tris	Trisaminomethane

U	Units
VEGF	Vascular endothelial growth factor
Wnt	Wingless-related integration site
μg	Microgram
μL	Microliter
μm	Micrometer
μM	Micromolar

7 List of Figures

Figure 1.1.1: Kellgren Lawrence grading system.	1
Figure 1.2.1: Structural changes during OA.	2
Figure 1.2.2: Zonal structure of articular cartilage.	4
Figure 1.4.1: Different imaging methods for the detection of articular calcification.	9
Figure 1.5.1: Calcium crystal formation is determined by extracellular phosphate (Pi) and pyrophosphate (PPi) ions.	12
Figure 3.1.1: Demographic information of the patient cohort and radiological detection of articular calcification.	30
Figure 3.1.2: Histological detection of articular calcification.	31
Figure 3.1.3: Identification of calcium crystals in cartilage by Raman spectroscopy.	32
Figure 3.1.4: Histological presentation of BCP and CPP deposition in articular cartilage.	33
Figure 3.1.5: Scanning electron imaging and energy dispersive X-ray spectroscopy (SEM-EDS) of cartilage calcifications.	34
Figure 3.2.1: Gene expression of PPi metabolism enzymes in cartilage in the presence (+) compared to the absence (-) of histological calcification.	35
Figure 3.2.2: Gene expression of PPi metabolism enzymes in cartilage classified by the type of calcification in the tissue.	37
Figure 3.2.3: TNAP and ENPP1 activity and concentrations of Pi and PPi in articular cartilage	38
Figure 3.3.1: In vitro calcification of human primary chondrocytes stimulated with calciprotein particles or ATP.	39
Figure 3.3.2: Synovial fluid concentrations of senescence-associated mediators classified by the crystal type detected in corresponding cartilage tissue.	41
Figure 3.3.3: Intracellular CPP deposition in meniscal fibrochondrocytes with von Kossa staining of corresponding menisci.	43

8 List of Tables

Table 1: List of instruments and equipment.	15
Table 2: List of reagents and manufacturer.	16
Table 3: List of consumables and manufacturer.	17
Table 4: List of kits and enzymes.	18
Table 5: Human primer sequences.	18
Table 6: List of buffers and solutions with ingredients.	19
Table 7: Reverse transcription master mix.	22
Table 8: Step-wise qRT-PCR protocol.	22
Table 9: Master mix for quantitative RT-PCR.	23

9 References

1. Coaccioli S, Sarzi-Puttini P, Zis P, Rinonapoli G, Varrassi G. Osteoarthritis: New Insight on Its Pathophysiology. *Journal of clinical medicine*. 2022;11(20).
2. Steinmetz JD, Culbreth GT, Haile LM, Rafferty Q, Lo J, Fukutaki KG, et al. Global, regional, and national burden of osteoarthritis, 1990–2020 and projections to 2050: a systematic analysis for the Global Burden of Disease Study 2021. *The Lancet Rheumatology*. 2023;5(9):e508-e22.
3. WHO. Osteoarthritis World Health Organization: World Health Organization; 2023 [updated 14.07.23; cited 2024 03.06.24]. Available from: <https://www.who.int/news-room/fact-sheets/detail/osteoarthritis#:~:text=Osteoarthritis%20is%20a%20degenerative%20joint,%2C%20hips%2C%20spine%20and%20hands.>
4. Shentu C-Y, Yan G, Xu D-C, Chen Y, Peng L-H. Emerging pharmaceutical therapeutics and delivery technologies for osteoarthritis therapy. *Frontiers in Pharmacology*. 2022;13.
5. Zhang W, Doherty M, Peat G, Bierma-Zeinstra MA, Arden NK, Bresnihan B, et al. EULAR evidence-based recommendations for the diagnosis of knee osteoarthritis. *Annals of the rheumatic diseases*. 2010;69(3):483.
6. Garifallia S, Philip GC, Weiya Z, Johannes WJB, Pernille B, Maria Antonietta D, et al. EULAR recommendations for the use of imaging in the clinical management of peripheral joint osteoarthritis. *Annals of the rheumatic diseases*. 2017;76(9):1484.
7. Bedson J, Croft PR. The discordance between clinical and radiographic knee osteoarthritis: a systematic search and summary of the literature. *BMC Musculoskelet Disord*. 2008;9:116.
8. Kellgren JH, Lawrence JS. Radiological assessment of osteo-arthrosis. *Annals of the rheumatic diseases*. 1957;16(4):494-502.
9. Kohn MD, Sassoon AA, Fernando ND. Classifications in Brief: Kellgren-Lawrence Classification of Osteoarthritis. *Clin Orthop Relat Res*. 2016;474(8):1886-93.
10. Pi S-W, Lee B-D, Lee MS, Lee HJ. Ensemble deep-learning networks for automated osteoarthritis grading in knee X-ray images. *Scientific Reports*. 2023;13(1):22887.
11. Vaienti E, Scita G, Ceccarelli F, Pogliacomì F. Understanding the human knee and its relationship to total knee replacement. *Acta Biomed*. 2017;88(2s):6-16.
12. Tamer TM. Hyaluronan and synovial joint: function, distribution and healing. *Interdisciplinary toxicology*. 2013;6(3):111-25.
13. Wilkinson LS, Pitsillides AA, Worrall JG, Edwards JC. Light microscopic characterization of the fibroblast-like synovial intimal cell (synoviocyte). *Arthritis and rheumatism*. 1992;35(10):1179-84.
14. Smith MD. The normal synovium. *Open Rheumatol J*. 2011;5:100-6.
15. Loeuille D, Chary-Valckenaere I, Champigneulle J, Rat AC, Toussaint F, Pinzano-Watrin A, et al. Macroscopic and microscopic features of synovial membrane inflammation in the

- osteoarthritic knee: correlating magnetic resonance imaging findings with disease severity. *Arthritis and rheumatism*. 2005;52(11):3492-501.
16. Benito MJ, Veale DJ, FitzGerald O, van den Berg WB, Bresnihan B. Synovial tissue inflammation in early and late osteoarthritis. *Annals of the rheumatic diseases*. 2005;64(9):1263-7.
 17. Chou CH, Jain V, Gibson J, Attarian DE, Haraden CA, Yohn CB, et al. Synovial cell cross-talk with cartilage plays a major role in the pathogenesis of osteoarthritis. *Sci Rep*. 2020;10(1):10868.
 18. Blom AB, van Lent PL, Libregts S, Holthuysen AE, van der Kraan PM, van Rooijen N, et al. Crucial role of macrophages in matrix metalloproteinase-mediated cartilage destruction during experimental osteoarthritis: involvement of matrix metalloproteinase 3. *Arthritis and rheumatism*. 2007;56(1):147-57.
 19. Wenham CY, Conaghan PG. The role of synovitis in osteoarthritis. *Ther Adv Musculoskelet Dis*. 2010;2(6):349-59.
 20. Sanchez-Lopez E, Coras R, Torres A, Lane NE, Guma M. Synovial inflammation in osteoarthritis progression. *Nature reviews Rheumatology*. 2022;18(5):258-75.
 21. Reimann I, Arnoldi CC, Nielsen OS. Permeability of synovial membrane to plasma proteins in human coxarthrosis: relation to molecular size and histologic changes. *Clin Orthop Relat Res*. 1980(147):296-300.
 22. Myers SL, Brandt KD, Eilam O. Even low-grade synovitis significantly accelerates the clearance of protein from the canine knee: implications for measurement of synovial fluid "markers" of osteoarthritis. *Arthritis & Rheumatism*. 1995;38(8):1085-91.
 23. Worrall JG, Bayliss MT, Edwards JC. Morphological localization of hyaluronan in normal and diseased synovium. *The Journal of rheumatology*. 1991;18(10):1466-72.
 24. Lu Y, Levick J, Wang W. *The Mechanism of Synovial Fluid Retention in Pressurized Joint Cavities*. *Microcirculation* (New York, NY : 1994). 2005;12:581-95.
 25. Ludwig TE, Hunter MM, Schmidt TA. Cartilage boundary lubrication synergism is mediated by hyaluronan concentration and PRG4 concentration and structure. *BMC Musculoskelet Disord*. 2015;16:386.
 26. Carlson AK, Rawle RA, Wallace CW, Brooks EG, Adams E, Greenwood MC, et al. Characterization of synovial fluid metabolomic phenotypes of cartilage morphological changes associated with osteoarthritis. *Osteoarthritis and cartilage*. 2019;27(8):1174-84.
 27. Homandberg GA, Wen C, Hui F. Cartilage damaging activities of fibronectin fragments derived from cartilage and synovial fluid. *Osteoarthritis and cartilage*. 1998;6(4):231-44.
 28. Yasuda T, Poole AR. A fibronectin fragment induces type II collagen degradation by collagenase through an interleukin-1-mediated pathway. *Arthritis and rheumatism*. 2002;46(1):138-48.
 29. Mendler M, Eich-Bender SG, Vaughan L, Winterhalter KH, Bruckner P. Cartilage contains mixed fibrils of collagen types II, IX, and XI. *The Journal of cell biology*. 1989;108(1):191-7.

30. Hsueh MF, Khabut A, Kjellström S, Önnerfjord P, Kraus VB. Elucidating the Molecular Composition of Cartilage by Proteomics. *J Proteome Res.* 2016;15(2):374-88.
31. Matzat SJ, van Tiel J, Gold GE, Oei EH. Quantitative MRI techniques of cartilage composition. *Quant Imaging Med Surg.* 2013;3(3):162-74.
32. Johnson K, Svensson CI, Etten DV, Ghosh SS, Murphy AN, Powell HC, et al. Mediation of spontaneous knee osteoarthritis by progressive chondrocyte ATP depletion in Hartley guinea pigs. *Arthritis & Rheumatism.* 2004;50(4):1216-25.
33. Sophia Fox AJ, Bedi A, Rodeo SA. The basic science of articular cartilage: structure, composition, and function. *Sports Health.* 2009;1(6):461-8.
34. Youn I, Choi JB, Cao L, Setton LA, Guilak F. Zonal variations in the three-dimensional morphology of the chondron measured in situ using confocal microscopy. *Osteoarthritis and cartilage.* 2006;14(9):889-97.
35. Moger CJ, Barrett R, Bleuet P, Bradley DA, Ellis RE, Green EM, et al. Regional variations of collagen orientation in normal and diseased articular cartilage and subchondral bone determined using small angle X-ray scattering (SAXS). *Osteoarthritis and cartilage.* 2007;15(6):682-7.
36. Havelka S, Horn V, Spohrová D, Valouch P. The calcified-noncalcified cartilage interface: the tidemark. *Acta Biol Hung.* 1984;35(2-4):271-9.
37. Brose T, Kubosch E, Schmal H, Stoddart M, Armiento A. Crosstalk Between Mesenchymal Stromal Cells and Chondrocytes: The Hidden Therapeutic Potential for Cartilage Regeneration. *Stem Cell Reviews and Reports.* 2021;17:1-19.
38. Salminen H, Vuorio E, Säämänen AM. Expression of Sox9 and type IIA procollagen during attempted repair of articular cartilage damage in a transgenic mouse model of osteoarthritis. *Arthritis and rheumatism.* 2001;44(4):947-55.
39. Stolz M, Gottardi R, Raiteri R, Miot S, Martin I, Imer R, et al. Early detection of aging cartilage and osteoarthritis in mice and patient samples using atomic force microscopy. *Nature Nanotechnology.* 2009;4(3):186-92.
40. Kirsch T, von der Mark K. Remodelling of collagen types I, II and X and calcification of human fetal cartilage. *Bone Miner.* 1992;18(2):107-17.
41. Li G, Zhang M, Huang Y, Yang J, Dong L, Shi H, et al. The relationship between abnormal Core binding factor- β expression in human cartilage and osteoarthritis. *BMC Musculoskelet Disord.* 2021;22(1):174.
42. Hashimoto S, Ochs RL, Rosen F, Quach J, McCabe G, Solan J, et al. Chondrocyte-derived apoptotic bodies and calcification of articular cartilage. *Proceedings of the National Academy of Sciences.* 1998;95(6):3094.
43. Hwang HS, Kim HA. Chondrocyte Apoptosis in the Pathogenesis of Osteoarthritis. *Int J Mol Sci.* 2015;16(11):26035-54.
44. Fox AJ, Bedi A, Rodeo SA. The basic science of human knee menisci: structure, composition, and function. *Sports Health.* 2012;4(4):340-51.

45. Seitz AM, Osthaus F, Schwer J, Warnecke D, Faschingbauer M, Sgroi M, et al. Osteoarthritis-Related Degeneration Alters the Biomechanical Properties of Human Menisci Before the Articular Cartilage. *Front Bioeng Biotechnol.* 2021;9:659989.
46. Englund M, Guermazi A, Lohmander LS. The Meniscus in Knee Osteoarthritis. *Rheumatic Disease Clinics of North America.* 2009;35(3):579-90.
47. Deng B, Wang F, Yin L, Chen C, Guo L, Chen H, et al. Quantitative study on morphology of calcified cartilage zone in OARSI 0~4 cartilage from osteoarthritic knees. *Current Research in Translational Medicine.* 2016;64(3):149-54.
48. Cox LGE, van Donkelaar CC, van Rietbergen B, Emans PJ, Ito K. Decreased bone tissue mineralization can partly explain subchondral sclerosis observed in osteoarthritis. *Bone.* 2012;50(5):1152-61.
49. Suri S, Gill SE, Massena de Camin S, Wilson D, McWilliams DF, Walsh DA. Neurovascular invasion at the osteochondral junction and in osteophytes in osteoarthritis. *Annals of the rheumatic diseases.* 2007;66(11):1423-8.
50. Junker S, Krumbholz G, Frommer KW, Rehart S, Steinmeyer J, Rickert M, et al. Differentiation of osteophyte types in osteoarthritis - proposal of a histological classification. *Joint Bone Spine.* 2016;83(1):63-7.
51. Grynpas MD, Alpert B, Katz I, Lieberman I, Pritzker KPH. Subchondral bone in osteoarthritis. *Calcified Tissue International.* 1991;49(1):20-6.
52. Mapp PI, Walsh DA. Mechanisms and targets of angiogenesis and nerve growth in osteoarthritis. *Nature Reviews Rheumatology.* 2012;8(7):390-8.
53. Bernabei I, So A, Busso N, Nasi S. Cartilage calcification in osteoarthritis: mechanisms and clinical relevance. *Nat Rev Rheumatol.* 2023;19(1):10-27.
54. Vidavsky N, Kunitake J, Estroff LA. Multiple Pathways for Pathological Calcification in the Human Body. *Adv Healthc Mater.* 2021;10(4):e2001271.
55. Grace MM, Letonoff EJ. Synovial Chondromatosis: An Unusual Case of Knee Pain and Swelling. *Federal practitioner : for the health care professionals of the VA, DoD, and PHS.* 2018;35(4):45-8.
56. Yang BY, Sartoris DJ, Resnick D, Clopton P. Calcium pyrophosphate dihydrate crystal deposition disease: frequency of tendon calcification about the knee. *The Journal of rheumatology.* 1996;23(5):883-8.
57. Derfus BA, Kurian JB, Butler JJ, Daft LJ, Carrera GF, Ryan LM, et al. The high prevalence of pathologic calcium crystals in pre-operative knees. *The Journal of rheumatology.* 2002;29(3):570-4.
58. Hubert J, Beil FT, Rolvien T, Butscheidt S, Hischke S, Püschel K, et al. Cartilage calcification is associated with histological degeneration of the knee joint: a highly prevalent, age-independent systemic process. *Osteoarthritis and cartilage.* 2020;28(10):1351-61.

59. Gordon GV, Villanueva T, Schumacher HR, Gohel V. Autopsy study correlating degree of osteoarthritis, synovitis and evidence of articular calcification. *The Journal of rheumatology*. 1984;11(5):681-6.
60. Ulian G, Moro D, Valdrè G. Hydroxylapatite and Related Minerals in Bone and Dental Tissues: Structural, Spectroscopic and Mechanical Properties from a Computational Perspective. *Biomolecules*. 2021;11(5).
61. Tariq U, Haider Z, Chaudhary K, Hussain R, Ali J. Calcium to phosphate ratio measurements in calcium phosphates using LIBS. *Journal of Physics: Conference Series*. 2018;1027(1):012015.
62. Dieppe PA, Crocker P, Huskisson EC, Willoughby DA. Apatite deposition disease. A new arthropathy. *Lancet (London, England)*. 1976;1(7954):266-9.
63. McCarty DJ, Lehr JR, Halverson PB. Crystal populations in human synovial fluid. Identification of apatite, octacalcium phosphate, and tricalcium phosphate. *Arthritis and rheumatism*. 1983;26(10):1220-4.
64. Bertrand J, Kräft T, Gronau T, Sherwood J, Rutsch F, Lioté F, et al. BCP crystals promote chondrocyte hypertrophic differentiation in OA cartilage by sequestering Wnt3a. *Annals of the rheumatic diseases*. 2020;79(7):975-84.
65. Fuerst M, Bertrand J, Lammers L, Dreier R, Echtermeyer F, Nitschke Y, et al. Calcification of articular cartilage in human osteoarthritis. *Arthritis and rheumatism*. 2009;60(9):2694-703.
66. Kräft T, Godmann L, Hubert J, Nitschke Y, Hawellek T, Liote F, et al. BCP crystals induce hypertrophic differentiation of chondrocytes by activating canonical wnt signaling. *Osteoarthritis and cartilage*. 2014;22:S170-S1.
67. Rong J, Pool B, Zhu M, Munro J, Cornish J, McCarthy GM, et al. Basic Calcium Phosphate Crystals Induce Osteoarthritis-Associated Changes in Phenotype Markers in Primary Human Chondrocytes by a Calcium/Calmodulin Kinase 2-Dependent Mechanism. *Calcified Tissue International*. 2019;104(3):331-43.
68. McCarthy GM, Westfall PR, Masuda I, Christopherson PA, Cheung HS, Mitchell PG. Basic calcium phosphate crystals activate human osteoarthritic synovial fibroblasts and induce matrix metalloproteinase-13 (collagenase-3) in adult porcine articular chondrocytes. *Annals of the rheumatic diseases*. 2001;60(4):399-406.
69. Nalesso G, Sherwood J, Bertrand J, Pap T, Ramachandran M, De Bari C, et al. WNT-3A modulates articular chondrocyte phenotype by activating both canonical and noncanonical pathways. *The Journal of cell biology*. 2011;193(3):551-64.
70. Corr EM, Cunningham CC, Helbert L, McCarthy GM, Dunne A. Osteoarthritis-associated basic calcium phosphate crystals activate membrane proximal kinases in human innate immune cells. *Arthritis Res Ther*. 2017;19(1):23.
71. Renaudin F, Sarda S, Campillo-Gimenez L, Séverac C, Léger T, Charvillat C, et al. Adsorption of Proteins on m-CPPD and Urate Crystals Inhibits Crystal-induced Cell Responses: Study on Albumin-crystal Interaction. *Journal of functional biomaterials*. 2019;10(2).

72. Nasi S, So A, Combes C, Daudon M, Busso N. Interleukin-6 and chondrocyte mineralisation act in tandem to promote experimental osteoarthritis. *Annals of the rheumatic diseases*. 2016;75(7):1372.
73. Nishida K, Doi T, Matsuo M, Ishiwari Y, Tsujigiwa H, Yoshida A, et al. Involvement of nitric oxide in chondrocyte cell death in chondro-osteophyte formation. *Osteoarthritis and cartilage*. 2001;9(3):232-7.
74. Ea HK, Uzan B, Rey C, Lioté F. Octacalcium phosphate crystals directly stimulate expression of inducible nitric oxide synthase through p38 and JNK mitogen-activated protein kinases in articular chondrocytes. *Arthritis Res Ther*. 2005;7(5):R915-26.
75. Kohn NN, Hughes RE, Mc CD, Jr., Faires JS. The significance of calcium phosphate crystals in the synovial fluid of arthritic patients: the "pseudogout syndrome". II. Identification of crystals. *Annals of internal medicine*. 1962;56:738-45.
76. Gras P, Rey C, André G, Charvillat C, Sarda S, Combes C. Crystal structure of monoclinic calcium pyrophosphate dihydrate (m-CPPD) involved in inflammatory reactions and osteoarthritis. *Acta Crystallographica Section B Structural Science, Crystal Engineering and Materials*. 2016;72:96-101.
77. Guerne PA, Terkeltaub R, Zuraw B, Lotz M. Inflammatory microcrystals stimulate interleukin-6 production and secretion by human monocytes and synoviocytes. *Arthritis and rheumatism*. 1989;32(11):1443-52.
78. Meyer F, Dittmann A, Kornak U, Herbster M, Pap T, Lohmann CH, et al. Chondrocytes From Osteoarthritic and Chondrocalcinosis Cartilage Represent Different Phenotypes. *Front Cell Dev Biol*. 2021;9(637).
79. Tasdemir N, Lowe SW. Senescent cells spread the word: non-cell autonomous propagation of cellular senescence. *The EMBO journal*. 2013;32(14):1975-6.
80. Coryell PR, Diekman BO, Loeser RF. Mechanisms and therapeutic implications of cellular senescence in osteoarthritis. *Nature Reviews Rheumatology*. 2021;17(1):47-57.
81. Del Rey MJ, Valín Á, Usategui A, Ergueta S, Martín E, Municio C, et al. Senescent synovial fibroblasts accumulate prematurely in rheumatoid arthritis tissues and display an enhanced inflammatory phenotype. *Immun Ageing*. 2019;16:29-.
82. Gao SG, Zeng C, Li LJ, Luo W, Zhang FJ, Tian J, et al. Correlation between senescence-associated beta-galactosidase expression in articular cartilage and disease severity of patients with knee osteoarthritis. *International journal of rheumatic diseases*. 2016;19(3):226-32.
83. Price JS, Waters JG, Darrah C, Pennington C, Edwards DR, Donell ST, et al. The role of chondrocyte senescence in osteoarthritis. *Aging Cell*. 2002;1(1):57-65.
84. Forsyth CB, Cole A, Murphy G, Bienias JL, Im HJ, Loeser RF, Jr. Increased matrix metalloproteinase-13 production with aging by human articular chondrocytes in response to catabolic stimuli. *The journals of gerontology Series A, Biological sciences and medical sciences*. 2005;60(9):1118-24.

85. Zhang W, Doherty M, Bardin T, Barskova V, Guerne PA, Jansen TL, et al. European League Against Rheumatism recommendations for calcium pyrophosphate deposition. Part I: terminology and diagnosis. *Annals of the rheumatic diseases*. 2011;70(4):563-70.
86. Abhishek A, Doherty S, Maciewicz R, Muir K, Zhang W, Doherty M. Evidence of a Systemic Predisposition to Chondrocalcinosis and Association Between Chondrocalcinosis and Osteoarthritis at Distant Joints: A Cross-Sectional Study. *Arthritis Care & Research*. 2013;65(7):1052-8.
87. Filippou G, Filippucci E, Tardella M, Bertoldi I, Di Carlo M, Adinolfi A, et al. Extent and distribution of CPP deposits in patients affected by calcium pyrophosphate dihydrate deposition disease: an ultrasonographic study. *Annals of the rheumatic diseases*. 2013;72(11):1836-9.
88. Pendleton A, Johnson MD, Hughes A, Gurley KA, Ho AM, Doherty M, et al. Mutations in ANKH cause chondrocalcinosis. *American journal of human genetics*. 2002;71(4):933-40.
89. Reijnierse M, Schwabl C, Klauser A. Imaging of Crystal Disorders:: Calcium Pyrophosphate Dihydrate Crystal Deposition Disease, Calcium Hydroxyapatite Crystal Deposition Disease and Gout Pathophysiology, Imaging, and Diagnosis. *Radiologic Clinics*. 2022;60(4):641-56.
90. Barskova VG, Kudaeva FM, Bozhieva LA, Smirnov AV, Volkov AV, Nasonov EL. Comparison of three imaging techniques in diagnosis of chondrocalcinosis of the knees in calcium pyrophosphate deposition disease. *Rheumatology (Oxford, England)*. 2013;52(6):1090-4.
91. Mitsuyama H, Healey RM, Terkeltaub RA, Coutts RD, Amiel D. Calcification of human articular knee cartilage is primarily an effect of aging rather than osteoarthritis. *Osteoarthritis and cartilage*. 2007;15(5):559-65.
92. Resnick D, Niwayama G, Goergen TG, Utsinger PD, Shapiro RF, Haselwood DH, et al. Clinical, Radiographic and Pathologic Abnormalities in Calcium Pyrophosphate Dihydrate Deposition Disease (CPPD): Pseudogout. *Radiology*. 1977;122(1):1-15.
93. Ledingham J, Regan M, Jones A, Doherty M. Radiographic patterns and associations of osteoarthritis of the knee in patients referred to hospital. *Annals of the rheumatic diseases*. 1993;52(7):520.
94. Patrick M, Hamilton E, Wilson R, Austin S, Doherty M. Association of radiographic changes of osteoarthritis, symptoms, and synovial fluid particles in 300 knees. *Annals of the rheumatic diseases*. 1993;52(2):97.
95. Miksanek J, Rosenthal AK. Imaging of calcium pyrophosphate deposition disease. *Curr Rheumatol Rep*. 2015;17(3):20.
96. Hubert J, Hawellek T, Hischke S, Bertrand J, Krause M, Püschel K, et al. Hyaline cartilage calcification of the first metatarsophalangeal joint is associated with osteoarthritis but independent of age and BMI. *BMC Musculoskeletal Disorders*. 2016;17(1):474.
97. Lumbreras B, Pascual E, Frasquet J, González-Salinas J, Rodríguez E, Hernández-Aguado I. Analysis for crystals in synovial fluid: training of the analysts results in high consistency. *Annals of the rheumatic diseases*. 2005;64(4):612.
98. Zell M, Aung T, Kaldas M, Rosenthal AK, Bai B, Liu T, et al. Calcium pyrophosphate crystal size and characteristics. *Osteoarthritis and cartilage open*. 2021;3(1).

99. Ivorra J, Rosas J, Pascual E. Most calcium pyrophosphate crystals appear as non-birefringent. *Annals of the rheumatic diseases*. 1999;58(9):582-4.
100. Kóssa G. Über die im Organismus künstlich erzeugbaren Verkalkungen. 1901.
101. Sun Y, Mauerhan DR, Honeycutt PR, Kneisl JS, Norton HJ, Zinchenko N, et al. Calcium deposition in osteoarthritic meniscus and meniscal cell culture. *Arthritis Res Ther*. 2010;12(2):R56.
102. Goldstein J. *Practical scanning electron microscopy: electron and ion microprobe analysis*: Springer Science & Business Media; 2012.
103. Miculescu F, Luță C, Constantinescu AE, Maidaniuc A, Mocanu AC, Miculescu M, et al. Considerations and Influencing Parameters in EDS Microanalysis of Biogenic Hydroxyapatite. *Journal of functional biomaterials*. 2020;11(4).
104. Nguyen C, Bazin D, Daudon M, Chatron-Colliet A, Hannouche D, Bianchi A, et al. Revisiting spatial distribution and biochemical composition of calcium-containing crystals in human osteoarthritic articular cartilage. *Arthritis Research & Therapy*. 2013;15(5):R103.
105. Fuerst M, Lammers L, Schäfer F, Niggemeyer O, Steinhagen J, Lohmann CH, et al. Investigation of calcium crystals in OA knees. *Rheumatology international*. 2010;30:623-31.
106. Butler HJ, Ashton L, Bird B, Cinque G, Curtis K, Dorney J, et al. Using Raman spectroscopy to characterize biological materials. *Nature Protocols*. 2016;11(4):664-87.
107. Shipp D, Sinjab F, Notingher I. Raman spectroscopy: techniques and applications in the life sciences. *Advances in Optics and Photonics*. 2017;9:315.
108. Pascart T, Norberciak L, Legrand J, Becce F, Budzik JF. Dual-energy computed tomography in calcium pyrophosphate deposition: initial clinical experience. *Osteoarthritis and cartilage*. 2019;27(9):1309-14.
109. Hosu CD, Moisoiu V, Stefancu A, Antonescu E, Leopold LF, Leopold N, et al. Raman spectroscopy applications in rheumatology. *Lasers in Medical Science*. 2019;34(4):827-34.
110. Hu DP, Ferro F, Yang F, Taylor AJ, Chang W, Miclau T, et al. Cartilage to bone transformation during fracture healing is coordinated by the invading vasculature and induction of the core pluripotency genes. *Development (Cambridge, England)*. 2017;144(2):221-34.
111. Villa-Bellosta R, Egido J. Phosphate, pyrophosphate, and vascular calcification: a question of balance. *European heart journal*. 2017;38(23):1801-4.
112. Anderson HC. VESICLES ASSOCIATED WITH CALCIFICATION IN THE MATRIX OF EPIPHYSEAL CARTILAGE. *Journal of Cell Biology*. 1969;41(1):59-72.
113. Kirsch T, Harrison G, Golub EE, Nah HD. The roles of annexins and types II and X collagen in matrix vesicle-mediated mineralization of growth plate cartilage. *The Journal of biological chemistry*. 2000;275(45):35577-83.
114. Sun Y, Mauerhan DR, Franklin AM, Zinchenko N, Norton HJ, Hanley EN, Jr., et al. Fibroblast-like synoviocytes induce calcium mineral formation and deposition. *Arthritis*. 2014;2014:812678.

115. Silver FH, Landis WJ. Deposition of apatite in mineralizing vertebrate extracellular matrices: A model of possible nucleation sites on type I collagen. *Connective tissue research*. 2011;52(3):242-54.
116. Nudelman F, Pieterse K, George A, Bomans PHH, Friedrich H, Brylka LJ, et al. The role of collagen in bone apatite formation in the presence of hydroxyapatite nucleation inhibitors. *Nature Materials*. 2010;9(12):1004-9.
117. Mbuyi-Muamba JM, Dequeker J, Gevers G. Collagen and non-collagenous proteins in different mineralization stages of human femur. *Acta anatomica*. 1989;134(4):265-8.
118. Landis WJ, Jacquet R. Association of Calcium and Phosphate Ions with Collagen in the Mineralization of Vertebrate Tissues. *Calcified Tissue International*. 2013;93(4):329-37.
119. Cornette P, Jaabar I, Wanherdrick K, Binder AC, Berenbaum F, Landoulsi J, et al. ROLE OF NON-COLLAGENOUS PROTEINS IN THE MINERALIZATION OF COLLAGEN FIBRILS: IMPLICATION IN OSTEOARTHRITIS. *Osteoarthritis and cartilage*. 2022;30:S322-S3.
120. Wuthier RE, Bisaz S, Russell RG, Fleisch H. Relationship between pyrophosphate, amorphous calcium phosphate and other factors in the sequence of calcification in vivo. *Calcified tissue research*. 1972;10(3):198-206.
121. Moreno EC, Aoba T, Margolis HC. Pyrophosphate adsorption onto hydroxyapatite and its inhibition of crystal growth. *Compend Suppl*. 1987(8):S256-8, s60, s62-6.
122. Addison WN, Azari F, Sørensen ES, Kaartinen MT, McKee MD. Pyrophosphate inhibits mineralization of osteoblast cultures by binding to mineral, up-regulating osteopontin, and inhibiting alkaline phosphatase activity. *The Journal of biological chemistry*. 2007;282(21):15872-83.
123. Rosenthal AK, McCarty BA, Cheung HS, Ryan M. A comparison of the effect of transforming growth factor β 1 on pyrophosphate elaboration from various articular tissues. *Arthritis & Rheumatism*. 1993;36(4):539-42.
124. Altman RD, Muniz OE, Pita JC, Howell DS. Articular chondrocalcinosis. Microanalysis of pyrophosphate (PPI) in synovial fluid and plasma. *Arthritis and rheumatism*. 1973;16 2:171-8.
125. Garimella R, Bi X, Anderson HC, Camacho NP. Nature of phosphate substrate as a major determinant of mineral type formed in matrix vesicle-mediated in vitro mineralization: An FTIR imaging study. *Bone*. 2006;38(6):811-7.
126. Thouverey C, Bechkoff G, Pikula S, Buchet R. Inorganic pyrophosphate as a regulator of hydroxyapatite or calcium pyrophosphate dihydrate mineral deposition by matrix vesicles. *Osteoarthritis and cartilage*. 2009;17(1):64-72.
127. Heinonen JK. *Biological role of inorganic pyrophosphate*: Springer Science & Business Media; 2001.
128. Ralph D, van de Wetering K, Uitto J, Li Q. Inorganic Pyrophosphate Deficiency Syndromes and Potential Treatments for Pathologic Tissue Calcification. *The American Journal of Pathology*. 2022;192(5):762-70.

129. Szeri F, Niaziyori F, Donnelly S, Fariha N, Tertyshnaia M, Patel D, et al. The Mineralization Regulator ANKH Mediates Cellular Efflux of ATP, Not Pyrophosphate. *Journal of Bone and Mineral Research*. 2022;37(5):1024-31.
130. Kaczmarek E, Koziak K, Sévigny J, Siegel JB, Anrather J, Beaudoin AR, et al. Identification and characterization of CD39/vascular ATP diphosphohydrolase. *The Journal of biological chemistry*. 1996;271(51):33116-22.
131. Caswell AM, Russell RG. Evidence that ecto-nucleoside-triphosphate pyrophosphatase serves in the generation of extracellular inorganic pyrophosphate in human bone and articular cartilage. *Biochimica et biophysica acta*. 1988;966(3):310-7.
132. Jin H, St Hilaire C, Huang Y, Yang D, Dmitrieva NI, Negro A, et al. Increased activity of TNAP compensates for reduced adenosine production and promotes ectopic calcification in the genetic disease ACDC. *Sci Signal*. 2016;9(458):ra121.
133. Stella J, Buers I, van de Wetering K, Höhne W, Rutsch F, Nitschke Y. Effects of Different Variants in the ENPP1 Gene on the Functional Properties of Ectonucleotide Pyrophosphatase/Phosphodiesterase Family Member 1. *Hum Mutat*. 2016;37(11):1190-201.
134. Li Q, Brodsky J, Conlin L, Pawel B, Glatz A, Gafni R, et al. Mutations in the ABCC6 Gene as a Cause of Generalized Arterial Calcification of Infancy: Genotypic Overlap with Pseudoxanthoma Elasticum. *The Journal of investigative dermatology*. 2013;134.
135. St Hilaire C, Ziegler SG, Markello TC, Brusco A, Groden C, Gill F, et al. NT5E mutations and arterial calcifications. *The New England journal of medicine*. 2011;364(5):432-42.
136. Cudrici CD, Newman KA, Ferrante EA, Huffstutler R, Carney K, Betancourt B, et al. Multifocal calcific periartthritis with distinctive clinical and radiological features in patients with CD73 deficiency. *Rheumatology (Oxford, England)*. 2021;61(1):163-73.
137. Weiss MJ, Cole DE, Ray K, Whyte MP, Lafferty MA, Mulivor R, et al. First identification of a gene defect for hypophosphatasia: evidence that alkaline phosphatase acts in skeletal mineralization. *Connective tissue research*. 1989;21(1-4):99-104.
138. Buchholz A, Stücker S, Koßlowski F, Lohmann CH, Bertrand J. High-Resolution Imaging Methods for Identification of Calcium Crystal Types in Osteoarthritis. *Gout, Urate, and Crystal Deposition Disease*. 2023;1(2):62-82.
139. Ehirchiou D, Bernabei I, Chobaz V, Castelblanco M, Hügle T, So A, et al. CD11b Signaling Prevents Chondrocyte Mineralization and Attenuates the Severity of Osteoarthritis. *Front Cell Dev Biol*. 2020;8:611757.
140. Stücker S, Koßlowski F, Buchholz A, Lohmann CH, Bertrand J. High frequency of BCP, but less CPP crystal-mediated calcification in cartilage and synovial membrane of osteoarthritis patients. *Osteoarthritis and Cartilage [Internet]*. Epub May 11 2024 [cited May 11 2024]; (24). Available from: <https://doi.org/10.1016/j.joca.2024.04.019>.
141. Stücker S, Koßlowski F, Buchholz A, Lohmann C, Bertrand J. BCP, but not CPP deposition, in osteoarthritis cartilage is associated with upregulated TNAP expression and elevated inorganic phosphate content. [Manuscript submitted for publication].

142. Maneiro E, Martín MA, de Andres MC, López-Armada MJ, Fernández-Sueiro JL, del Hoyo P, et al. Mitochondrial respiratory activity is altered in osteoarthritic human articular chondrocytes. *Arthritis and rheumatism*. 2003;48(3):700-8.
143. Diekman BO, Loeser RF. Aging and the emerging role of cellular senescence in osteoarthritis. *Osteoarthritis and cartilage*. 2024;32(4):365-71.
144. Stücker S, Koßlowski F, Buchholz A, Lohmann C, Bertrand J. CPP deposition in cartilage is associated with an elevated senescence associated secretory phenotype in synovial fluid. [Unpublished manuscript].
145. Yavorsky A, Hernandez-Santana A, McCarthy G, McMahon G. Detection of calcium phosphate crystals in the joint fluid of patients with osteoarthritis - analytical approaches and challenges. *The Analyst*. 2008;133(3):302-18.
146. Fisseler-Eckhoff A, Müller KM. Arthroscopy and chondrocalcinosis. *Arthroscopy : the journal of arthroscopic & related surgery : official publication of the Arthroscopy Association of North America and the International Arthroscopy Association*. 1992;8(1):98-104.
147. Ibad HA, Kwee RM, Ghotbi E, Roemer FW, Guermazi A, Demehri S. Radiographically detectable intra-articular mineralization: Predictor of knee osteoarthritis outcomes or only an indicator of aging? A brief report from the osteoarthritis initiative. *Osteoarthritis and cartilage open*. 2023;5(2):100348.
148. Abreu M, Johnson K, Chung CB, de Lima JE, Trudell D, Terkeltaub R, et al. Calcification in calcium pyrophosphate dihydrate (CPPD) crystalline deposits in the knee: anatomic, radiographic, MR imaging, and histologic study in cadavers. *Skeletal Radiology*. 2004;33(7):392-8.
149. Karimzadeh H, Sirous M, Sadati SN, Bashshash M, Mottaghi P, Ommani B, et al. Prevalence of Chondrocalcinosis in Patients above 50 Years and the Relationship with Osteoarthritis. *Adv Biomed Res*. 2017;6:98-.
150. Zhang Y, Terkeltaub R, Nevitt M, Xu L, Neogi T, Aliabadi P, et al. Lower prevalence of chondrocalcinosis in Chinese subjects in Beijing than in white subjects in the United States: the Beijing Osteoarthritis Study. *Arthritis and rheumatism*. 2006;54(11):3508-12.
151. Sirotti S, Becce F, Sconfienza LM, Terslev L, Naredo E, Zufferey P, et al. Reliability and Diagnostic Accuracy of Radiography for the Diagnosis of Calcium Pyrophosphate Deposition: Performance of the Novel Definitions Developed by an International Multidisciplinary Working Group. *Arthritis & rheumatology (Hoboken, NJ)*. 2023;75(4):630-8.
152. Tanikawa H, Ogawa R, Okuma K, Harato K, Niki Y, Kobayashi S, et al. Detection of calcium pyrophosphate dihydrate crystals in knee meniscus by dual-energy computed tomography. *J Orthop Surg Res*. 2018;13(1):73.
153. Cipolletta E, Filippou G, Scirè CA, Di Matteo A, Di Battista J, Salaffi F, et al. The diagnostic value of conventional radiography and musculoskeletal ultrasonography in calcium pyrophosphate deposition disease: a systematic literature review and meta-analysis. *Osteoarthritis and cartilage*. 2021;29(5):619-32.
154. Misra D, Guermazi A, Sieren JP, Lynch J, Torner J, Neogi T, et al. CT imaging for evaluation of calcium crystal deposition in the knee: initial experience from the Multicenter Osteoarthritis (MOST) study. *Osteoarthritis and cartilage*. 2015;23(2):244-8.

155. Riestra JL, Sánchez A, Rodríques-Valverde V, Castillo E, Calderón J. Roentgenographic features of the arthropathy associated with CPPD crystal deposition disease. A comparative study with primary osteoarthritis. *The Journal of rheumatology*. 1985;12(6):1154-8.
156. Latourte A, Rat AC, Ngueyon Sime W, Ea HK, Bardin T, Mazières B, et al. Chondrocalcinosis of the Knee and the Risk of Osteoarthritis Progression: Data From the Knee and Hip Osteoarthritis Long-term Assessment Cohort. *Arthritis & rheumatology (Hoboken, NJ)*. 2020;72(5):726-32.
157. Jarraya M, Guerhazi A, Liew JW, Tolstykh I, Lynch JA, Aliabadi P, et al. Prevalence of intra-articular mineralization on knee computed tomography: the multicenter osteoarthritis study. *Osteoarthritis and cartilage*. 2023;31(8):1111-20.
158. Neogi T, Nevitt M, Niu J, LaValley MP, Hunter DJ, Terkeltaub R, et al. Lack of association between chondrocalcinosis and increased risk of cartilage loss in knees with osteoarthritis: results of two prospective longitudinal magnetic resonance imaging studies. *Arthritis and rheumatism*. 2006;54(6):1822-8.
159. Hawellek T, Hubert J, Hischke S, Vettorazzi E, Wegscheider K, Bertrand J, et al. Articular cartilage calcification of the humeral head is highly prevalent and associated with osteoarthritis in the general population. *Journal of Orthopaedic Research*. 2016;34(11):1984-90.
160. Hawellek T, Hubert J, Hischke S, Krause M, Bertrand J, Pap T, et al. Articular cartilage calcification of the hip and knee is highly prevalent, independent of age but associated with histological osteoarthritis: evidence for a systemic disorder. *Osteoarthritis and cartilage*. 2016;24(12):2092-9.
161. Felson DT, Anderson JJ, Naimark A, Kannel W, Meenan RF. The prevalence of chondrocalcinosis in the elderly and its association with knee osteoarthritis: the Framingham Study. *The Journal of rheumatology*. 1989;16(9):1241-5.
162. Jung YK, Han MS, Park HR, Lee EJ, Jang JA, Kim GW, et al. Calcium-phosphate complex increased during subchondral bone remodeling affects early stage osteoarthritis. *Sci Rep*. 2018;8(1):487.
163. DeGroot J, Verzijl N, Bank RA, Lafeber FP, Bijlsma JW, TeKoppele JM. Age-related decrease in proteoglycan synthesis of human articular chondrocytes: the role of nonenzymatic glycation. *Arthritis and rheumatism*. 1999;42(5):1003-9.
164. Oliviero F, Baggio C, Favero M, Damasco AC, Boscaro C, Tietto D, et al. Synovial Fluid from Patients with Osteoarthritis Shows Different Inflammatory Features Depending on the Presence of Calcium Pyrophosphate Crystals. *Int J Mol Sci*. 2023;25(1).
165. Swan A, Chapman B, Heap P, Seward H, Dieppe P. Submicroscopic crystals in osteoarthritic synovial fluids. *Annals of the rheumatic diseases*. 1994;53(7):467-70.
166. Gibilisco PA, Schumacher Jr HR, Hollander JL, Soper KA. Synovial fluid crystals in osteoarthritis. *Arthritis & Rheumatism*. 1985;28(5):511-5.
167. Halverson PB, McCarty DJ. Patterns of radiographic abnormalities associated with basic calcium phosphate and calcium pyrophosphate dihydrate crystal deposition in the knee. *Annals of the rheumatic diseases*. 1986;45(7):603-5.

-
168. Niessink T, Stassen RHMJ, Kischkel B, Vuscan P, Emans PJ, van den Akker GGH, et al. Discovery of calcite as a new pro-inflammatory calcium-containing crystal in human osteoarthritic synovial fluid. *Osteoarthritis and cartilage*. 2024.
 169. Frallonardo P, Oliviero F, Peruzzo L, Tauro L, Scanu A, Galozzi P, et al. Detection of Calcium Crystals in Knee Osteoarthritis Synovial Fluid: A Comparison Between Polarized Light and Scanning Electron Microscopy. *JCR: Journal of Clinical Rheumatology*. 2016;22(7).
 170. Frallonardo P, Ramonda R, Peruzzo L, Scanu A, Galozzi P, Tauro L, et al. Basic calcium phosphate and pyrophosphate crystals in early and late osteoarthritis: relationship with clinical indices and inflammation. *Clinical rheumatology*. 2018;37(10):2847-53.
 171. Ryu K, Iriuchishima T, Oshida M, Kato Y, Saito A, Imada M, et al. The prevalence of and factors related to calcium pyrophosphate dihydrate crystal deposition in the knee joint. *Osteoarthritis and cartilage*. 2014;22(7):975-9.
 172. McCarty DJJ, Hogan JM, Gatter RA, Grossman M. Studies on Pathological Calcifications in Human Cartilage: I. PREVALENCE AND TYPES OF CRYSTAL DEPOSITS IN THE MENISCI OF TWO HUNDRED FIFTEEN CADAVERA. *JBJS*. 1966;48(2).
 173. Tedeschi SK, Yoshida K, Huang W, Solomon DH. Confirming Prior and Identifying Novel Correlates of Acute Calcium Pyrophosphate Crystal Arthritis. *Arthritis Care & Research*. 2023;75(2):283-8.
 174. Taverna D, Boraldi F, De Santis G, Caprioli RM, Quaglino D. Histology-directed and imaging mass spectrometry: An emerging technology in ectopic calcification. *Bone*. 2015;74:83-94.
 175. Burt HM, Dutt YC. Growth of monosodium urate monohydrate crystals: effect of cartilage and synovial fluid components on in vitro growth rates. *Annals of the rheumatic diseases*. 1986;45(10):858-64.
 176. Shidham V, Chivukula M, Basir Z, Shidham G. Evaluation of Crystals in Formalin-Fixed, Paraffin-Embedded Tissue Sections for the Differential Diagnosis of Pseudogout, Gout, and Tumoral Calcinosis. *Modern Pathology*. 2001;14(8):806-10.
 177. MacMullan P, McMahan G, McCarthy G. Detection of basic calcium phosphate crystals in osteoarthritis. *Joint Bone Spine*. 2011;78(4):358-63.
 178. Andrés M, Vela P, Jovaní V, Pascual E. Most needle-shaped calcium pyrophosphate crystals lack birefringence. *Rheumatology (Oxford, England)*. 2019;58(6):1095-8.
 179. Schumacher HR, Cherian PV, Reginato AJ, Bardin T, Rothfuss S. Intra-articular apatite crystal deposition. *Annals of the rheumatic diseases*. 1983;42 Suppl 1(Suppl 1):54-9.
 180. Bjelle AO, Sundström KG. An ultrastructural study of the articular cartilage in calcium pyrophosphate dihydrate (CPPD) crystal deposition disease (chondrocalcinosis articularis). *Calcified tissue research*. 1975;19(1):63-71.
 181. Bertrand J, Kräft T, Nitschke Y, Rutsch F, Liote F, Pap T. BCP crystals drive chondrocyte hypertrophic differentiation via binding WNT ligands and activation of canonical WNT signaling. *Osteoarthritis and cartilage*. 2018;26:S62-S3.

182. Kourí JB, Aguilera JM, Reyes J, Lozoya KA, González S. Apoptotic chondrocytes from osteoarthrotic human articular cartilage and abnormal calcification of subchondral bone. *The Journal of rheumatology*. 2000;27(4):1005-19.
183. Ralph Schumacher H. Ultrastructural findings in chondrocalcinosis and pseudogout. *Arthritis & Rheumatism*. 1976;19(S3):413-25.
184. Boivin G, Lagier R. An ultrastructural study of articular chondrocalcinosis in cases of knee osteoarthritis. *Virchows Arch A Pathol Anat Histopathol*. 1983;400(1):13-29.
185. Pritzker KP, Cheng PT, Renlund RC. Calcium pyrophosphate crystal deposition in hyaline cartilage. Ultrastructural analysis and implications for pathogenesis. *The Journal of rheumatology*. 1988;15(5):828-35.
186. Ohira T, Ishikawa K, Masuda I, Yokoyama M, Honda I. Histologic localization of lipid in the articular tissues in calcium pyrophosphate dihydrate crystal deposition disease. *Arthritis and rheumatism*. 1988;31(8):1057-62.
187. Bjelle AO. Morphological study of articular cartilage in pyrophosphate arthropathy. (Chondrocalcinosis articularis or calcium pyrophosphate dihydrate crystal deposition diseases). *Annals of the rheumatic diseases*. 1972;31(6):449-56.
188. Steinbach LS, Resnick D. Calcium pyrophosphate dihydrate crystal deposition disease: imaging perspectives. *Current problems in diagnostic radiology*. 2000;29(6):209-29.
189. Beutler A, Rothfuss S, Clayburne G, Sieck M, Schumacher HR, Jr. Calcium pyrophosphate dihydrate crystal deposition in synovium. Relationship to collagen fibers and chondrometaplasia. *Arthritis and rheumatism*. 1993;36(5):704-15.
190. Oca P, Zaka R, Dion AS, Freeman TA, Williams CJ. Phosphate and calcium are required for TGFbeta-mediated stimulation of ANK expression and function during chondrogenesis. *Journal of cellular physiology*. 2010;224(2):540-8.
191. Wang J, Tsui HW, Beier F, Tsui FW. The CPPDD-associated ANKH M48T mutation interrupts the interaction of ANKH with the sodium/phosphate cotransporter PiT-1. *The Journal of rheumatology*. 2009;36(6):1265-72.
192. Kudryavtsev I, Serebriakova M, Zhiduleva E, Murtazaliev P, Titov V, Malashicheva A, et al. CD73 Rather Than CD39 Is Mainly Involved in Controlling Purinergic Signaling in Calcified Aortic Valve Disease. *Frontiers in genetics*. 2019;10:604.
193. Rutsch F, Ruf N, Vaingankar S, Toliat MR, Suk A, Höhne W, et al. Mutations in ENPP1 are associated with 'idiopathic' infantile arterial calcification. *Nature Genetics*. 2003;34(4):379-81.
194. Ralph D, Nitschke Y, Levine MA, Caffet M, Wurst T, Saeidian AH, et al. ENPP1 variants in patients with GACI and PXE expand the clinical and genetic heterogeneity of heritable disorders of ectopic calcification. *PLOS Genetics*. 2022;18(4):e1010192.
195. Bertrand J, Nitschke Y, Fuerst M, Hermann S, Schäfers M, Sherwood J, et al. Decreased levels of nucleotide pyrophosphatase phosphodiesterase 1 are associated with cartilage calcification in osteoarthritis and trigger osteoarthritic changes in mice. *Annals of the rheumatic diseases*. 2012;71(7):1249-53.

196. Jin Y, Cong Q, Gvozdenovic-Jeremic J, Hu J, Zhang Y, Terkeltaub R, et al. Enpp1 inhibits ectopic joint calcification and maintains articular chondrocytes by repressing hedgehog signaling. *Development (Cambridge, England)*. 2018;145(18).
197. Nam HK, Liu J, Li Y, Kragor A, Hatch NE. Ectonucleotide pyrophosphatase/phosphodiesterase-1 (ENPP1) protein regulates osteoblast differentiation. *The Journal of biological chemistry*. 2011;286(45):39059-71.
198. Johnson K, Hashimoto S, Lotz M, Pritzker K, Goding J, Terkeltaub R. Up-regulated expression of the phosphodiesterase nucleotide pyrophosphatase family member PC-1 is a marker and pathogenic factor for knee meniscal cartilage matrix calcification. *Arthritis and rheumatism*. 2001;44(5):1071-81.
199. Savinov AY, Salehi M, Yadav MC, Radichev I, Millán JL, Savinova OV. Transgenic Overexpression of Tissue-Nonspecific Alkaline Phosphatase (TNAP) in Vascular Endothelium Results in Generalized Arterial Calcification. *Journal of the American Heart Association*. 2015;4(12):e002499.
200. Fakhry M, Roszkowska M, Briolay A, Bougault C, Guignandon A, Diaz-Hernandez JI, et al. TNAP stimulates vascular smooth muscle cell trans-differentiation into chondrocytes through calcium deposition and BMP-2 activation: Possible implication in atherosclerotic plaque stability. *Biochimica et Biophysica Acta (BBA) - Molecular Basis of Disease*. 2017;1863(3):643-53.
201. Yamamoto K, Kishida T, Sato Y, Nishioka K, Ejima A, Fujiwara H, et al. Direct conversion of human fibroblasts into functional osteoblasts by defined factors. *Proceedings of the National Academy of Sciences*. 2015;112(19):6152-7.
202. Kirsch T, Swoboda B, Nah H. Activation of annexin II and V expression, terminal differentiation, mineralization and apoptosis in human osteoarthritic cartilage. *Osteoarthritis and cartilage*. 2000;8(4):294-302.
203. Derfus B, Kranendonk S, Camacho N, Mandel N, Kushnaryov V, Lynch K, et al. Human osteoarthritic cartilage matrix vesicles generate both calcium pyrophosphate dihydrate and apatite in vitro. *Calcif Tissue Int*. 1998;63(3):258-62.
204. Miao D, Scutt A. Histochemical Localization of Alkaline Phosphatase Activity in Decalcified Bone and Cartilage. *Journal of Histochemistry & Cytochemistry*. 2002;50(3):333-40.
205. Rees JA, Ali SY. Ultrastructural localisation of alkaline phosphatase activity in osteoarthritic human articular cartilage. *Annals of the rheumatic diseases*. 1988;47(9):747-53.
206. Patrick M, Hamilton E, Hornby J, Doherty M. Synovial fluid pyrophosphate and nucleoside triphosphate pyrophosphatase: comparison between normal and diseased and between inflamed and non-inflamed joints. *Annals of the rheumatic diseases*. 1991;50(4):214-8.
207. Doherty M, Chuck A, Hosking D, Hamilton E. Inorganic pyrophosphate in metabolic diseases predisposing to calcium pyrophosphate dihydrate crystal deposition. *Arthritis and rheumatism*. 1991;34(10):1297-303.
208. Russell RGG, Bisaz S, Fleisch H, Currey HLF, Rubinstein HM, Dietz AA, et al. INORGANIC PYROPHOSPHATE IN PLASMA, URINE, AND SYNOVIAL FLUID OF PATIENTS WITH PYROPHOSPHATE ARTHROPATHY (CHONDROCALCINOSIS OR PSEUDOGOUT). *The Lancet*. 1970;296(7679):899-902.

-
209. Doherty M, Belcher C, Regan M, Jones A, Ledingham J. Association between synovial fluid levels of inorganic pyrophosphate and short term radiographic outcome of knee osteoarthritis. *Annals of the rheumatic diseases*. 1996;55(7):432.
210. Jiang J, Leong NL, Mung JC, Hidaka C, Lu HH. Interaction between zonal populations of articular chondrocytes suppresses chondrocyte mineralization and this process is mediated by PTHrP. *Osteoarthritis and cartilage*. 2008;16(1):70-82.
211. Tang Z, Chen H, He H, Ma C. Assays for alkaline phosphatase activity: Progress and prospects. *TrAC Trends in Analytical Chemistry*. 2019;113:32-43.
212. Mandel NS, Mandel GS. A model for human calcium pyrophosphate crystal deposition disease: crystallization kinetics in a gelatin matrix. *Scan Electron Microsc*. 1984(Pt 4):1779-92.
213. Johnson KA, Hessle L, Vaingankar S, Wennberg C, Mauro S, Narisawa S, et al. Osteoblast tissue-nonspecific alkaline phosphatase antagonizes and regulates PC-1. *American journal of physiology Regulatory, integrative and comparative physiology*. 2000;279(4):R1365-77.
214. Aghagolzadeh P, Radpour R, Bachtler M, van Goor H, Smith ER, Lister A, et al. Hydrogen sulfide attenuates calcification of vascular smooth muscle cells via KEAP1/NRF2/NQO1 activation. *Atherosclerosis*. 2017;265:78-86.
215. Boskey AL, Bullough PG. Cartilage calcification: normal and aberrant. *Scan Electron Microsc*. 1984(Pt 2):943-52.
216. Zamboulis DE, Marr N, Moustafa A, Meeson R, Orriss IR, Thorpe CT. Pathological calcification in canine tendon-derived cells is modulated by extracellular ATP. *Veterinary Research Communications*. 2024;48(3):1533-43.
217. Cutarelli A, Marini M, Tancredi V, D'Arcangelo G, Murdocca M, Frank C, et al. Adenosine Triphosphate stimulates differentiation and mineralization in human osteoblast-like Saos-2 cells. *Development, growth & differentiation*. 2016;58(4):400-8.
218. Villa-Bellosta R, Wang X, Millán JL, Dubyak GR, O'Neill WC. Extracellular pyrophosphate metabolism and calcification in vascular smooth muscle. *Am J Physiol Heart Circ Physiol*. 2011;301(1):H61-8.
219. Ryan LM, Rachow JW, McCarty DJ. Synovial fluid ATP: a potential substrate for the production of inorganic pyrophosphate. *The Journal of rheumatology*. 1991;18(5):716-20.
220. Boskey AL, Doty SB, Binderman I. Adenosine 5'-triphosphate promotes mineralization in differentiating chick limb-bud mesenchymal cell cultures. *Microsc Res Tech*. 1994;28(6):492-504.
221. Nakano Y, Addison WN, Kaartinen MT. ATP-mediated mineralization of MC3T3-E1 osteoblast cultures. *Bone*. 2007;41(4):549-61.
222. Campillo-Gimenez L, Renaud M, Gras P, Renaudin F, Mellouk A, Bobe P, et al. Calcium pyrophosphate dihydrate crystals induce IL-1beta production by monocytes through ATP release- and ROS production-dependent pathways – involvement of potassium efflux. *Osteoarthritis and cartilage*. 2016;24:S327-S8.

-
223. Venegas FC, Sánchez-Rodríguez R, Luisetto R, Angioni R, Viola A, Canton M. Oxidative Stress by the Mitochondrial Monoamine Oxidase B Mediates Calcium Pyrophosphate Crystal-Induced Arthritis. *Arthritis & Rheumatology*. 2024;76(2):279-84.
224. Volonte D, Benson CJ, Daugherty SL, Beckel JM, Trebak M, Galbiati F. Purinergic signaling promotes premature senescence. *Journal of Biological Chemistry*. 2024;300(4).
225. Gao X, Di X, Li J, Kang Y, Xie W, Sun L, et al. Extracellular ATP-induced calcium oscillations regulating the differentiation of osteoblasts through aerobic oxidation metabolism pathways. *J Bone Miner Metab*. 2023;41(5):606-20.
226. Kan S, Duan M, Liu Y, Wang C, Xie J. Role of Mitochondria in Physiology of Chondrocytes and Diseases of Osteoarthritis and Rheumatoid Arthritis. *Cartilage*. 2021;13(2_suppl):1102s-21s.
227. Zhao T, Niu D, Chen Y, Fu P. The role of mitochondrial quality control mechanisms in chondrocyte senescence. *Experimental gerontology*. 2024;188:112379.
228. Ruiz-Romero C, Calamia V, Mateos J, Carreira V, Martínez-Gomariz M, Fernández M, et al. Mitochondrial dysregulation of osteoarthritic human articular chondrocytes analyzed by proteomics: a decrease in mitochondrial superoxide dismutase points to a redox imbalance. *Mol Cell Proteomics*. 2009;8(1):172-89.
229. Nasi S, Castelblanco M, Chobaz V, Ehrchiou D, So A, Bernabei I, et al. Xanthine Oxidoreductase Is Involved in Chondrocyte Mineralization and Expressed in Osteoarthritic Damaged Cartilage. *Front Cell Dev Biol*. 2021;9:612440.
230. Nasi S, Ea HK, Lioté F, So A, Busso N. Sodium Thiosulfate Prevents Chondrocyte Mineralization and Reduces the Severity of Murine Osteoarthritis. *PloS one*. 2016;11(7):e0158196.
231. Coppé JP, Desprez PY, Krtolica A, Campisi J. The senescence-associated secretory phenotype: the dark side of tumor suppression. *Annu Rev Pathol*. 2010;5:99-118.
232. Mas-Bargues C, Borrás C, Alique M. The Contribution of Extracellular Vesicles From Senescent Endothelial and Vascular Smooth Muscle Cells to Vascular Calcification. *Frontiers in Cardiovascular Medicine*. 2022;9.
233. Gardner SE, Humphry M, Bennett MR, Clarke MC. Senescent Vascular Smooth Muscle Cells Drive Inflammation Through an Interleukin-1 α -Dependent Senescence-Associated Secretory Phenotype. *Arterioscler Thromb Vasc Biol*. 2015;35(9):1963-74.
234. Muñoz JC, Martín R, Alonso C, Gutiérrez B, Nieto ML. Relation between serum levels of chemotaxis-related factors and the presence of coronary artery calcification as expression of subclinical atherosclerosis. *Clinical Biochemistry*. 2017;50(18):1048-55.
235. Velard F, Laurent-Maquin D, Guillaume C, Bouthors S, Jallot E, Nedelec JM, et al. Polymorphonuclear neutrophil response to hydroxyapatite particles, implication in acute inflammatory reaction. *Acta Biomater*. 2009;5(5):1708-15.
236. Mikhaylova L, Malmquist J, Nurminskaya M. Regulation of in vitro vascular calcification by BMP4, VEGF and Wnt3a. *Calcif Tissue Int*. 2007;81(5):372-81.

-
237. Inoue M, Itoh H, Ueda M, Naruko T, Kojima A, Komatsu R, et al. Vascular Endothelial Growth Factor (VEGF) Expression in Human Coronary Atherosclerotic Lesions. *Circulation*. 1998;98(20):2108-16.
238. Hachicha M, Naccache PH, McColl SR. Inflammatory microcrystals differentially regulate the secretion of macrophage inflammatory protein 1 and interleukin 8 by human neutrophils: a possible mechanism of neutrophil recruitment to sites of inflammation in synovitis. *The Journal of experimental medicine*. 1995;182(6):2019-25.
239. Wang J, Fang CL, Noller K, Wei Z, Liu G, Shen K, et al. Bone-derived PDGF-BB drives brain vascular calcification in male mice. *J Clin Invest*. 2023;133(23).
240. Lange S, Heger J, Euler G, Wartenberg M, Piper HM, Sauer H. Platelet-derived growth factor BB stimulates vasculogenesis of embryonic stem cell-derived endothelial cells by calcium-mediated generation of reactive oxygen species. *Cardiovasc Res*. 2009;81(1):159-68.
241. Loro E, Ramaswamy G, Chandra A, Tseng WJ, Mishra MK, Shore EM, et al. IL15RA is required for osteoblast function and bone mineralization. *Bone*. 2017;103:20-30.
242. Warner SC, Nair A, Marpadga R, Chubinskaya S, Doherty M, Valdes AM, et al. IL-15 and IL15RA in Osteoarthritis: Association With Symptoms and Protease Production, but Not Structural Severity. *Front Immunol*. 2020;11:1385.
243. Sun JM, Sun LZ, Liu J, Su BH, Shi L. Serum interleukin-15 levels are associated with severity of pain in patients with knee osteoarthritis. *Dis Markers*. 2013;35(3):203-6.
244. Jenei-Lanzl Z, Meurer A, Zaucke F. Interleukin-1 β signaling in osteoarthritis – chondrocytes in focus. *Cellular signalling*. 2019;53:212-23.
245. Del Carlo M, Schwartz D, Erickson EA, Loeser RF. Endogenous production of reactive oxygen species is required for stimulation of human articular chondrocyte matrix metalloproteinase production by fibronectin fragments. *Free Radical Biology and Medicine*. 2007;42(9):1350-8.
246. Martin JA, Klingelhutz AJ, Moussavi-Harami F, Buckwalter JA. Effects of oxidative damage and telomerase activity on human articular cartilage chondrocyte senescence. *The journals of gerontology Series A, Biological sciences and medical sciences*. 2004;59(4):324-37.
247. Peng R, Shang J, Jiang N, Chi-Jen H, Gu Y, Xing B, et al. Klf10 is involved in extracellular matrix calcification of chondrocytes alleviating chondrocyte senescence. *Journal of Translational Medicine*. 2024;22(1):52.
248. Shang J, Lin N, Peng R, Jiang N, Wu B, Xing B, et al. Inhibition of Klf10 Attenuates Oxidative Stress-Induced Senescence of Chondrocytes via Modulating Mitophagy. *Molecules*. 2023;28(3).
249. Richter E, Lohmann CH, Dell'Accio F, Goettsch C, Bertrand J. Sortilin Is Upregulated in Osteoarthritis-Dependent Cartilage Calcification and Associated with Cellular SenescenceEpub [cited; 24(15)].
250. Watanabe W, Baker DG, Schumacher HR, Jr. Comparison of the acute inflammation induced by calcium pyrophosphate dihydrate, apatite and mixed crystals in the rat air pouch model of a synovial space. *The Journal of rheumatology*. 1992;19(9):1453-7.

-
251. Laquerriere P, Grandjean-Laquerriere A, Jallot E, Balossier G, Frayssinet P, Guenounou M. Importance of hydroxyapatite particles characteristics on cytokines production by human monocytes in vitro. *Biomaterials*. 2003;24(16):2739-47.
252. Mallat Z, Besnard S, Duriez M, Deleuze V, Emmanuel F, Bureau MF, et al. Protective Role of Interleukin-10 in Atherosclerosis. *Circulation Research*. 1999;85(8):e17-e24.
253. Altomare A, Corrado A, Maruotti N, Cici D, Cantatore FP. The role of Interleukin-1 receptor antagonist as a treatment option in calcium pyrophosphate crystal deposition disease. *Mol Biol Rep*. 2021;48(5):4789-96.
254. Isoda K, Matsuki T, Kondo H, Iwakura Y, Ohsuzu F. Deficiency of Interleukin-1 Receptor Antagonist Induces Aortic Valve Disease in BALB/c Mice. *Arteriosclerosis, Thrombosis, and Vascular Biology*. 2010;30(4):708-15.
255. Hegner B, Schaub T, Janke D, Zickler D, Lange C, Girndt M, et al. Targeting proinflammatory cytokines ameliorates calcifying phenotype conversion of vascular progenitors under uremic conditions in vitro. *Scientific Reports*. 2018;8(1):12087.
256. Grandjean-Laquerriere A, Laquerriere P, Guenounou M, Laurent-Maquin D, Phillips TM. Importance of the surface area ratio on cytokines production by human monocytes in vitro induced by various hydroxyapatite particles. *Biomaterials*. 2005;26(15):2361-9.
257. Campillo-Gimenez L, Renaudin F, Jalabert M, Gras P, Gosset M, Rey C, et al. Inflammatory Potential of Four Different Phases of Calcium Pyrophosphate Relies on NF- κ B Activation and MAPK Pathways. 2018;9(2248).
258. Scanu A, Oliviero F, Luisetto R, Ramonda R, Doria A, Punzi L, et al. Effect of pathogenic crystals on the production of pro- and anti-inflammatory cytokines by different leukocyte populations. *Immunobiology*. 2021;226(1):152042.
259. Loeser RF. Aging and osteoarthritis: the role of chondrocyte senescence and aging changes in the cartilage matrix. *Osteoarthritis and cartilage*. 2009;17(8):971-9.
260. Dijkgraaf LC, Liem RSB, de Bont LGM, Boering G. Calcium pyrophosphate dihydrate crystal deposition disease: a review of the literature and a light and electron microscopic study of a case of the temporomandibular joint with numerous intracellular crystals in the chondrocytes. *Osteoarthritis and cartilage*. 1995;3(1):35-45.
261. Vijen S, Hawes C, Runions J, Russell RGG, Wordsworth BP, Carr AJ, et al. Differences in intracellular localisation of ANKH mutants that relate to mechanisms of calcium pyrophosphate deposition disease and craniometaphyseal dysplasia. *Sci Rep*. 2020;10(1):7408.
262. Lust G, Nuki G, Seegmiller JE. Inorganic pyrophosphate and proteoglycan metabolism in cultured human articular chondrocytes and fibroblasts. *Arthritis and rheumatism*. 1976;19 Suppl 3:479-87.
263. Caswell A, Guillard-Cumming DF, Hearn PR, McGuire MK, Russell RG. Pathogenesis of chondrocalcinosis and pseudogout. Metabolism of inorganic pyrophosphate and production of calcium pyrophosphate dihydrate crystals. *Annals of the rheumatic diseases*. 1983;42 Suppl 1(Suppl 1):27-37.

-
264. Johnson K, Vaingankar S, Chen Y, Moffa A, Goldring MB, Sano K, et al. Differential mechanisms of inorganic pyrophosphate production by plasma cell membrane glycoprotein-1 and B10 in chondrocytes. *Arthritis and rheumatism*. 1999;42(9):1986-97.
265. Terkeltaub R, Rosenbach M, Fong F, Goding J. Causal link between nucleotide pyrophosphohydrolase overactivity and increased intracellular inorganic pyrophosphate generation demonstrated by transfection of cultured fibroblasts and osteoblasts with plasma cell membrane glycoprotein-1. *Arthritis & Rheumatism*. 1994;37(6):934-41.
266. Johnson K, Jung A, Murphy A, Andreyev A, Dykens J, Terkeltaub R. Mitochondrial oxidative phosphorylation is a downstream regulator of nitric oxide effects on chondrocyte matrix synthesis and mineralization. *Arthritis and rheumatism*. 2000;43(7):1560-70.
267. Mansurova SE. Inorganic pyrophosphate in mitochondrial metabolism. *Biochimica et Biophysica Acta (BBA) - Bioenergetics*. 1989;977(3):237-47.
268. Terkeltaub RA. Inorganic pyrophosphate generation and disposition in pathophysiology. 2001;281(1):C1-C11.
269. Ho AM, Johnson MD, Kingsley DM. Role of the Mouse ank Gene in Control of Tissue Calcification and Arthritis. *Science (New York, NY)*. 2000;289(5477):265-70.
270. Polewski MD, Johnson KA, Foster M, Millán JL, Terkeltaub R. Inorganic pyrophosphatase induces type I collagen in osteoblasts. *Bone*. 2010;46(1):81-90.
271. Kogaya Y, Furuhashi K. Comparison of the calcium distribution pattern among several kinds of hard tissue forming cells of some living vertebrates. *Scanning Microsc*. 1988;2(4):2029-43.
272. Wuthier RE, Chin JE, Hale JE, Register TC, Hale LV, Ishikawa Y. Isolation and characterization of calcium-accumulating matrix vesicles from chondrocytes of chicken epiphyseal growth plate cartilage in primary culture. *Journal of Biological Chemistry*. 1985;260(29):15972-9.
273. Blanco FJ, López-Armada MJ, Maneiro E. Mitochondrial dysfunction in osteoarthritis. *Mitochondrion*. 2004;4(5-6):715-28.
274. Raynard C, Tessier N, Huna A, Warnier M, Flaman JM, Van Coppenolle F, et al. Expression of the Calcium-Binding Protein CALB1 Is Induced and Controls Intracellular Ca(2+) Levels in Senescent Cells. *Int J Mol Sci*. 2022;23(16).
275. Wierzbicki A, Dalal P, Madura JD, Cheung HS. Molecular Dynamics Simulation of Crystal-Induced Membranolysis. *The Journal of Physical Chemistry B*. 2003;107(44):12346-51.
276. Dalal P, Zanotti K, Wierzbicki A, Madura JD, Cheung HS. Molecular Dynamics Simulation Studies of the Effect of Phosphocitrate on Crystal-Induced Membranolysis. *Biophysical Journal*. 2005;89(4):2251-7.
277. Bjelle A. Cartilage matrix in hereditary pyrophosphate arthropathy. *The Journal of rheumatology*. 1981;8(6):959-64.

10 Publications

Stücker S, Koßlowski F, Buchholz A, Lohmann CH, Bertrand J. CPP deposition in cartilage is associated with an elevated senescence associated secretory phenotype in synovial fluid. **(Unpublished manuscript)**

Stücker S, Koßlowski F, Lohmann CH, Bertrand J. BCP, but not CPP deposition, in osteoarthritis cartilage is associated with upregulated TNAP expression and elevated inorganic phosphate content. *Arthritis & Rheumatology* **(Manuscript under review)**

Stücker, S., Koßlowski, F., Buchholz, A., Lohmann, C. H., & Bertrand, J. (2024). High frequency of BCP, but less CPP crystal-mediated calcification in cartilage and synovial membrane of osteoarthritis patients. *Osteoarthritis and cartilage*, S1063-4584(24)01176-2. Advance online publication. <https://doi.org/10.1016/j.joca.2024.04.019>

Feldmann, A., Nitschke, Y., Linß, F., Mulac, D., **Stücker, S.**, Bertrand, J., Buers, I., Langer, K., & Rutsch, F. (2023). Improved Reversion of Calcifications in Porcine Aortic Heart Valves Using Elastin-Targeted Nanoparticles. *International journal of molecular sciences*, 24(22), 16471. <https://doi.org/10.3390/ijms242216471>

Buchholz A., **Stücker S.**, Koßlowski F., Lohmann CH., Bertrand J. (2023). High-Resolution Imaging Methods for Identification of Calcium Crystal Types in Osteoarthritis. *Gout, Urate, and Crystal Deposition Disease*, 1(2):62-82. <https://doi.org/10.3390/gucdd1020007>

Stolberg-Stolberg, J., Boettcher, A., Sambale, M., **Stuecker, S.**, Sherwood, J., Raschke, M., Pap, T., & Bertrand, J. (2022). Toll-like receptor 3 activation promotes joint degeneration in osteoarthritis. *Cell death & disease*, 13(3), 224. <https://doi.org/10.1038/s41419-022-04680-5>

Stücker S., Bollmann M., Garbers C., Bertrand J. (2021). The role of calcium crystals and their effect on osteoarthritis pathogenesis. *Best practice & research. Clinical Rheumatology*, 35(4):101722. <https://doi.org/10.1016/j.berh.2021.101722>

12 Declaration of Honour

I hereby declare that I prepared this thesis without the impermissible help of third parties and that none other than the aids indicated have been used; all sources of information are clearly marked, including my own publications.

In particular I have not consciously:

- fabricated data or rejected undesirable results,
- misused statistical methods with the aim of drawing other conclusions than those warranted by the available data,
- plagiarized external data or publications,
- presented the results of other researchers in a distorted way.

I am aware that violations of copyright may lead to injunction and damage claims by the author and also to prosecution by the law enforcement authorities. I hereby agree that the thesis may be electronically reviewed with the aim of identifying plagiarism.

This work has not yet been submitted as a doctoral thesis in the same or a similar form in Germany, nor in any other country. It has not yet been published as a whole.

(Place, Date)

(Signature)